

**Untersuchungen zur Struktur-Eigenschafts-Beziehung
selbstassoziiierender Photosensibilisatoren mittels zeitaufgelöster
Spektroskopie
(Investigations on structure-property-relationship of self-
associating photosensitizers by means of time-resolved
spectroscopy)**

Dissertation

**zur Erlangung des akademischen Grades
doktor rerum naturalium
(Dr. rer. nat.)**

vorgelegt dem Rat der Physikalisch-Astronomischen Fakultät der Friedrich-
Schiller-Universität Jena

vom Diplomphysiker
Laimonas Kelbauskas
Geboren am 7. Dezember 1973 in Jonava (Litauen)

Gutachter:

1. Prof. Dr. Roland Sauerbrey
2. Prof. Dr. R. Pottier
3. Prof. Dr. R. Rotomskis

Tag des Rigorosums: 07.07.2003

Tag der öffentlichen Verteidigung: 17.07.2003

Contents

Chapter 1. Self-association/aggregation of planar macrocyclic molecules (tetrapyrroles)

| | |
|---|----|
| 1.1. Introduction | 1 |
| 1.2. Influence of self-association (aggregation) on physico-chemical properties of tetrapyrrolic molecules | |
| 1.2.1. Structural and spectral properties of monomeric tetrapyrroles | 6 |
| 1.2.2. Aggregatio/disaggregation behavior of tetrapyrrolic sensitizers in various environments | 8 |
| 1.2.3. Structure-activity relationship of a congeneric series of pyropheophorbide a ether derivatives | 12 |
| 1.3. Self-association of molecular components in various media. Properties of macromolecular assemblies | |
| 1.3.1. Formation of J-aggregates of a water-soluble porphyrin | 15 |
| 1.3.2. Exciton-exciton interaction in molecular aggregates | 16 |

Chapter 2. Techniques and methods

| | |
|--|----|
| 2.1. Methods for investigation of aggregation behavior of photosensitizers | |
| 2.1.1. Experimental techniques for fluorescence investigation with high temporal resolution | 26 |
| 2.1.2. Optimization of experimental techniques for highly resolved fluorescence measurements in time domain | 26 |
| 2.1.3. Time-resolved fluorescence measurements on sensitizers in homogenous solutions | 28 |
| 2.1.4. Experimental techniques for fluorescence investigations with high spatial resolution. Principles of confocal laser-scanning fluorescence microscopy | 31 |
| 2.1.5. Determination of two-photon absorption spectra of sensitizers and fluorescent probes | 34 |

| | |
|--|----|
| 2.2. Techniques of spectroscopy measurements | 37 |
| Chapter 3. Results and discussion | |
| 3.1. Investigation of energy relaxation mechanisms and structure of J-aggregates of TPPS₄ | |
| 3.1.1. Steady-state measurements | 42 |
| 3.1.2. Fluorescence kinetics spectroscopy | 45 |
| 3.1.3. Investigation of nonlinear properties and structure of TPPS ₄ J-aggregates | 50 |
| 3.2. Aggregation state and subcellular localization patterns of a series of pyropheophorbide - a and chlorin e6 derivatives | |
| 3.2.1. Steady-state absorption and fluorescence measurements | 56 |
| 3.2.1.1. Photoproduct formation | 56 |
| 3.2.1.2. Absorption and emission properties | 56 |
| 3.2.2. Time-resolved fluorescence measurements in homogenous solution | 59 |
| 3.2.3. Investigations on interaction of the sensitizers with biological membranes | 63 |
| 3.2.4 Time-resolved fluorescence measurements in tumor cells | 65 |
| 3.2.4.1. Derivatives of pyropheophorbide a ether | 65 |
| 3.2.4.2. Chlorin e6 derivatives | 68 |
| 3.2.5. Investigations on the uptake kinetics and subcellular localization patterns of PS in tumor cells | 70 |
| 3.2.5.1. Derivatives of pyropheophorbide a ether | 71 |
| 3.2.5.2. Chlorin e6 derivatives. Fluorescence lifetime imaging (FLIM, τ - imaging) | 72 |
| 3.2.5.3. Endocytotic uptake in tumor cells | 74 |
| 3.2.6. Summary and discussion of the obtained results | 75 |
| Summary | 78 |
| Zusammenfassung | 81 |
| References | 85 |
| Appendix | 92 |

Glossary of used definitions

Amphiphilicity or amphiphilic

Ampiphilic molecules possess in their structure both a hydrophilic and a lipophilic region. Amphiphilic substances are therefore soluble in polar and non-polar solvents. Because of the lipophilic properties, most amphiphiles tend to form self-assemblies in aqueous environment.

Congeneric series

Derivatives of a substance possessing a particular physico-chemical or structural property which changes gradually within the series with other properties being very similar or identical to the unmodified molecule. The congeneric series of a substance are synthesized in order to investigate the influence of a property to the activity of the substance (property-activity relationship).

Endocytosis

{Endo (within) cytos (cell) } a process of active uptake in cells in which a substance gains entry into a cell without crossing the cell membrane. The cell ingulfs the substance by folding inward a portion of its outer membrane (plasma membrane). Most hydrophobic molecules needed for metabolic processes in the cell are internalised by endocytosis.

Endosomes

Or endocytic vesicles, are formed during endocytosis in which localized regions of plasma membrane invaginate and pinch off producing a closed 'bag' which contains molecules to internalise.

Hydrophilicity or hydrophilic

is a characteristic of materials exhibiting an affinity for water. Hydrophilic literally means "water-loving" and such materials readily adsorb water. Hydrophilic molecules also possess the ability to form "hydrogen-bonds" with water.

Lipophilicity or lipophilic

materials possessing this characteristic have the opposite response to water interaction compared to hydrophilic materials. Lipophilic molecules ("fat-loving") have little or no tendency to adsorb water molecules and tend to self-assembly (aggregation) in aqueous environment. Lipophilic molecules lack active regions in their structure for formation of "hydrogen-bonds" with water molecules.

Lysosomes

Lysosomes are cell organelles containing mainly hydrolytic enzymes (proteins) used for the controlled intracellular digestion of macromolecules. For optimal activity the hydrolytic enzymes require an acid environment (pH ~5), which is maintained in the interior of lysosomes.

Photodynamic therapy

A non-invasive treatment of tumor and other diseases, which is based on the selective retention of light-sensitive substances (photosensitizers) and their subsequent activation with light of appropriate wavelength. The activation of photosensitizer molecules initiates formation of highly reactive cytotoxic species, such as singlet oxygen and free radicals which lead to the destruction of cells. The selective retention of the photosensitizer by neoplastic cells causes the destruction of the cancerous tissue without affecting the healthy tissue.

Glossary of acronyms:

CCD – coupled charge device

Chl – chlorin e6

ChlC6, ChlC9 – derivatives of Chl with alkyl side chains

FWHM – full width at half maximum

LSM – laser-scanning microscope

MCP-PMT – multichannel plate photomultiplier

mTHPC – tetra(m-hydroxyphenyl)chlorin

OPA – optical parametric amplifier

OPE – one-photon excitation

OMA – optical multichannel analyzer

PBS – phosphate buffered saline

PDT – photodynamic therapy

Ppe – pyropheophorbide a ether

PpeC1...C9 – derivatives of Ppe with alkyl side chains

PS – photosensitizer

TCSPC – time-correlated single photon counting

TPPS₄ – meso-tetrasulfonatophenyl porphine

TPE –two-photon excitation

Chapter 1

**Self-association/aggregation of planar
macrocyclic molecules (tetrapyrroles)**

1.1. Introduction

Owing to strong interaction, self-associated molecular aggregates possess chemical and optical properties which can differ significantly from those of the individual molecules.

In recent years, many efforts have been made to investigate aggregation processes and structure-property relationships of diverse molecular aggregates due to their unique physicochemical properties. An important reason for the strongly increased interest in molecular aggregates was their potential technological application in various fields.

The self-association of molecules plays a significant role in the nature, particularly in living systems. All membranes of animal cells are based on self-assembled molecules of phospholipids, which tend to aggregate in aqueous environments due to the so called hydrophobic (water-insoluble) interaction forming molecular layers and closed structures (vesicles). In biophysics, molecular aggregates of chlorophyll have been found to mediate the primary light-harvesting and charge-transfer processes in the photosynthetic unit of plants [1-3]. The importance of the aggregation for vital key processes attracted attention of many researchers and initiated numerous studies.

In technological fields, molecular aggregates have been employed as potential organic photoconductors [4], as materials with enhanced nonlinear optical properties [5,6] for use in nonlinear optics devices [7-9] and for information processing and storage [10]. They are widely used in photographic materials as antenna systems on the surface of silver halide microcrystals to collect light for the photographic process [11,12]. Moreover, there has been renewed interest in molecular aggregates because their properties can be exploited for superconductivity.

J-aggregates represent a particular case of molecular assemblies. Discovered in the mid thirties by Scheibe [13,14] and Jelley [15,16], the J-aggregates of pseudo-isocyanine (PIC) have been an object of extensive investigations due to their unusual optical properties [17-19]. The special interest in these molecular formations arises from collective effects that are caused by strong interaction between the molecules within aggregates. The strong intermolecular interaction results in the formation of collective eigenstates, the so called excitonic states, which are delocalized over many molecules within the aggregate. As a result, interesting collective effects, such as giant optical nonlinearities and exciton superradiance can occur. Despite the number of relevant studies conducted, the structure-property relationship and the energy transformation processes in J-aggregates are as yet not well understood.

The **first aim** of this study was *to investigate the energy relaxation processes and structure of the J-aggregates*. The investigations were carried out on a water-soluble tetrapyrrolic photosensitizer (PS) by means of steady-state and time-resolved fluorescence spectroscopy.

The **second aim** was *to investigate the structure-property relationship of photosensitizers using appropriate physical methods and to gain additional knowledge on how the structure of a photosensitizer molecule can modulate its photodynamic efficacy*.

Aggregation of the photosensitizers used in the so called photodynamic (photochemical) therapy of tumors (PDT) has *empirically* been found to play a decisive role for their photodynamic activity [20,21]. The principle of the photodynamic therapy is a very promising modality for the non-invasive treatment of tumors and other diseases. Still being investigated by many research groups worldwide, it has recently been approved by several countries (USA, Canada, Japan, some European countries) for esophageal and lung cancer. Its use in other cancers, including breast and ovarian is now undergoing trials.

PDT is based on a selective retention of a light-sensitive substance, photosensitizer, in tumor cells and its subsequent activation with light at appropriate wavelength. The photodynamic effect arises due to the energy- and/or charge transfer from the PS to an acceptor molecule and the formation of cytotoxic species such as highly reactive singlet oxygen or free radicals. In the past decades, a great number of PS for PDT have been developed but only a few of them show a more or less satisfactory tumor selectivity and phototoxicity. Up to now the method to find an effective sensitizer has been an *empirical* one. The important key question of how the structure of the sensitizers is related to their photodynamic activity, remains to be clarified.

The self-association of sensitizer molecules can be caused by different reasons, *e.g.* by interaction between sensitizer and solvent molecules. Sensitizer molecules, which possess a hydrophobic region in their structure, tend to isolate it from the contact with water molecules and self-associate in order to minimize the free energy of the system. In aggregated form, sensitizers show no or only a negligible photodynamic activity. This is due to the fast radiationless energy relaxation, which precludes energy- and/or charge transfer from the sensitizer to acceptor molecules. The subsequent formation of highly active singlet oxygen species or radicals that induce the photodynamic effect is hindered. However, it has been found that amphiphilic sensitizers, which are soluble both in water and lipid environment and tend to self-associate in aqueous solutions, exhibit photodynamic efficacy which is much higher than that of the pure hydrophilic (water-soluble) and pure lipophilic (oil-soluble)

sensitizers [20,22-24]. Interestingly, a study on the structure-activity relationship performed on amphiphilic porphyrinoids with varying lipophilicity (bearing lipophilic side chains of varying length) showed that the tumor response does not correlate with the increasing lipophilicity but exhibits a maximum for alkyl side chain lengths of 5 or 6 carbon atoms [20]. No clear explanation for this intriguing and contradictional fact could be provided so far. On the other hand, steric modifications of the molecular structure of sensitizers has also been found to exert a strong influence on their photodynamic activity [21,24]. These observations suggest that the aggregation may play a key role in the understanding of the structure-activity relationship of the PS.

Knowledge about the relationship between the aggregation and the photodynamic efficacy would facilitate the further development of the drug design and could contribute significantly to a more efficient PDT. However, studies concerning the structure-activity relationship of the sensitizers are rather rare and there is still a lack of knowledge on the influence of aggregation on the photodynamic efficacy of the sensitizers *in vitro* and *in vivo*. This is mainly caused by the absence of appropriate experimental techniques, which could enable a sensitive and non-invasive examination of the physical state of sensitizer molecules inside living cells.

Since molecular aggregates can be differentiated from other molecules by their spectroscopic features, spectroscopic methods are most suitable for investigations of aggregate formation. However, due to the complexity of the microenvironmental conditions and possible interaction with intracellular compounds, steady-state spectroscopic measurements have only limited value for investigations of aggregation states on the subcellular level. This is, because steady-state spectral information lacks of specificity and can be misinterpreted when manifold interaction with the environment takes place. In contrast to this, time-resolved measurements make it possible to distinguish sensitizer aggregates from its non-associated species by their characteristic energy relaxation properties, which are much more sensitive to changes in the aggregation state than the steady-state characteristics. Thus, measurements in the time domain should allow one to detect and follow up changes in the aggregation state of molecules. Though widely employed for measurements of optical properties in homogenous media, most time-resolved spectroscopic methods are almost non-applicable for studies of biological objects, especially on the subcellular level. The main shortcomings of most time domain techniques, such as transient absorption measurements, are high absorptivity, high photon flux densities and/or long integration times required in order to achieve a sufficient signal-to-noise ratio. In addition, spectroscopic measurements inside cells

have to be conducted with a high spatial resolution which means reduced irradiation volumes with small numbers of molecules, and thus, extremely weak signals. This leads to prolonged measurement intervals and higher irradiation doses experienced by the cell. High irradiation doses can cause photochemical and thermal effects in the cell interior. This leads to a partial or complete destruction of cells making experiments of this kind almost impossible.

Time-resolved fluorescence measurements are more advantageous in this regard because they are based on a direct detection of photons emitted by molecules after their excitation and therefore do not require high optical densities and high excitation intensities to be used (as far as one-photon excitation of fluorescence is used). In particular, time-resolved fluorescence microscopy has been shown to be a potential tool for tumor detection by measuring the fluorescence lifetime of exogenous compounds [25], for the determination of pH, and the aggregation state of hydrophilic porphyrins in cells [26]. It has been used as a unique technique for following binding of phthalocyanine molecules to proteins, photodegradation [27], internalization processes [28,29] and localization of PS [30-32]. Excitation with laser pulses down to the ps time scale has been widely applied for time domain fluorescence measurements in living cells [27,31-37]. The interpretation of the results obtained, particularly concerning aggregation state of the sensitizers, has been rather complicated owing to the relatively low temporal resolution achieved in these early measurements. Namely, interactions of PS with biomolecules in the cell interior could also result in fluorescence lifetimes of PS comparable to those of aggregated PS species (< 1 ns).

This shortcoming can be avoided when strongly aggregated PS with short fluorescence lifetimes are used which can clearly be distinguished from those of other sensitizer species. As a rule, such PS show a very low fluorescence quantum yield (they are “nearly non fluorescent”) and their detection inside cells is even more complicated by small excitation volumes. These two limitations make an appropriate measurement apparatus with high detection sensitivity necessary. In addition, technique with a high temporal resolution is required, because the excited state lifetimes of highly aggregated species are as a rule in the order of sub-picoseconds to hundreds of picoseconds.

Therefore, a technique providing both high temporal and spectral resolutions and a high sensitivity have to be found for measurements of aggregation behavior of sensitizers on the intracellular level.

The aggregation/disaggregation behavior of selected sensitizers with varying lipophilicity belonging to the congeneric series of two different classes (porphyrins and

chlorins) was studied in homogenous solutions and in tumor cells by means of steady-state and time-resolved fluorescence spectroscopy and microscopy.

In the following sections of this chapter an introduction to the molecular structure, overview of spectroscopic and photodynamical properties of the widely used sensitizer classes - porphyrins and reduced porphyrins (chlorins) - are given. The theory of the excitonic interactions in J-aggregates is described in the second part of the chapter.

A description of experimental techniques for measurements in the time domain, contributions to their optimization and the principles of laser scanning microscopy are presented in Chapter 2. Experimental techniques used in this study are described. Chapter 3 represents the experimental results obtained and their interpretation.

1.2. Influence of self-association (aggregation) on physico-chemical properties of tetrapyrrolic molecules

1.2.1. Spectral and structural properties of monomeric tetrapyrroles

Tetrapyrrolic molecules possess a conjugated π electron system, which mainly determines its spectral properties. The energy term scheme of a tetrapyrrolic molecule with a conjugated π electron system is depicted in Fig. 1.1. When excited to the first (S_1) or higher singlet states (the transition $S_0 \rightarrow T_1$ is spin-forbidden), the molecule can relax to the ground state either via the internal conversion (k_{IC}) or by emitting a fluorescence photon from S_1 state (k_{FI}). Also, the molecule can cross to the triplet (T_1) state and relax to the ground state by emitting a photon. As the transition $S_1 - T_1$ is spin-forbidden, the intersystem crossing (ISC) rates k_{ISC} are much lower ($\sim 10^8 \text{ s}^{-1}$) than those of the internal conversion k_{IC} and the fluorescence transition rates k_{FI} from the S_1 state. The efficiency of the ISC is defined as $E(\text{ISC}) = k_{ISC} / (k_{IC} + k_{FI} + k_{ISC})$. While strongly fluorescent dye molecules exhibit low ISC

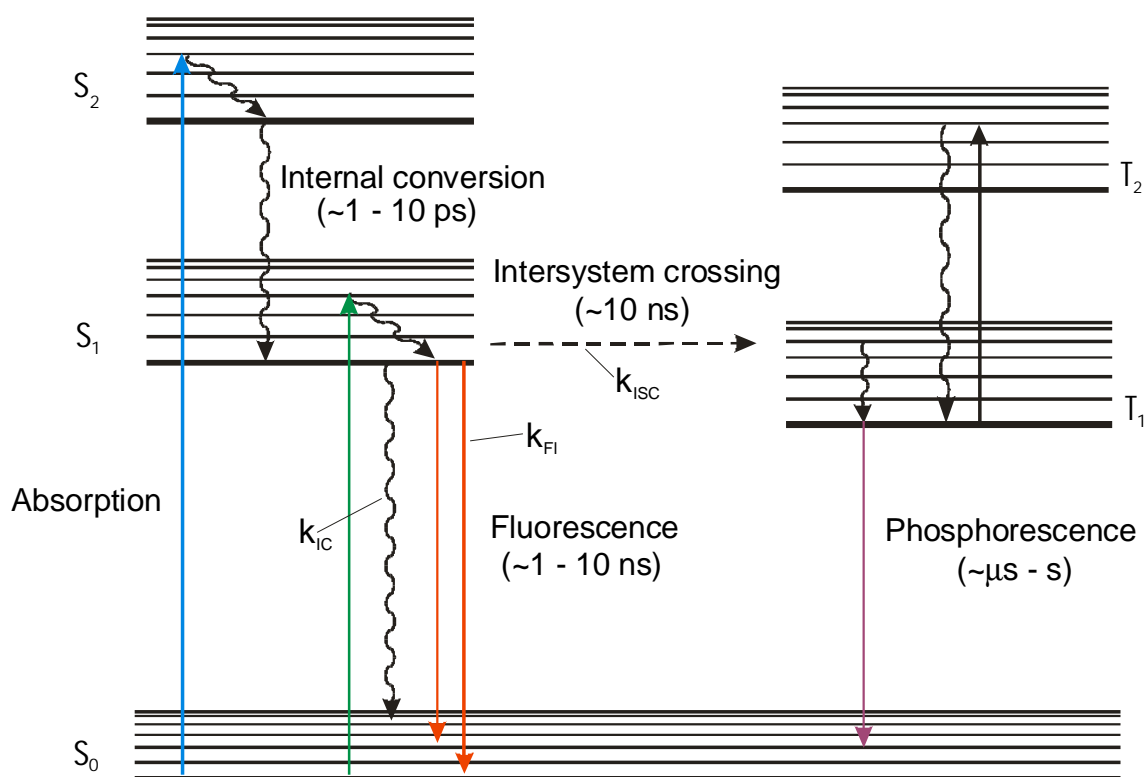


Fig. 1.1. Energy term scheme (Jablonski-diagram) of a tetrapyrrolic molecule with conjugated π -electron system. The non-radiative transitions are depicted by the sinuous line. The straight lines represent radiative transitions. Typical lifetimes of each relaxation channel are given in brackets below. k_{FI} , k_{ISC} , k_{IC} denote the rates of the fluorescence, intersystem crossing and internal conversion transitions, respectively.

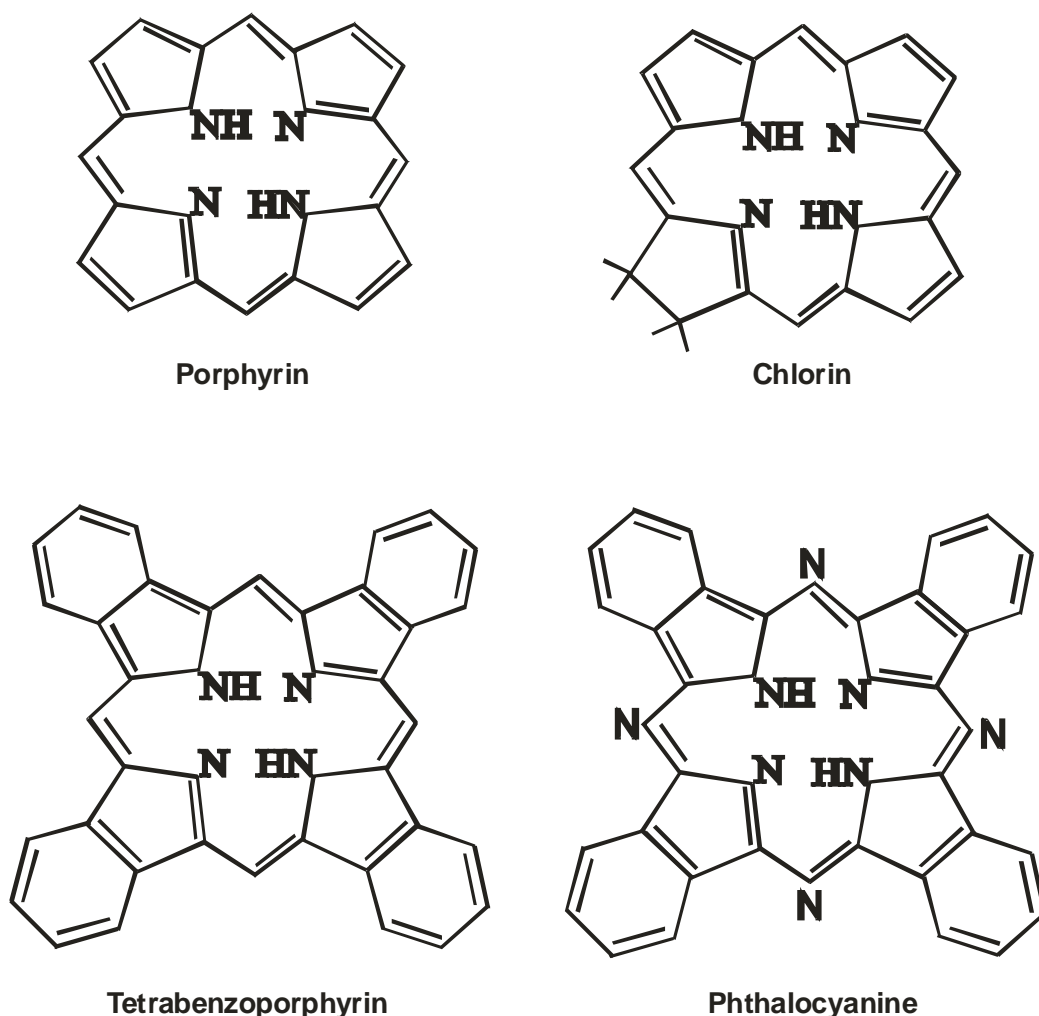


Fig. 1.2. Simplified molecular structure of some of tetrapyrrolic compounds

efficiencies (~ 0.01 or less), $E(\text{ISC})$ of the sensitizers can reach values of up to 0.7.

The intrinsic lifetime of the T_1 state is typically much longer than that of the singlet states, so that the excitation energy of a molecule in the T_1 state is ‘stored’ over longer times. As a consequence, charge- and energy-transfer processes from this state become much more probable as compared to the singlet states. The high ISC quantum yield and the long lifetime of the T_1 state are the preconditions for an efficient induction of charge- and energy-transfer processes from the sensitizer molecule. Such energy transfer mechanisms make it possible to excite target molecules in higher energy states that cannot be accessed by the direct excitation due to forbidden transitions or molecular symmetry restrictions. Among other energy and charge transfer processes, generation of highly reactive singlet oxygen ($^1\text{O}_2$) species upon energy transfer from an activated sensitizer (donor) to an oxygen molecule (acceptor) has been suggested to be the main photodynamic mechanism which causes damages of tumor

tissue and cancer cells [38]. On the other hand, highly reactive radicals of other molecules can also be formed when the charge transfer processes take place.

Since the first reports on the photodynamic principle of disease treatment [39], many photosensitizing agents (hereafter referred to as photosensitizers or sensitizers) have been developed with more or less satisfactory results of their applications in light-mediated destruction of tumor cells. Within the great variety of all PS developed so far, tetrapyrrolic sensitizers and their derivatives belong to the most efficient agents and are most promising for PDT applications (Fig. 1.2).

1.2.2. Aggregation/disaggregation behavior of tetrapyrrolic sensitizers in various environments

Due to the planar molecular structure, many tetrapyrrolic sensitizers tend to self-associate to form dimers or higher aggregates [40-47]. For the flat pyrrolic rings, it is energetically favorable to be surrounded by other pyrrolic rings. This phenomena is driven by the interaction forces between the molecules.

In general, four different types of intermolecular interactions can be distinguished: dipole \leftrightarrow dipole (electrostatic), dipole \leftrightarrow induced-dipole (induction), induced dipole \leftrightarrow induced dipole (London or dispersion), and short range repulsion (Pauli repulsion). All four are also referred to as Van der Waals interactions [48,49]. Because of the small local dipole moments and the high polarizability of the porphyrinoids, the dispersive interaction between two tetrapyrrolic rings (often referred to as π - π interaction), is the largest attractive force which contributes to the total interaction. However, the electrostatic component of side chains attached to the porphyrins ring may also play an important role in determining the geometry of two interacting tetrapyrrolic molecules.

The aggregation process of unsubstituted porphyrinoids dissolved in aqueous solutions can be driven by two different forces - van der Waals (enthalpy-driven) and/or hydrophobic interaction with solvent molecules (entropy-driven) [50]. When dissolved in polar solvents, tetrapyrrolic compounds with hydrophobic side chains cause an increase of the free energy in the system. This is due to the energetically unfavorable interaction between the non-polar hydrophobic regions and the polar solvent molecules. The hydrophobic interaction forces the system 'tetrapyrrole-solvent' to minimize its free energy. The minimum of the free energy in such a system is reached, when the hydrophobic regions are isolated from the interaction with solvent molecules by forming self-assemblies of the tetrapyrrolic molecules. The hydrophobic

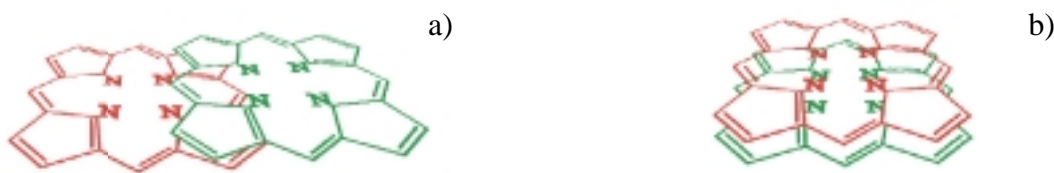


Fig. 1.3. Simplified structure of a) J- and b) H-aggregates (dimers) of tetrapyrroles

regions are directed to the inside, thus precluding the solvent molecules from interacting with the hydrophobic (polar) regions.

The typical intrinsic spectral properties of the sensitizer aggregates with respect to the monomers are: red-shifted and broadened absorption spectrum, significantly shorter lifetime of the lowest excited singlet state (S_1), low fluorescence quantum yield, and no or only negligible energy- and charge-transfer. Thus, singlet oxygen generation is negligible. The low fluorescence and singlet oxygen quantum yields are caused by strong interaction between the tetrapyrrolic macrocycles, which results in a splitting of their energy levels, thus ‘opening’ a fast, non-radiative deactivation channel of the excited level. As a result, the fluorescence lifetime shortens considerably and the quantum yield of the intersystem crossing to the triplet level (T_1) drops nearly to zero [30,37,51-53]. Accordingly, in aggregated form, the PS exhibit no or only a negligible photodynamic efficiency [45,54,55].

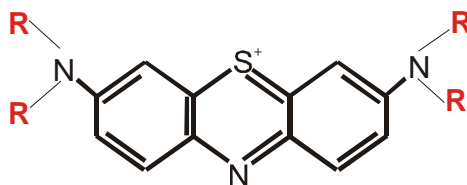
Molecular aggregates, in which individual molecules are arranged in a specific manner, are of particular interest due to their unique properties. Depending on their actual geometry, two types of aggregates are distinguished – ‘head-to-tail’ or J-aggregates and ‘face-to-face’ or H- aggregates (Fig. 1.3). J-aggregates represent macromolecular assemblies of individual molecules with the transition moments of the individual molecules aligned nearly parallel to the line joining their centers. Due to the strong intermolecular interaction, molecular eigenstates in these formations are perturbed and partially or fully delocalized over the aggregate. This results in the occurrence of charge or energy migration and excitonic processes within the aggregates. An important characteristic spectral feature of J-aggregates is the additional narrow absorption band, also called ‘excitonic band’, which is shifted to the red with respect to the monomeric absorption. It results from the cooperative effects in the optical response of the J-aggregates.

Within the great variety of the sensitizers developed for PDT so far, it seems to be obvious, that PS with the most direct activity on neoplastic cells exhibit an amphiphilic

character [56]. In contrast to other molecules, amphiphilic compounds consist of both a hydrophilic (polar) and a lipophilic (non polar) region on opposite sides. In aqueous solutions amphiphilic molecules tend to aggregate because of their lipophilic properties [36,57,58]. The strength of the self-assembly for an amphiphilic PS is modulated by the lipophilicity and structural properties of the molecule. Because aggregated sensitizers are photodynamically inactive due to the low singlet oxygen generation [54,59], the aggregation of PS is often considered to be unfavorable for PDT applications. However, from the early studies on the PS hematoporphyrin derivative (HpD) it is known that the aggregated species of HpD are essential to the tumor treatment whereas the monomeric species are not [60]. Furthermore, it has been reported that monomers and equilibrium monomers of HpD are taken up from the aqueous phase by membranes only to a negligible extent [61]. *It is obvious, that when internalizing a sensitizer in aggregated form, tumor cells must be able to disaggregate/unfold it in order to make it photodynamically active. The monomerization of the photodynamic less efficient aggregates is the precondition for the photosensitizing ability of the aggregated photosensitizers.* Aggregates of amphiphilic sensitizers can be monomerized by cell membranes, because membranes consist merely of the phospholipids and represent therefore a lipophilic medium. Depending on the aggregation state, aggregates can be monomerized by the cell membranes to different extents. The monomerization process can take place at both the plasma and inner cell membranes [58,62,63]. Since aggregates, in common with macromolecules, can hardly cross the plasma membrane of cells by passive diffusion, this finding raises two important questions: *can photosensitizers in aggregated form be internalized by tumor cells, and are the cells then able to monomerize them?* These questions are still a matter of discussion and are closely related to hydro-/lipophilicity characteristics [60] as well as to the structure-activity relationship [64] of the sensitizers. The monomerization at the inner membranes can occur when aggregates are internalized via endocytosis. The uptake and the intracellular distribution of sensitizers play key roles for their photodynamic efficiency [56]. It has been reported, that the distribution of the porphyrins within the cell is dependent on the structure of pendant side chains [21,31,56,65].

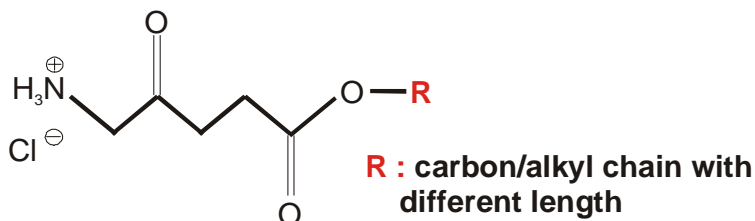
There have been many attempts to investigate the internalization pathways of sensitizers in cells. Unfortunately, the internalization mechanisms for most sensitizers still remain insufficiently elucidated. The granulated fluorescence of endosomes/lysosomes observed using stationary fluorescence microscopy was attributed to an endocytotic pathway of internalization [21,26]. In this particular case, the uptake of aggregates and their monomerization in endosomes/lysosomes can be supposed but an endocytotic internalization

Methylene blue



Phototoxicity (fibrosarcoma cells): R = C1, C2, C3, C4, C5, C6

Aminolaevulinic acid (ALA) ester



Phototoxicity (pancreatoma cells): R = C3, C4, C5, C6

Phototoxicity (A549 cells): R = C1, C2, C4, C6, C8

Chlorin ethers

Tumour response (fibrosarcoma): R = C1, C3, C6, C7

Fig. 1.4. Sensitizers and the pro-drug ALA with varying lipophilicity and their photodynamic efficacy. The lipophilicity was changed by attaching alkyl side chains of varying length to the host molecules. The number of carbon atoms in alkyl chain for which the photodynamic efficacy was significantly higher are shown in green. The blue-marked numbers of carbon atoms in the alkyl chain denotes the most efficient compound within the series (from [21,24,67]).

of monomers integrated in the plasma membrane cannot be excluded. It has also been shown [21], that the internalization pathways can be influenced by the aggregation state of the sensitizer. Lipophilicity seems to be one of the most crucial parameters determining the photodynamic efficiency of a sensitizer, and therefore it can be hypothesized that it is determined by the degree of aggregation in aqueous media. As noted by Margaron et al. [23] and Kessel et al. [66], the lipophilicity may be an important factor in the photodynamic activity because it may affect the localization by determining the aggregation of sensitizers. Increasing the lipophilicity by attaching lipophilic alkyl chains of different length to methylene blue resulted in an increased tumor response [67]. A similar dependence of the photodynamic activity has also been observed for the sensitizer chlorin e6 [24]. Furthermore, a maximum of protoporphyrin IX production efficacy was observed for the pro-drug aminolaevulinic acid ester (ALA) bearing alkyl chains with 5 carbon atoms [22] (s. Fig. 1.4. for details). The latter fact suggests that the uptake of ALA is influenced by the lipophilicity.

1.2.3. The structure-activity relationship of a congeneric series of pyropheophorbide a ether derivatives

A congeneric series of a substance makes it possible to change one or several particular parameters of the substance and to investigate their influence on the physico-chemical properties.

To gain information on the relation between the structure and the photodynamic efficacy of the sensitizers, a congeneric series of the pyropheophorbide a ether (Ppe) derivatives bearing alkyl side chains of different length (Fig. 1.5) was investigated. The substances were synthesized by the group of Th. J. Dougherty [68]. Main properties and the photodynamic activity of all compounds are summarized in Table I [20]. Within the series, the lipophilicity (expressed by the partition coefficient logP) of the compounds increases linearly with the length of the attached carbon chain. The singlet oxygen quantum yield in methylene chloride (CH_2Cl_2), where the compounds are present in the monomeric form, is almost the same for all compounds. This suggests a comparable phototoxicity of the

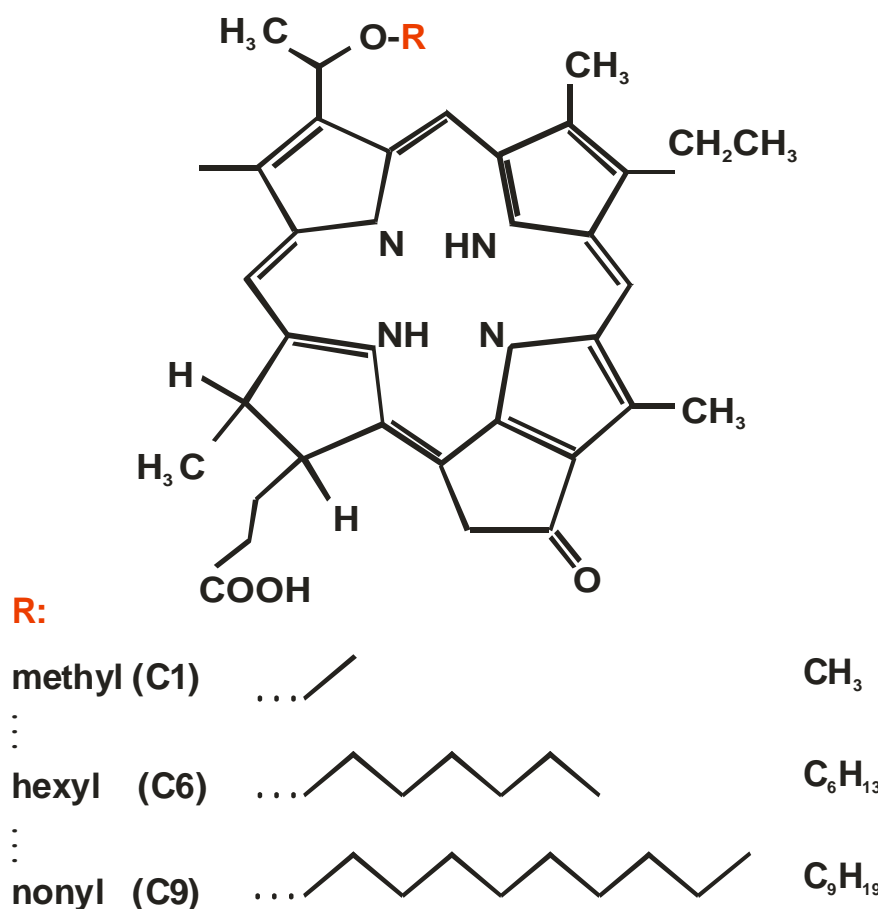


Fig. 1.5. Chemical structure of pyropheophorbide a ether derivatives with linear alkyl side chains of different lengths.

Table I. Some physico-chemical properties and the photodynamic efficacy (tumour response) of a congeneric series of pyropheophorbide derivatives (from [20, 21]).

| Alkyl chain R | Lipophilicity Octanol/water partition coefficient log P | ¹ O ₂ generation quantum yield in CH ₂ Cl ₂ | Pharmacokinetics | | Tumour response (treatment 24 h after application in mice, fibrosarcoma) |
|-------------------------|---|--|------------------|------------|---|
| | | | maximum uptake | clearance | |
| C1 : C3 | 3.0 4.0 | 0.45 | minutes | hour | poor |
| C5 C6 C7 | 5.0 5.5 6.1 | 0.44 0.48 0.48 | hours | hours/days | efficient to very efficient |
| C9 : C12 | 7.1 8.6 | 0.41 | >24 hours | days | poor |

compounds. However, the tumor response in an animal model at 24 hours after injection into the tissue was low or very low for the least lipophilic compounds (C1..C3) and for the most lipophilic (C9..C12) compounds. It exhibited a maximum for those with intermediate chain lengths, C5, C6, C7. Since changes in the observed photodynamic efficiency are not strictly correlated with the lipophilicity, the oxygen generation quantum yield seems not to be the only factor which determines the photodynamic efficiency of a sensitizer *in vivo*. While the low tumor response of the most hydrophilic C1..C3 can be explained by the rapid clearance from the tissue observed during the measurement and thus an insufficient accumulation of the PS in cells at the time of testing, the low photodynamic efficiency in the case of the most lipophilic C9..C12 seems to be more controversial. The lower clearance rate of C9..C12 (see Table I) and their higher concentrations in tumor and plasma [20] should lead to an increased photodynamic efficiency as in the case of C1..C3 compounds. Unfortunately, no explanation of the observed relation between the length of the alkyl chains/lipophilicity and the photodynamic efficacy could be provided so far. From the experimental findings presented above it can be concluded, that the lipophilicity influences strongly the photodynamic efficacy of the sensitizers *in vivo*. However, the photodynamic efficacy increases not linearly with the increasing lipophilicity, but exhibits a maximum for the alkyl chains of the middle length.

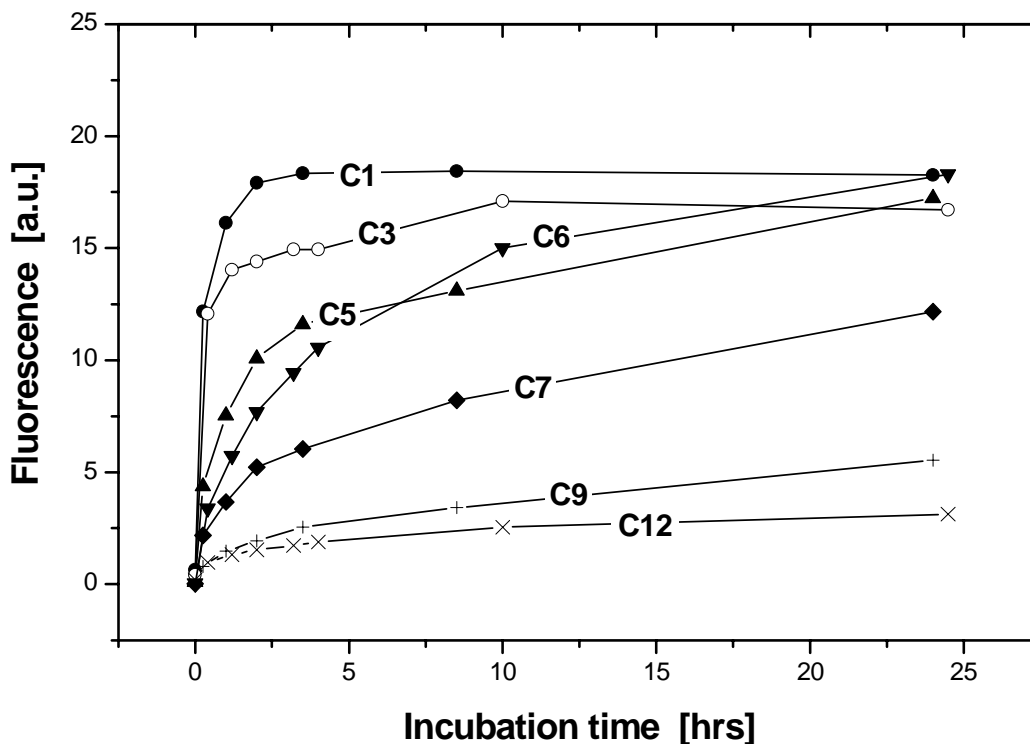


Fig. 1.6. Time course of the disaggregation of the pyropheophorbide a derivatives in the presence of erythrocyte ghosts. The monomerization was monitored by measuring of the fluorescence intensity as a function of the incubation time

The intracellular concentrations of the *monomeric* species of Ppe derivatives has been found to decrease with the increasing lipophilicity [21]. Furthermore, distinct intracellular localization patterns for compounds with different lipophilicity were obtained in the same study: the most lipophilic derivatives localized mainly to the lysosomes, whereas compounds with the intermediate chain length localized preferentially to the mitochondria.

The experimental findings presented above initiate the following question: what biological and/or physico-chemical mechanisms of interaction between sensitizer molecules and living cells underlie such a structure-activity relationship?

It has been shown in previous investigations conducted by our group, that the ability of the cell membrane to monomerize the aggregates decreases with the increasing length of the alkyl chains. The disaggregation kinetics of the Ppe derivatives in erythrocyte ghosts are depicted in Fig. 1.6. The most hydrophilic compounds (C1..C3) are monomerized fast as compared to the most lipophilic PpeC9..C12 which undergo a much slower disaggregation process. Derivatives with alkyl chains of more than 10 carbons are strongly aggregated so that they can hardly be monomerized by the biological membranes. These results imply that the disaggregation kinetics in the cell membrane strongly depends on the lipophilicity of the molecule.

1.3. Self-association of molecular components in various media. Properties of macromolecular assemblies

1.3.1. Formation of J-aggregates of a water-soluble porphyrin

Meso-5,10,15,20-sulfonatophenyl porphine ($\text{H}_2\text{TPPS}_4^{4-}$) is a water-soluble tetrapyrrolic dye (Fig.1.7). It has been shown that $\text{H}_2\text{TPPS}_4^{4-}$ can self-associate to form H- and J-aggregates depending on the dye concentration, pH and ionic strength [69-72]. In an acidic medium ($\text{pH} < 5$), the nitrogen atoms of $\text{H}_2\text{TPPS}_4^{4-}$ can be protonated resulting in a diprotonated form $\text{H}_4\text{TPPS}_4^{2-}$. The diprotonated tetraphenyl porphyrin shows, in contrast to its neutral form, a near to coplanar conformation of the phenyl rings to the tetrapyrrolic ring. This allows the approach of the sulfonato groups to the central part of the tetrapyrrolic ring thereby forming J-aggregates [73]. The formation of J-aggregates is indicated by the appearance of a sharp intense absorption band that is shifted to the red with respect to the monomeric Soret band [69]. There have been many attempts to clarify the structure of the J-aggregates of TPPS_4 by using UV-VIS and FT-IR spectroscopy [18,69,74], hole-burning [75], pump-probe spectroscopy [76], elastic and dynamic light scattering [77], circular dichroism

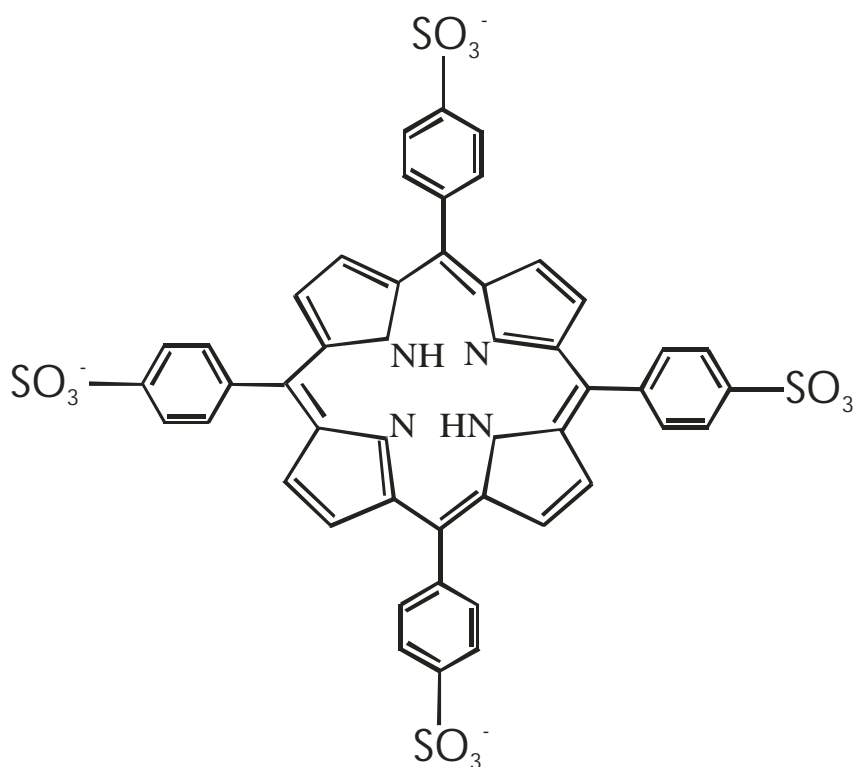


Fig. 1.7. Chemical structure of meso-5,10,15,20-sulfonatophenyl porphine ($\text{H}_2\text{TPPS}_4^{4-}$)

[78] etc. It has been proposed, that TPPS₄ forms in aqueous solution mesoaggregates which can associate to larger clusters with fractal properties [79]. The aggregation of TPPS₄ results in a delocalization of the excitation energy over a number of the aggregated molecules due to the intermolecular interaction within aggregated domains [79]. Additional energy relaxation processes, and exciton-exciton annihilation in particular, may appear [19,80-82]. Despite the number of relevant studies conducted, the structure of J-aggregates formed by TPPS₄ remains unclear. Measurements of the excitation relaxation kinetics in TPPS₄ reported by other authors show relatively large discrepancies [76,83-85] making a generalization of the reported results rather complicated.

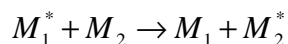
1.3.2. Exciton interaction in molecular aggregates

When distances between atoms or molecules are within the order of their sizes, they can interact strongly and behave as a collective system. The optical properties of such a system differ from those of individual atoms or molecules, so that the system acts as a whole and a splitting of energetic levels takes place. As a result, light absorption results in a delocalization of the electronic excitation energy over the whole system. Such an excitation can be described by a planar wave, which can propagate in the structure over long distances. The degree of excitation delocalization and the type of motion initiated by an external field depends strongly on the interaction between the molecules in the system. In terms of the quantum mechanics, the exciton is defined as a molecular state consisting of an excited electron and an 'unoccupied' highest occupied molecular orbital (so-called 'hole') in the same molecule, which interacts with other molecules in its surroundings. A molecular state consisting of both electron and hole localized on the same molecule in an aggregate is called Frenkel exciton. Frenkel excitons occur in associated and non-covalently bound complexes, such as molecular crystals of benzene or naphthalene. Aggregates of dye molecules are another important class of the Frenkel exciton systems. Most investigated and characterized so far are aggregates of isocyanine and pseudo-isocyanine [19,86], phthalocyanine [81,87], and thiocyanine dyes [82].

Upon aggregation, dye molecules form rod-like structures consisting of several hundreds of molecules or more. Depending on the interaction between associated molecules, changes in steady-state absorption and/or emission spectra may occur. An inherent indication for the formation of the aggregate is the change of the absorption spectrum from monomeric absorption bands to shifted and/or additionally formed narrow excitonic absorption bands of

the aggregate. This narrowing occurs due to the mutual interaction of the molecules in the aggregate.

The theoretical considerations presented in what follows deal with Frenkel excitons only, so that the notion ‘Frenkel’ will be omitted and only ‘exciton’ will be used. The exciton migration between two molecules occurs according to the general scheme (Fig. 1.8):



Depending on the relaxation characteristics, two types of excitons are distinguished: coherent (free) and noncoherent (localized) ones. According to Davydov, the free exciton in a molecular assembly occurs when the excitation transfer between the molecules is much faster than their vibrational relaxation and intramolecular nuclear motions. In the case of localized exciton, the excitation transfer rate is slower than the vibrational relaxation rate, so that the excitation energy may be considered to be localized on the molecule as the relaxation travels through the assembly.

The behavior of excitons in molecular aggregates has been a subject of intense interest since the idea of the nonradiative electronic excitation energy transfer in a molecular system was proposed by J. Perrin in the 1920’s. The first theoretical model was developed in terms of quantum mechanics by F. Perrin, which showed that electronic excitation energy can be

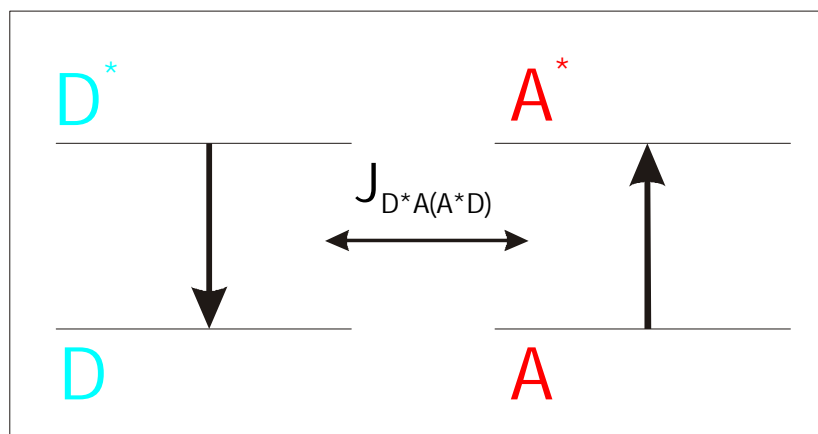


Fig. 1.8. Resonance excitation energy transfer between two spatially separated molecules. J denotes interaction between donor (D) and acceptor (A) molecules

transferred over distances of hundreds or even thousands of angstroms. Later, a theoretical study based on the quantum mechanical perturbation theory and experiments on dye solutions presented by Th. Förster [88,89] concluded that energy transfer can take place over distances up to 100 Å. In the 1950’s, the theory of the excitation energy transfer was advanced by the

idea of an ‘inductive-resonance’ between the molecules separated at such distances [90]. Förster’s theoretical approach has been frequently used by other researchers and therefore considered as a fundamental model for the characterization of intermolecular energy transfer, although it has limitations and shows some inadequacies with experiments due to theoretical assumptions made. Förster’s theory was further extended by Dexter, which accounted for Coulomb interactions of higher order and allowed for contribution of exchange interactions.

In the theory of exciton migration two distinct cases have to be considered depending on the excitation-diffusion length and the aggregate size: the ‘small aggregate’ case is assumed when the exciton diffusion length is much larger than the size of the aggregate. Here, the aggregate can be considered as a supermolecule with energy levels representing different numbers of excitations in the aggregate. Therefore, the statistical approach can be used to treat the exciton relaxation dynamics in such molecular assemblies [91]. The opposite case of ‘large aggregates’ is met, when the actual exciton diffusion length is comparable or smaller than the size of the aggregate. For the description of the exciton relaxation in such aggregates a kinetic model can be used. In order to elucidate these two cases in more detail, the underlying theoretical models are briefly summarized in the following section.

The ‘Small aggregate’ approach

According to the statistical approach for small aggregates proposed by Paillotin et al. [91], the aggregate state can be characterized by the number of excitations l present at any particular time interval t after an excitation event at $t = 0$. Thus, a state of l excitons in the aggregate may disappear due to the relaxation of one exciton owing to a single-exciton process (i.e. by radiative decay, internal conversion, intersystem crossing, quenching by the reaction centers etc.) or after an annihilation event. Depending on the relaxation mechanism, the aggregate passes to a lower state with $l-1$ or $l-2$ excitons. In this approach, it is assumed that excitons interact only within the aggregate and no interaction between exciton in different aggregates occurs. It is also assumed, that the simultaneous annihilation of more than 2 excitons at one time is less probable and can be neglected. Before dealing with annihilation it has to be noted, that different types of annihilation are distinguished depending on the initial state of interacting excitons involved: singlet – singlet, triplet – triplet, singlet – triplet and triplet - singlet. It has been shown that when picosecond laser pulses are used for excitation, the major exciton interaction process is singlet-singlet annihilation [92]. The other exciton

annihilation processes may be neglected [93]. The singlet-singlet annihilation is referred to as the following process:



where S_1 and S_0 are excited and ground singlet states, respectively, T_1 is the lowest triplet state. $\gamma^{(1)}$ and $\gamma^{(2)}$ are the annihilation rate constants. Indexes 1 and 2 denote the disappearance of one or both interacting excitons during annihilation, respectively. The final transition states of the molecules do not influence the annihilation kinetics itself, and are given only to account for the possible energy relaxation pathways. Nevertheless, their quantum yields can be quite different depending on the symmetry properties of the system. According to the theoretical considerations, the transition rate from an energy level with l excitations to a lower one $l-1$ due to a single exciton relaxation process is:

$$T_{\text{single}}(n \rightarrow n-1) = Kn \quad (1.3)$$

where K represents the sum of the decay rate constants of all singlet-exciton relaxation paths mentioned above. The transition rate from n to $n-1$ level due to annihilation is given by:

$$T^{(v)}(n \rightarrow n-1) = \gamma_{12}^{(v)} + \gamma_{13}^{(v)} + \dots + \gamma_{1n}^{(v)} + \gamma_{23}^{(v)} + \dots + \gamma_{2n}^{(v)} + \dots = \sum_{k=1}^n \sum_{i=k+1}^n \gamma_{ki}^{(v)}. \quad (1.4)$$

Here, the index $v=1$ or 2 , depending whether one (eq. 1.1) or both (eq. 1.2) excitons disappear during annihilation. γ_{ki} is the annihilation rate, which depends on the positions of the k th and i th excitons in the domain. If one assume a random exciton distribution within a domain, eq. 1.4 simplifies to:

$$T^{(v)}(n \rightarrow n-1) = \frac{1}{2} n(n-1) \gamma^{(v)} \quad (1.5)$$

where

$$\gamma^{(v)} = \frac{1}{M^2} \sum_{n=1}^M \sum_{p=1}^M \gamma_{np}^{(v)} \quad (1.6)$$

Assuming a delta function for the excitation pulse and neglecting the quenching by triplets the Pauli master equation describing the temporal evolution of the excitation in the domain is:

$$\begin{aligned} \frac{dp_n(n_0, t)}{dt} = & T_{\text{single}}(n+1 \rightarrow n)p_{n+1}(n_0, t) + \sum_{v=1,2} T^{(v)}(n+v \rightarrow n)p_{n+v}(n_0, t) - \\ & - T_{\text{single}}(n \rightarrow n-1)p_n(n_0, t) - \sum_{v=1,2} T^{(v)}(n \rightarrow n-v)p_n(n_0, t) \end{aligned} \quad (1.7)$$

where $T_{\text{single}}(n+1 \rightarrow n)$ denotes the single-exciton relaxation rate (s. a.) from a energy level with $n+1$ excitons to a lower one with n excitons. $p_n(n_0, t)$ represents the probability that at a time t there are n excitons on a domain, given the initial number of excitons in a domain created by the excitation pulse n_0 . Now, using eq. 1.3 and 1.5 one obtains:

$$\begin{aligned} \frac{dp_n(n_0, t)}{dt} = & K(n+1)p_{n+1}(n_0, t) + \gamma^{(1)} \frac{n(n+1)}{2} p_{n+1}(n_0, t) + \gamma^{(2)} \frac{(n+1)(n+2)}{2} p_{n+2}(n_0, t) - \\ & - (Kn + \gamma^{(1)} \frac{n(n-1)}{2} + \gamma^{(2)} \frac{n(n-1)}{2}) p_n(n_0, t). \end{aligned} \quad (1.8)$$

Physically $p_n(n_0, t)$ can be interpreted in terms of the average number of excitons $\langle n \rangle$ in a domain at time t as:

$$\langle n \rangle = \sum_{i=1}^{n_0} np_n(n_0, t) \quad (1.9)$$

Using the latter expression the Pauli master equation can be expressed in terms of $\langle n \rangle$ when an appropriate summing over all terms is performed:

$$\frac{d\langle n \rangle}{dt} = -K\langle n \rangle - (\gamma^{(2)} + \frac{\gamma^{(1)}}{2})\langle n(n-1) \rangle \quad (1.10)$$

Assuming a sufficiently large domain, the exciton density can be treated as a continuous variable, so that $\langle n(n-1) \rangle \cong \langle n \rangle^2$ yields a differential equation, which describes the energy relaxation in the domain in the presence of the annihilation.

The fluorescence intensity of a domain, which possesses n_0 excitons at $t=0$ can be expressed as:

$$I_{fl}(t) = \frac{1}{n_0} \sum_{n=1}^{n_0} np_n(n_0, t) \quad (1.11)$$

Here, the $I_{fl}(t)$ is normalized to unity at $t=0$. The integrated fluorescence quantum yield is given by:

$$\phi = k_{fl} \int_0^{\infty} I_{fl}(t) dt \quad (1.12)$$

where k_{fl} is the fluorescence decay rate. When calculating these quantities, one has to take into account the fact, that each domain in the system may have absorbed different number of excitons. This is partially due to domain size differences. Experimentally measurable is only

the mean initial number of excitations per domain. Assuming a Poisson distribution of the probability that a domain contains n excitons at $t=0$, eq. 1.11 and 1.12 convert into:

$$I_{fl}(t) = \frac{1}{y} \sum_{n_0=0}^{\infty} \frac{y^{n_0-1} e^{-y}}{(n_0-1)!} I_{fl}(n_0, t) \quad (1.13)$$

and

$$\phi = \sum_{n_0=1}^{\infty} \frac{y^{n_0-1} e^{-y}}{(n_0-1)!} \phi_{n_0}, \quad (1.14)$$

respectively. y is related to the excitation intensity and represents the number of excitation photons per domain.

In order to determine the fluorescence quantum yield and fluorescence intensity, the Pauli equation has to be solved. For the sake of simplicity, the entire solution procedure is not presented here. A complete derivation is available in [91]. According to the solution, $I_{fl}(t)$ can be expressed as a sum of exponents:

$$I_{fl}(t) = \sum_{d=0}^{\infty} (-1)^d \exp(-(p+1)(p+r)\tau)\theta_p \quad (1.15)$$

where

$$\theta_p = \sum_{k=d}^{\infty} \frac{(-1)^k k! \eta^k (r+1+2p)}{d!(k-d)!(r+d+1)\dots(r+d+1+k)} \quad (1.16)$$

With $\tau = \gamma \frac{t}{2}$, $\gamma = \gamma^{(1)} + \gamma^{(2)}$, $r = 2K/\gamma$, $\eta = y(1+\gamma^{(2)}/\gamma)$. γ represents the ‘common’ excitation decay rate constant due to annihilation. The parameter r expresses the ratio of the single exciton and annihilation decay rates. Accordingly, the fluorescence quantum yield can be expressed as:

$$\phi = \phi_0 r \sum_{k=0}^{\infty} (-1)^k \frac{\eta^k}{r(r+1)\dots(r+k)k+1} \quad (1.17)$$

where ϕ_0 denotes the fluorescence quantum yield in the absence of annihilation.

Regarding to the ratio of the single-exciton relaxation rate and annihilation rate constants, two limiting cases can be distinguished: $r \rightarrow 0$ and $r \rightarrow \infty$. In the former case $2K \ll \gamma$, i. e. the single exciton relaxation is much slower than the relaxation via annihilation. Such conditions occur in ‘small’ domains, where the possibility for two excitons to collide is high. This approximation leads to the following expressions for $I_{fl}(t)$ and ϕ :

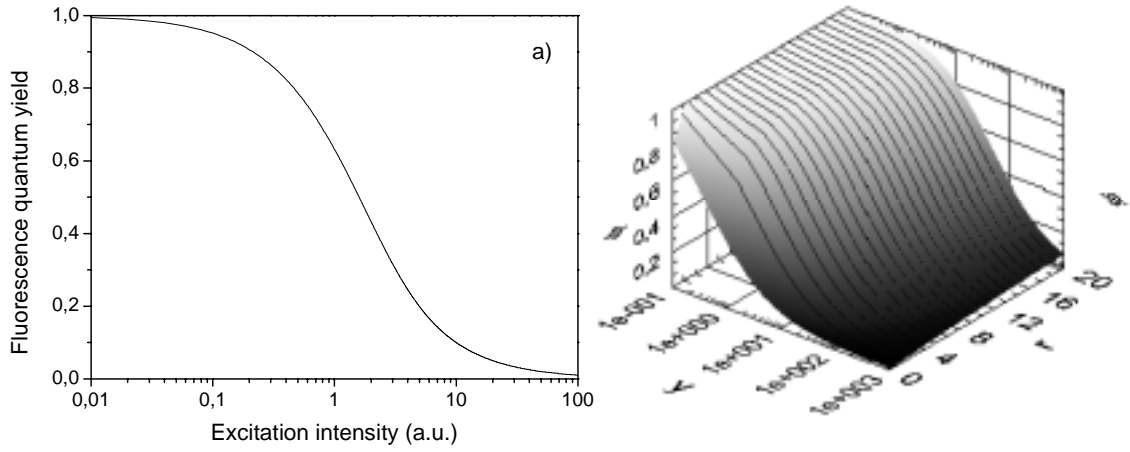


Fig. 1.9. Fluorescence quantum yield as a function of the excitation intensity y for the two limiting cases $r \rightarrow \infty$ (a, eq. (1.18)) and $r \rightarrow 0$ (b, eq. (1.19)).

$$I_n(t) = \frac{1 - e^{-\eta}}{\eta} e^{-Kt}, I_n(0) = 1 \quad (1.18)$$

$$\phi = \phi_0 (1 - e^{-\eta}) \eta$$

In the opposite case, i. e. $r \rightarrow \infty$, the latter equations can be expanded as:

$$I_n(t) = \frac{1}{(e^{Kt} (1 + \eta/r) - \eta/r)} \quad (1.19)$$

$$\phi = \frac{k_n}{\eta} \int_0^{\infty} I_n(t) dt = \phi_0 \frac{r}{\eta} \ln\left(1 + \frac{\eta}{r}\right)$$

where ϕ_0 is the fluorescence quantum yield under annihilation-free conditions (s. Fig. 1.9 for graphical representation).

These equations describe the decay of the fluorescence and its integrated quantum yield in ‘large’ domains, where the probability for a single exciton to decay via a single-exciton relaxation mechanism is much higher than annihilation with another exciton.

In the Pauli master equation (eq. 1.7) the influence of the excitation pulse shape on the initial distribution of excitations in time is not taken into account and a delta excitation pulse is assumed. The contribution of the excitation temporal profile can be taken into account by adding a generation term describing the time envelope of the exciting pulse $\sigma I(t)(n-1)p_{n-1}(n_0, t)$. Here, σ is the absorption cross section, $I(t)$ expresses the temporal profile of the excitation pulse intensity. In this case eq. 1.7 has to be solved numerically.

The 'Extended aggregate' approach

When the aggregate size is comparable to or greater than the exciton diffusion length, the relaxation kinetics can be described using a kinetic model, which was first proposed for characterization of the energy relaxation in molecular crystals [94]. Later, this model was extended for large molecular aggregates [95,96]. Here, the excitation relaxation kinetics is described by the following differential equation:

$$\frac{dn}{dt} = \sigma I(t)(N - (1 + \frac{\sigma_{em}}{\sigma})n) - kn - \frac{\gamma(t)}{2} n^2 \quad (1.20)$$

where N is the number of molecules per aggregate, n is the total number of excited molecules in the aggregate, σ_{em} and σ are the molecular cross sections of the absorption and stimulated emission, respectively, k is the linear energy decay rate, $I(t)$ is the excitation intensity, and $\gamma(t)$ is the singlet-singlet annihilation rate. After the excitation has finished, the generating term on the right side of eq. 1.20 can be neglected and the relation turns into a Ricatti's equation, which can be solved to give the relation:

$$n(t) = \frac{n_0 \exp(-kt)}{1 + (n_0 / 2) \int_0^t \gamma(t') \exp(-kt') dt'} \quad (1.21)$$

The time dependence of $\gamma(t)$ is given by:

$$\gamma(t) = \int d^d \lambda(\vec{r}) g(\vec{r}, t) \quad (1.22)$$

where d is the spectral dimension of the aggregate, $\lambda(\vec{r})$ is the relaxation rate, which in the case of the Förster-type interaction is given by:

$$\lambda(\vec{r}) = k_{fl} \left(\frac{R_A}{r} \right) \quad (1.23)$$

where R_A is the Förster annihilation radius and k_{fl} is the radiative relaxation rate.

In general, the two particles correlation function $g(\vec{r}, t)$ can be defined by the following differential equation:

$$\frac{\partial g(\vec{r}, t)}{\partial t} = 2D \nabla_r^2 g(\vec{r}, t) + F(g(\vec{r}, t)) \quad (1.24)$$

where D is the excitation diffusion coefficient of S_1 excitation,

$$F(g(\vec{r}, t)) = -2(\lambda(\vec{r}) + \frac{I(t) + n_2(k_2 - I(t))}{n_1} - I(t))g(\vec{r}, t) + 2n_1(2\gamma(t) - \sum_k (\lambda(\vec{k}) + \lambda(\vec{r} - \vec{k})) \frac{g(\vec{r}, \vec{k}, t)}{g(\vec{r}, t)})g(\vec{r}, t) \quad (1.25)$$

$g(\vec{r}, \vec{k}, t)$ denotes the three-particle correlation function and $I(t)$ is the excitation intensity. Deriving the latter expressions it has been assumed, that only S_1 - S_1 annihilation occurs and S_1 - S_2 annihilation has been neglected. The equation of the three-particle correlation function $g(\vec{r}, \vec{k}, t)$ involves a four-particle correlation function, which contains contributions of five-particle distribution etc. The expression of $g(\vec{r}, \vec{k}, t)$ is in general very bulky and can be simplified using the Kirkwood approximation for low excitation density to:

$$g(\vec{r}, \vec{k}, t) = g(\vec{r}, t)g(\vec{k}, t)g(\vec{r} - \vec{k}, t) \quad (1.26)$$

A further simplification of the latter expression can be made by developing $g(\vec{r} - \vec{k}, t)$ in a Taylor series in the point \vec{r} and neglecting terms of higher orders. Now, substituting eq. (1.26) into eq. (1.25) and assuming that the excitation pulse is over, i. e. $I(t)=0$, the expression of the $g(\vec{r}, t)$ becomes:

$$\frac{dg(\vec{r}, t)}{dt} = 2D\nabla_r^2 g(\vec{r}, t) - 2\lambda(\vec{r})g(\vec{r}, t) + 2\gamma(t)ng(\vec{r}, t)[1 - g(\vec{r}, t)] \quad (1.27)$$

where n is the S_1 excitation density. Under assumption of the dipole-dipole Förster-type interaction between molecules, the time dependence of $\gamma(t)$ can be asymptotically expressed as [97]:

$$\gamma(t) = \gamma_0 t^{-h} \quad (1.28)$$

where h is a parameter related to the spectral dimension of the domain. The spectral dimension describes the probability P_a for an exciton to decay after an excitation event within a time t in the presence of the annihilation:

$$P_a \sim t^{-d_s/2} \quad (1.29)$$

where d_s is the spectral dimension.

At this point of theoretical considerations, it is useful to provide some comparisons with the above treated case of small aggregates. In this theoretical treatment, depending on the ratio of excitation diffusion length and domain size, two different exciton interaction mechanisms are distinguished: static and diffusion-limited. The annihilation is considered as static when the correlation distances of excitons are smaller than a reaction radius R , which, in the case of the long-range Förster dipole-dipole interaction, is determined as:

$$R = (R_A / R_M)^{3/2} a \quad (1.30)$$

where R_A and R_M are the Förster radiuses of annihilation and migration, respectively, and a is the distance between nearest neighbor molecules. When static annihilation takes place, each

domain can be considered as a supermolecule in which only the number of excitations in S_1 determines the annihilation process, whereas the energy migration does not play an important role. Therefore, it can be assumed that the annihilation rate $\gamma(t)$ is time-independent and only the initial distribution of excitons defines it. This situation resembles that described by Paillotin's model (s. a.), where the annihilation rate is a constant and is independent of time.

In the opposite case, the diffusion-limited exciton annihilation takes place and the annihilation rate is defined by the diffusion of the excitations. The parameter h is related to the spectral dimension d_s as:

$$\begin{aligned} h &= 1 - d_s/6 && \text{static annihilation} \\ h &= 1 - d_s/2 && \text{diffusion-limited annihilation} \end{aligned} \quad (1.31)$$

Substituting eq. 1.23 into eq. 1.20 and assuming that the excitation pulse is over, one obtains:

$$\frac{dn}{dt} = -kn - \gamma_0 t^{-h} n^2 \quad (1.32)$$

If the annihilation occurs much faster than the monomolecular decay, i.e. $k \ll \gamma_0$, the first term on the right side in eq. 1.32 may be neglected yielding the following solution:

$$n = \frac{N_0}{N_0 \gamma_0 \frac{1}{1-h} t^{1-h} + 1} \quad (1.33)$$

where N_0 is the exciton density at $t=0$.

The parameters γ_0, N_0, h can be evaluated by fitting eq. 1.33 to experimental data. When their values are known, some excitonic motion parameters on the domain can be determined. It has been shown that the exciton singlet-singlet annihilation can be described utilizing the theory of the one-dimensional diffusion-limited motion. Accordingly, the diffusion coefficient D of the exciton in the domain can be expressed as:

$$D = \frac{\pi d N \gamma_0^2}{16} \quad (1.34)$$

where d is the distance between the molecules and N is the initial exciton density.

Then, the characteristic exciton hopping time can be evaluated by using:

$$\tau = \frac{d^2}{2D} \quad (1.35)$$

Chapter 2

Techniques and methods

2.1. Methods for investigation of aggregation behavior of photosensitizers

2.1.1. Experimental techniques for fluorescence investigation with high temporal resolution

The highest temporal resolution required for examination of the sensitizers aggregate state by fluorescence can be achieved when upconversion or ultrafast gating methods are used.

The method of fluorescence upconversion provides ultimate time resolution, which is in general determined by the excitation laser pulse width and thus can reach ~100 fs or better. The limitations for applying fluorescence upconversion in biochemical applications rely on complex detection apparatus which is required in order to record rather weak upconverted signals.

In order to record the fluorescence decay the fluorescence signal is induced by a repetitively pulsed excitation while the delay between the excitation and gating pulses is increased constantly. The gating procedure can be performed by a rapid switching of the fluorescence signal using the non-linear optical Kerr-effect. In this case, the temporal resolution in this case is mainly determined by the duration of the excitation pulse, when a Kerr-medium with a fast response time is used.

2.1.2. Optimization of experimental techniques for highly resolved fluorescence measurements in time domain

The technique of ultrafast gating of the fluorescence was used for investigations of the aggregation state of sensitizers. In this work, the all-optical Kerr effect was investigated in different materials in order to find an appropriate Kerr-medium with a fast response times and large induced anisotropy.

In the optical Kerr effect (Fig. 2.1), a strong polarized monochromatic pump beam induces a complex anisotropic change in the refractive indices experienced by a weak probe pulse. Being anisotropic, these changes cause a rotation of the polarisation direction of the probe beam in the Kerr medium and thereby the exciting polarized probe beam to be partially transmitted through a polarizer that normally blocks it. The transmission of such an optical system depends directly on the nonlinear refractive index of the Kerr medium:

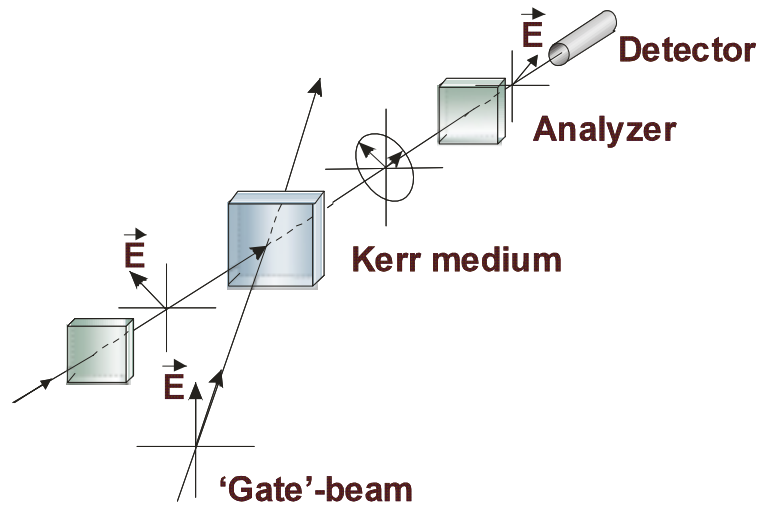


Fig. 2.1. Principle of 'gating' based on the all-optical Kerr effect

$$T(t) = \sin^2\left(\frac{1}{2}\Delta\varphi(t)\right) \quad (2.1)$$

Where $\Delta\varphi(t)$ is the time dependent phase difference between the ordinary and extraordinary optical axes in the medium expressed as follows:

$$\Delta\varphi(t) = 2\pi\Delta n(t)d / \lambda \quad (2.2)$$

where d is the length of the medium, λ - wavelength of the gate beam, $\Delta n(t) = n_2 I(t)$, with $I(t)$ being the power density of the gate beam and n_2 the nonlinear refractive index.

Measurements of the optical Kerr effect performed with the experimental setup

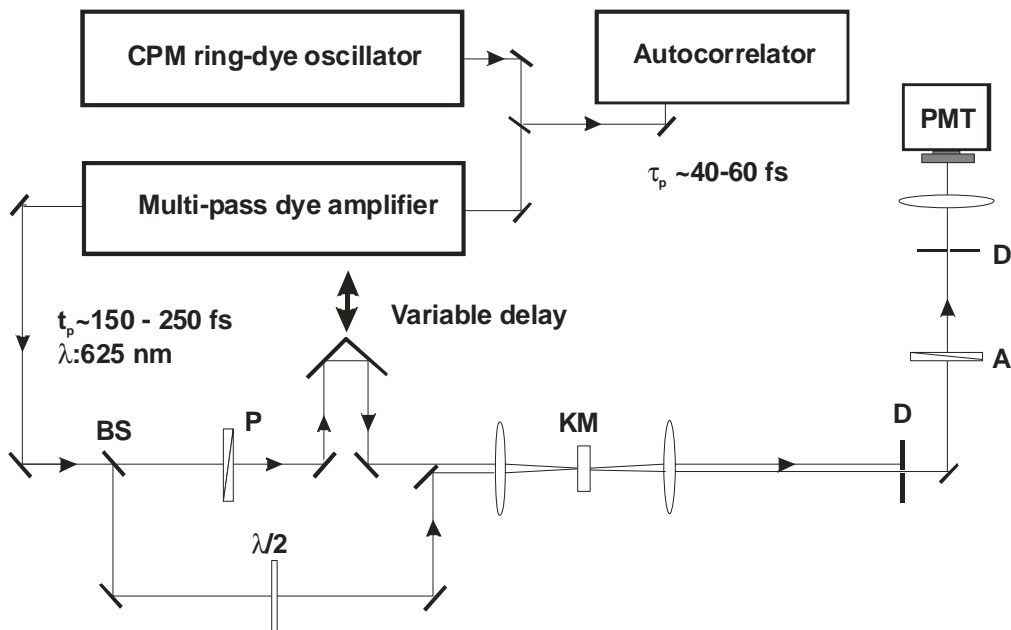


Fig. 2.2. Experimental setup for measurements of the optical Kerr effect. KM – Kerr medium, BS – beam splitter, P – polariser, A – analyser, PMT – photomultiplier, $\lambda/2$ – phase retardation plate, D – diaphragm. CPM – colliding pulse mode-locking

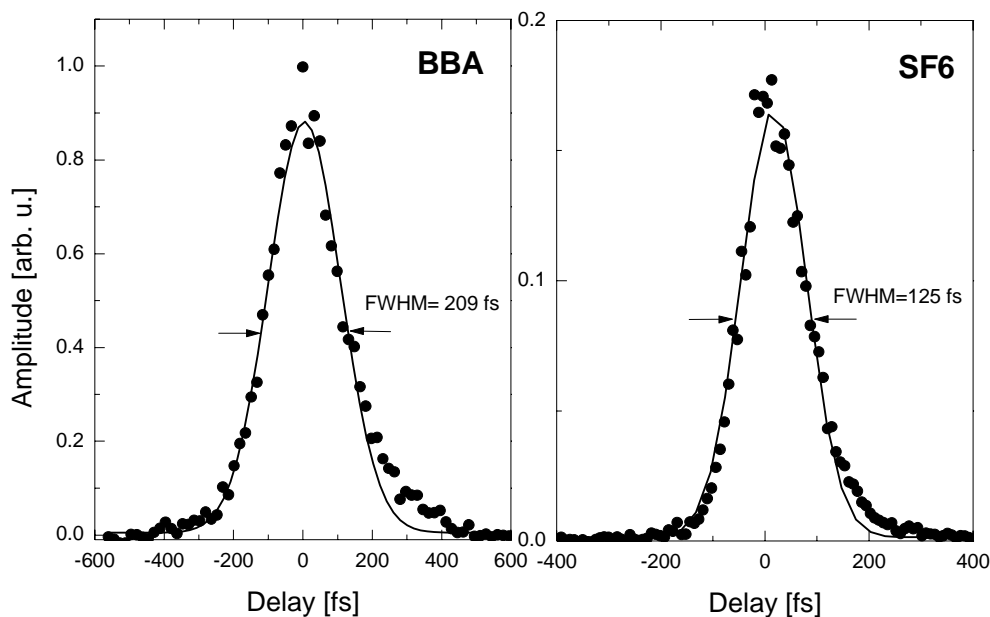


Fig. 2.3. Optical Kerr effect in chalcogenide (BBA) and SF6 glasses measured using the experimental set-up shown in Fig. 2.2. The full-width-at-half-maximum values correspond the duration of the ‘gate’ pulses.

presented in Fig. 2.2 showed ultrashort response times of chalcogenide (BBA) and SF6 glasses (Fig. 2.3) so that the temporal resolution of such a system is determined mainly by the duration of the ‘gate’ pulse. With obtained transmission maximum of ~30% obtained, BBA and SF6 glasses were found to be most suitable as Kerr medium. These results show, that the Kerr effect-based fluorescence gating technique can be used for measurements of a high temporal resolution (~100 fs).

2.1.3. Time-resolved fluorescence measurements on sensitizers in homogenous solutions

Preliminary investigations conducted on the sensitizers in homogenous solutions revealed that: i) aggregates of Ppe and Chl derivatives exhibit fluorescence decay times in the order of ~ 10 – 100 ps, ii) that can clearly be differentiated from the monomeric species lifetimes, which exhibit characteristic decay times of 1 – 6 ns, thus being at least one order of magnitude longer than those of highly aggregated species, iii) the measured fluorescence decay times of the aggregated sensitizer species make the use of an experimental technique with a high temporal resolution (under 10 ps) not necessary. Nevertheless, a technique allowing registration of fluorescence photons with a high sensitivity is crucial for examination of aggregated states of sensitizers due to their low fluorescence quantum yields.

Time-correlated single photon counting (TCSPC)

The use of this technique is based on the measurement of the time-dependent intensity of fluorescence $I(t)$ following the excitation pulse, which is preferably much shorter than the fluorescence lifetime τ . The fluorescence lifetime is determined from a plot of $I(t)$ versus t at a point where the fluorescence intensity drops to $1/e$ from its initial value at $t=0$ or by calculating the slope of a plot $\log I(t)$ versus t . Among other techniques introduced above, the latter is more advantageous due to its extremely high sensitivity. The high detection sensitivity is of particular interest when weakly fluorescent molecular aggregates are investigated. In this case, high-repetition rate of pico- and femtosecond laser sources are employed for excitation of the fluorescence. High-speed detectors, such as multichannel plate photomultipliers, enable temporal resolutions in the order of several 10 ps. It can further be improved when appropriate deconvolution algorithms for data analysis are used.

The principle of the method is based on statistical counting of emission photons and measurement of the time interval between a start signal and a counting event (time-correlated counting). The general scheme is depicted in Fig. 2.4. The probe is excited repetitively by a train of light pulses. The 'start' signal is generated using the same pulse train by a photodiode with a short response rise time, which has to be shorter than the reciprocal of the repetition rate of the exciting pulses. After a 'start' signal has been produced, the time-to-amplitude converter (TAC) starts a voltage ramp, which is proportional to the time. A 'stop' signal is generated when first emission photon reaches the photomultiplier and a counting event occurs. In this study the so called 'reversed start-stop' method of the photon counting was used. In this case the 'start' signal is generated by a fluorescence photon arrived in the PMT and the 'stop' signal is generated by the synchronizing diode. This reduces the speed of the TAC has to work with, since its processing cycles have to be performed with the photon detection rate instead of considerably higher pulse repetition rate. The TAC provides an output pulse whose voltage is proportional to the time between the 'start' and 'stop' signals. This voltage is converted by the analog-to-digital (ADC) converter into a digital signal and processed by the multi-channel analyzer, which increases the numerical value of a corresponding memory/time channel by one. By counting emission photons repeatedly over a time period, a histogram of number of counts versus time channels is built up. The number of counts in each channel represents the probability of a photon being emitted from the probe within a time period. Thus, the histogram of counts versus time interval represents the temporal profile of the energy relaxation process. The most important condition for

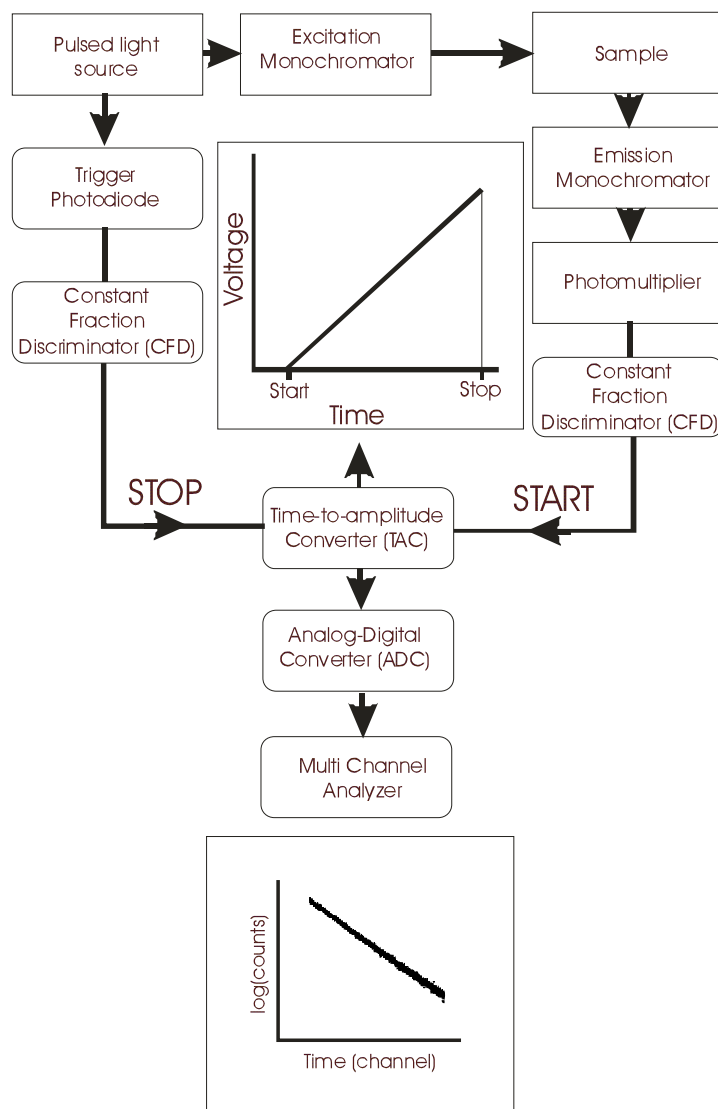


Fig. 2.4. General scheme of time-correlated single photon counting (TCSPC) method

appropriate measurements with TCSPC is that the probability for counting one emission photon per excitation pulse has to be limited to 0.01 – 0.1. This is due to the fact, that in order to achieve high detection sensitivity, the detector gain is in most cases set to about $10^5 - 10^6$, so that the detector is saturated by a first arriving photon. This means that the detector will count the emission photon properly unless no more than one photon arrives following one excitation pulse. Otherwise, i. e. when two or more photons reach the detector simultaneously, they will be detected as one photon, so that the reconstruction of the decay profile will be distorted. Thus, in order to assure proper photon counting statistics, the probability of counting of one photon per excitation pulse has to be below 0.01. In order to avoid long measurement times, excitation repetition rates usually used for measurements are 100 kHz – 5 MHz. The upper limit of the repetition rate is determined by the excitation source and by the processing time of the electronics.

2.1.4. Experimental techniques for fluorescence investigations with high spatial resolution. Principles of confocal laser-scanning fluorescence microscopy

In conventional wide-field fluorescence microscopy the image of the whole object is formed in the confocal plane. One of the most crucial obstacles of this visualization method is that the fluorescence is excited in the whole volume along the cone of the excitation beam, so that scattered fluorescence as well as fluorescence from outside the focal plane can strongly interfere with the fluorescence signal from the excitation focus. As a result, the image is blurred.

An important advance has been achieved by the so-called confocal configuration of the fluorescence detection [98-100]. The visualization in the case of confocal laser-scanning fluorescence microscopy is based on a point-to-point imaging of the probe by precisely moving (scanning) a tightly focused exciting laser beam over the probe and synchronously detecting and acquiring fluorescence photons at each point. The confocal detection of the fluorescence is realized by placing a pinhole diaphragm at the conjugated focus plane of the microscope objective in front of the fluorescence detector (Fig. 2.5). As a result, only the fluorescence originating from the focal plane is detected, whereas scattered and out-of-focus fluorescence is efficiently suppressed by the pinhole diaphragm. Thus, by moving the focus of the excitation beam in a vertical direction,

it is possible to detect the fluorescence signal separately from different depths of the specimen. By combining detected fluorescence points from the horizontal and vertical scans (slices), a three-dimensional image of the object can be constructed. Depending on

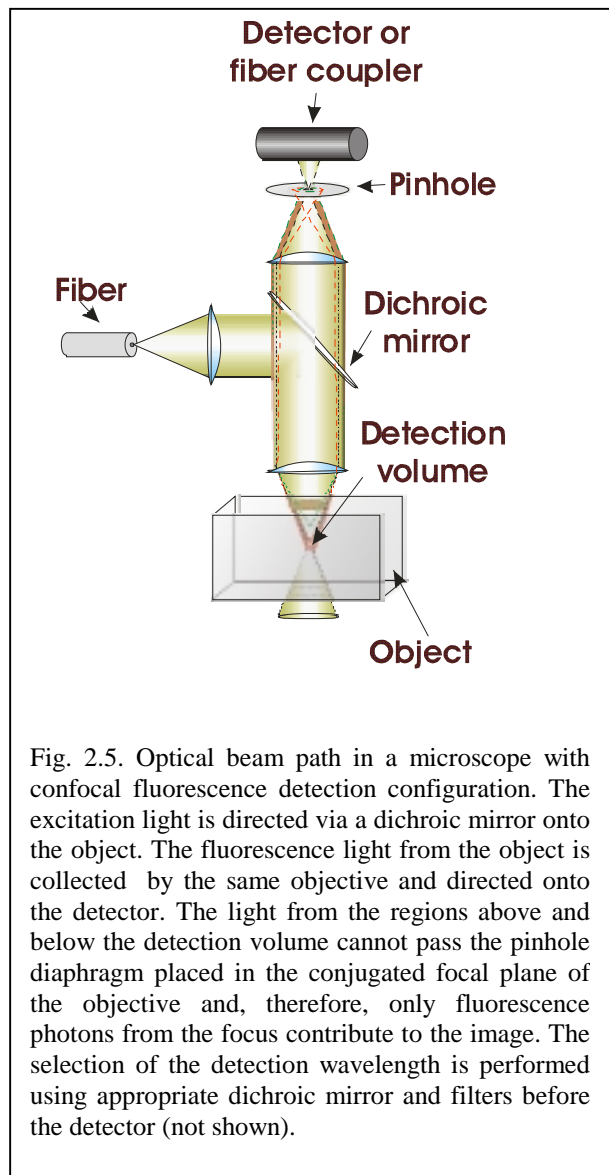


Fig. 2.5. Optical beam path in a microscope with confocal fluorescence detection configuration. The excitation light is directed via a dichroic mirror onto the object. The fluorescence light from the object is collected by the same objective and directed onto the detector. The light from the regions above and below the detection volume cannot pass the pinhole diaphragm placed in the conjugated focal plane of the objective and, therefore, only fluorescence photons from the focus contribute to the image. The selection of the detection wavelength is performed using appropriate dichroic mirror and filters before the detector (not shown).

applications, the pinhole diameter has to be adjusted in order to achieve optimal sensitivity and resolution.

One- and two-photon excitation (OPE and TPE) of fluorescence

The main shortcoming of one-photon confocal laser scanning fluorescence microscopy arises from the fact that the fluorescence is being excited along the whole cone of the exciting laser beam in the object. As a result, not only chromophores in the detection volume, but all molecules within the excitation cone are excited and subjected to photobleaching. Moreover, especially in case of biological objects, other photochemical processes originating from molecules in excited electronic energy states can occur, resulting in photodamage and destruction of the object. Due to the phototoxicity of the sensitizer molecules, this becomes crucial when fluorescence properties of sensitizers are investigated in living cells.

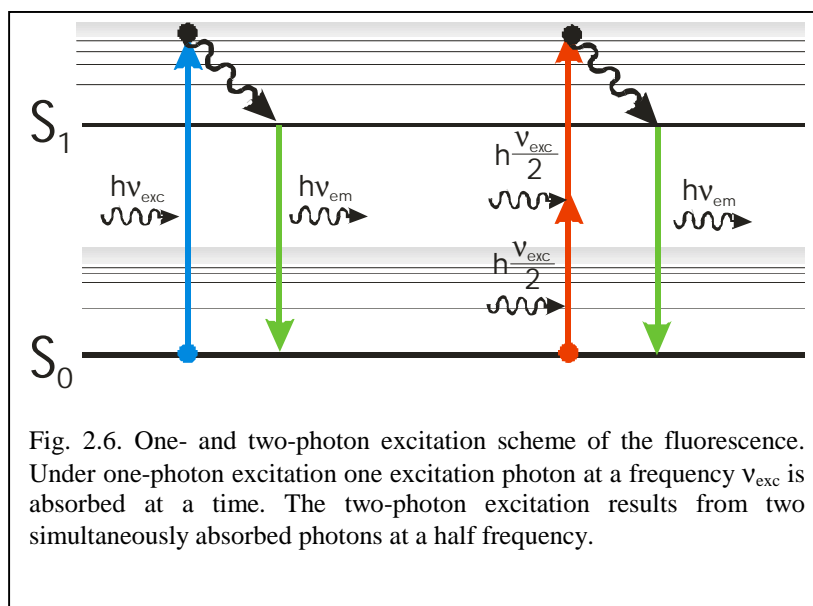
An important advance in laser-scanning fluorescence microscopy has been achieved using multi-photon fluorescence excitation. Thus, instead of being excited by the absorption of one photon in the visible region, chromophores are excited by absorption of two or more photons in the infrared,

where $\nu_{\text{VIS}} = 2\nu_{\text{IR}}$ (Fig.

2.6). In order to be absorbed simultaneously, two infrared photons with the same polarization have to be localized at the same place at the same time. The probability of such an absorption event is much lower than that of one photon absorption

(typical absorption cross-

sections are $\sim 10^{-50} \text{ cm}^4/\text{s}/\text{photon}$ for two-photon absorption and 10^{-17} cm^2 for one-photon absorption). Therefore, high excitation photon fluxes are necessary under two-photon excitation conditions in order to acquire fluorescence signals as high as with one-photon excitation. This can be achieved by employing lasers generating short laser pulses with a high peak power as excitation sources and by tightly focusing the laser beam. Because excitation



intensities needed for two-photon fluorescence excitation are only achieved in the vicinity of the focal volume, and appreciable fluorescence excitation is restricted to the focus of the laser beam. An excitation volume down to $<1\mu\text{m}^3$ can be formed when microscope objectives with high numerical apertures (NA ~ 1.4) are used.

The idea of application of two-photon excitation in fluorescence microscopy for high resolution 3D imaging was first proposed by Denk et al. [101]. Potential application possibilities of nonlinear fluorescence microscopy [102-118] caused an increasing interest in its further development. In general, two-photon fluorescence excitation allows imaging of microscopic objects with a resolution comparable to that of confocal microscopes with one-photon excitation, but has some important advantageous features: i) restriction of fluorescence excitation to a sub-micron volume. Since no out-of-focus fluorescence is present, no confocal diaphragm is necessary in the detection path. Since excitation of fluorescence takes place only in the close vicinity of the focus, molecules lying outside are not affected by photobleaching [119]. This enables longer exposition times and also prevents photodamage of the specimen, which may be crucial for biological objects, ii) due to the much larger separation of exciting wavelengths from emission wavelengths under two-photon excitation, the excitation photons can be filtered out without rejecting any fluorescence photons. As a result, significantly better sensitivity and signal to background fluorescence ratio can be achieved than in a confocal microscope. iii) two-photon excitation is less affected by scattering and absorption in the specimen.

The main drawback of two-photon fluorescence excitation is that a high excitation intensity is required to achieve sufficient absorption. This can cause unwanted thermal effects, leading to the destruction of the sensitizer or even the entire specimen. To minimize excitation intensities, it is therefore indispensable to know the two-photon absorption maxima of the substance. Because two-photon absorption spectra of most tetrapyrrolic sensitizers and fluorescent cellular probes were unexploited so far, measurements were conducted in order to ascertain their two-photon absorption characteristics.

2.1.5. Determination of two-photon absorption spectra of sensitizers and fluorescent probes

Theoretical background

In the case of one-photon excitation in a weak absorbing medium, the detected fluorescence photon flux is given by:

$$F_{fl}^{OPE} = G\Phi_1\sigma_1(\lambda)F_{exc}(\lambda)lC \quad (2.3)$$

where Φ_1 is the one-photon excited fluorescence quantum yield; $\sigma_1(\lambda)$ is the one-photon absorption cross-section at a given wavelength; $F_{exc}(\lambda)$ is the excitation intensity; l is the length of the optical path of the laser beam in the solution and C is the number of molecules in a unit volume of the solution. The factor G depends on the parameters of the experimental arrangement, such as the numerical aperture of the optical set-up used, transmittance of the optics and the spectral sensitivity of the detector. It can easily be determined by measuring the fluorescence of a reference substance, whose absorption and fluorescence properties (spectrum and quantum yield) are well known.

Because the two-photon excitation is a second-order process, the fluorescence intensity depends on the square law of the excitation intensity and is proportional to the two-photon absorption cross-section of the molecule or atom. When exciting the fluorescence by means of two-photon absorption, the fluorescence intensity relates to the excitation intensity in the following manner:

$$F_{fl}^{TPE} = \frac{1}{2}G\Phi_2\sigma_2(\lambda)F_{exc}^2(\lambda)lC \quad (2.4)$$

where Φ_2 and σ_2 are the TPE fluorescence quantum yield and two-photon absorption cross-section [in photons/cm⁴s], respectively. The other parameters are identical to those in eq. 2.3.

The factor $\frac{1}{2}$ is included since two excitation photons produce only one fluorescence photon.

A direct comparison of TPE fluorescence with OPE fluorescence allows one to determine the absolute values of TPE cross section under the assumption of equal emission quantum efficiencies [120]. It is known that in most cases the fluorescence quantum yield of molecules is determined by the energy relaxation mechanisms from the lowest excited electronic level S_1 . Therefore, it is reasonable to expect that the fluorescence quantum yields are equal in both cases. Using equations (2.3) and (2.4) and assuming a sech^2 (hyperbolic secant) excitation

pulse shape and the same factor G in both cases, one can estimate the absolute TPE absorption cross-section by:

$$\sigma_2 = 1.55 \frac{F_{fl}^{TPE} r^4 (f \tau \pi h c)^2}{GC \Phi I (P_{ave}^{TPE})^2 \lambda_2^2} \quad (2.5)$$

where c is the velocity of light in vacuum, P_{ave} is the average laser power, h is Planck's constant, τ is the pulse duration, r is the cross section of the focused laser beam and f is the repetition rate of the laser.

Experimental

The experimental setup used for the measurements of two-photon absorption spectra is shown in Fig. 2.7. For the excitation of fluorescence a Titanium-Sapphire (Ti:Sa) laser system was used, which consisted of an oscillator pumped by a cw frequency-doubled Nd:YAG laser and a Ti:Sa multi-pass amplifier. It generated laser pulses of 70-80 fs (FWHM) duration at a central wavelength of 800 nm with an average power of 1 W and a repetition rate of 1 kHz. An optical parametric amplifier (OPA) was employed for sum/difference frequency generation. This arrangement allowed for tuning the excitation wavelength in the wavelength region 480 - 1150 nm. The pulses from the OPA were determined to be 100-110 fs (FWHM) long with an average power of 1-20 mW, depending on the type of non-linear frequency

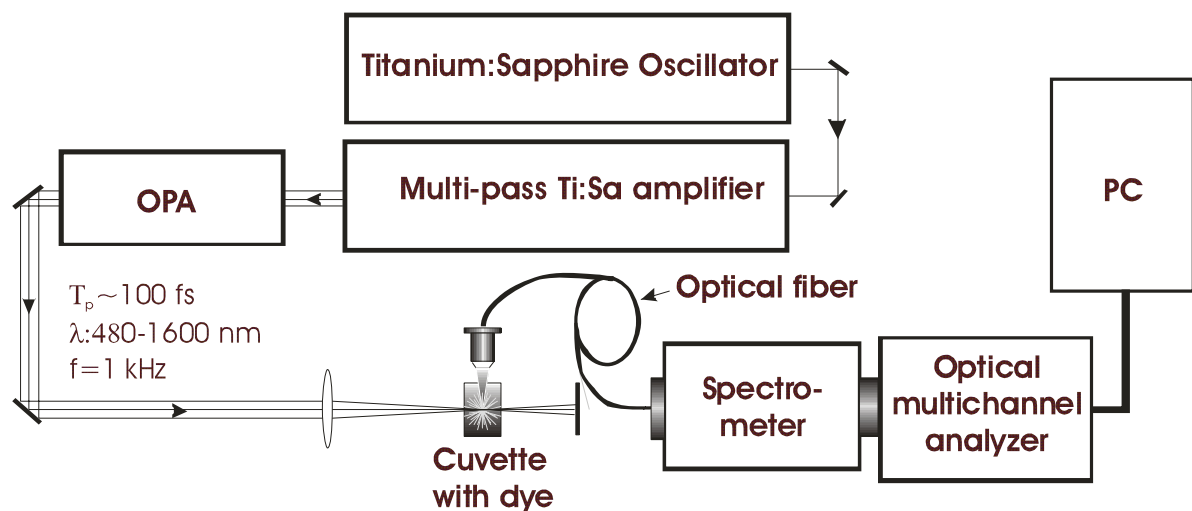


Fig. 2.7. Experimental arrangement of two-photon absorption measurement. OPA – optical parametric oscillator. PC- personal computer

mixing process used for generation of light at a particular frequency.

Fluorescence photons were collected via an optical fiber with a cross-section of 400 μm and a numeric aperture of 0.38. The fiber exit was imaged onto the entrance slit of the spectrometer. An optical multichannel analyzer (OMA) consisting of a spectrometer with a grating of 150 lines/mm and a multichannel plate intensifier with a cooled (-70 C°) CCD detector. The spectral resolution of the OMA was set to 2 nm.

The TPE absorption cross-section was calculated using equation (2.5). Rhodamine B dissolved in methanol was used as a reference substance with the well defined one-photon absorption cross-section and fluorescence quantum yield ($\Phi_1=0.7$ [121]). The calculated values of the TPE absorption cross-section for rhodamine B in MeOH agree with those measured by other authors at corresponding wavelengths [122]. For other dyes, for which the OPE fluorescence quantum yield was not known, the quantity $\Phi_2\sigma_2$ was determined (Fig. 2.8). The two-photon absorption maxima determined for the fluorescent probes are presented in Table II (see Appendix for the complete spectra).

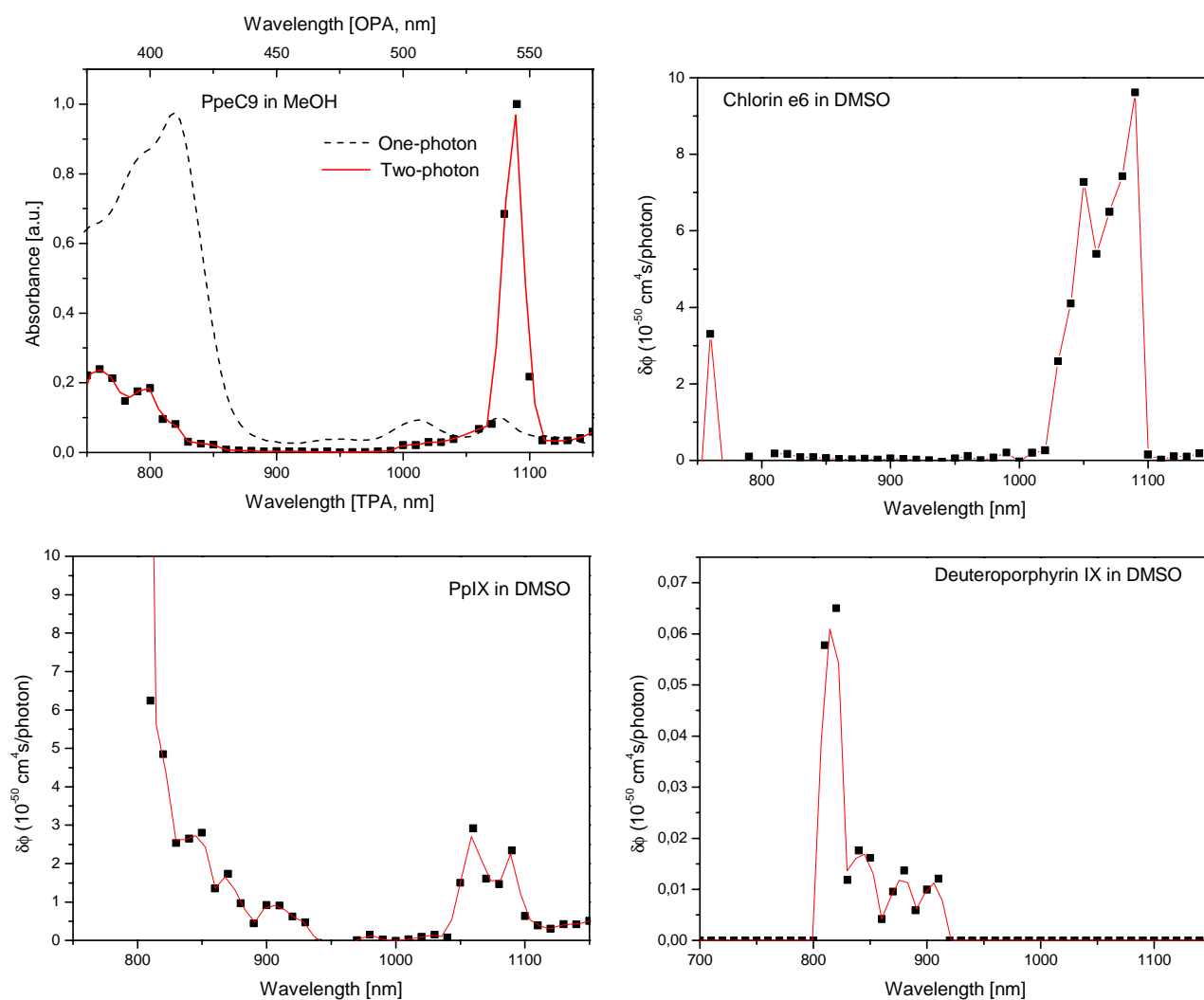


Fig. 2.8. Two-photon absorption spectra of some selected tetrapyrrolic sensitizers. One-photon absorption spectrum of PpeC9 is given for comparison purposes.

Table II. Two-photon absorption maxima of the investigated fluorescent cellular probes (Molecular Probes Europe BV, Netherlands. Please refer www.probes.com for more information).

| Material | $\lambda_{\max, \text{TPE}}$ (nm) |
|----------------------|-----------------------------------|
| Alexa Fluor™ 488 | 660 |
| Alexa Fluor™ 546 | 600 |
| Alexa Fluor™ 350 | 676 |
| Acridine orange | 640 |
| Dextran, rhodamine B | 810 |
| Indo-1 | 760 |
| Propidium iodide | 640 |
| Hoechst 33342 | 750 |
| Texas Red-X | 850 |
| FITC 'Isomer I' | 660 |
| FITC 'Isomer II' | 660 |
| AMCA-X, SE | 680 |
| Lucifer yellow AB | 875 |
| Cell Tracker™ CM-Dil | 660 |
| Nile red | 690 |
| DAPI | 620 |

2.2. Techniques of spectroscopy measurements

a. Steady-state spectroscopy

Absorption spectra of the sensitizers were recorded using a dual beam spectrometer employing glass cuvettes of different pathlengths. The absorption of the solvents was compensated by using cuvettes of the same type with pure solvent in the reference arm of the spectrometer.

Fluorescence was excited using the 488 nm or 514 nm Ar⁺-ion laser line with an average power of 10 mW (0,2 W/cm²). Spectra were recorded employing a polychromator coupled to an optical multichannel analyser (OMA) with a cooled CCD detector. Excitation and detection of the fluorescence was performed at the front side of the cuvettes to reduce the reabsorption. Scattered excitation light was blocked by using appropriate colour glass filters in front of the entrance slit of the polychromator.

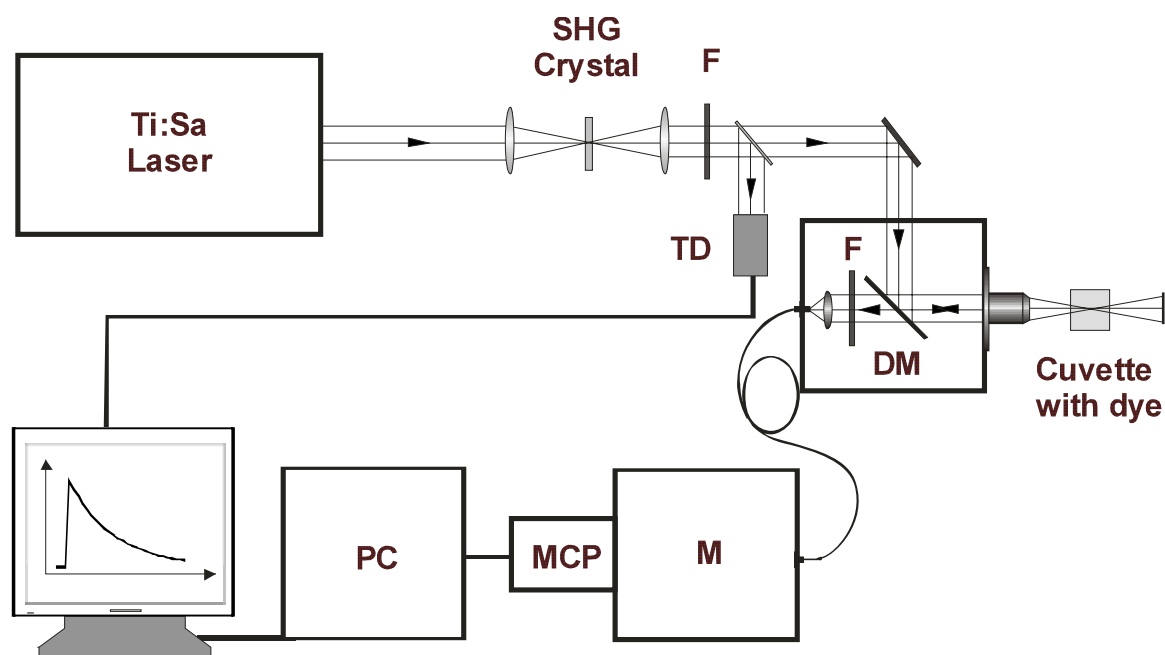


Fig. 2.9. Experimental setup used for the time-resolved fluorescence measurements of TPPS₄ in homogenous solutions. SHG – second harmonic generation, F – filters, TD – trigger diode, DM – dichroic mirror, M – monochromator, MCP – multichannel-plate photomultiplier, PC – computer with acquisition board.

b. Time-resolved fluorescence spectroscopy of TPPS₄

The fluorescence kinetic spectroscopy equipment used to perform measurements of the fluorescence kinetics of TPPS₄ is shown in Fig.2.9. A Kerr-lens mode-locked titanium:sapphire laser, which was pumped by an Ar⁺-ion laser was used as an excitation source. The laser was operated at a central wavelength of 800 nm or 860 nm with an average power of ~ 500 mW; the pulse duration was 140 fs (FWHM). The 76 MHz pulse repetition rate of the laser was reduced to 4.75 MHz (average power 11 mW) by using a Bragg diffraction crystal. The second harmonics of the 860 nm irradiation were generated in a lithium-niobate (LiNbO₃) crystal (thickness 2.5 mm) of type I (oo-e) yielding an average power of approx. 1 mW. The excitation light was focused onto a cuvette containing the solution of TPPS₄ using one of three microscope objectives with different magnifications and numerical apertures (10x, 63x; both water immersion, and 100x; oil immersion, with NA=0.45, 1.3, 1.4, respectively). The focusing optics and continuously adjustable neutral density filters allowed for variations in the excitation intensity over 6 orders of magnitude ($\sim 10^{10}$ - 10^{16} photons/cm²·pulse). Fluorescence was collected by the same microscope objective and directed onto the entrance slit of a monochromator via an optical fiber. The entrance and

the output slits of the monochromator were set to 2 mm, resulting in a full spectral width at half maximum (FWHM) of 8 nm.

A micro-channel plate photomultiplier (MCP-PMT) with an instrument response of 25 ps at FWHM was employed for counting fluorescence photons. A time-correlated single photon-counting unit and the corresponding software were used for the acquisition of fluorescence kinetic data. The data were analyzed with a fluorescence decay data analysis software package (FluoFit, Picoquant, Berlin, Germany), which permits the deconvolution of measured data with the instrument response function. The fit procedure used the Levenberg-Marquardt method. The number of decay components (mono-, bi-, or triexponential decay) for the fit was chosen according to the χ^2 value and its relative decrease when the number of the components was increased. The fit model was considered to be correct, when an increase in the number of the components resulted only in a negligible change of the χ^2 value (< 10 %). The time resolution attained with this system was approx. 20 ps. For the calculation of annihilation parameters, an additional program was written based on the LabView (National Instruments) software package.

The signal collection factor G, which accounts for both the geometry of the detecting system and spectral properties (monochromator spectral transparency, photomultiplier quantum efficiency, etc.), expresses the ratio between the fluorescence photons emitted from the excitation volume and those detected by the photomultiplier. It was determined by measuring over a certain period of time the integral fluorescence intensity of rhodamine 6G dye, which was used as a reference substance. Since the absorption and emission properties of this dye are well known, the number of photons emitted from the excitation volume could be calculated. The factor G was evaluated according to the ratio between the detected and calculated number of emitted photons per time unit.

All measurements of the fluorescence kinetics were performed under the condition that the probability for detecting one fluorescence photon per excitation pulse was between 0.01 – 0.1.

c. Time-resolved fluorescence measurements of Ppe and Chl derivatives in homogenous solution and in vitro

The experimental setup used for the measurements of Ppe and Chl derivatives in homogenous solution (Fig. 2.10a) is similar to that used for TPPS₄ measurements (Fig. 2.9). A home-build Kerr-lens mode-locked titanium-sapphire laser was pumped by the second harmonics of a NdYVO₄ laser and generated laser pulses at a central wavelength of 800 nm

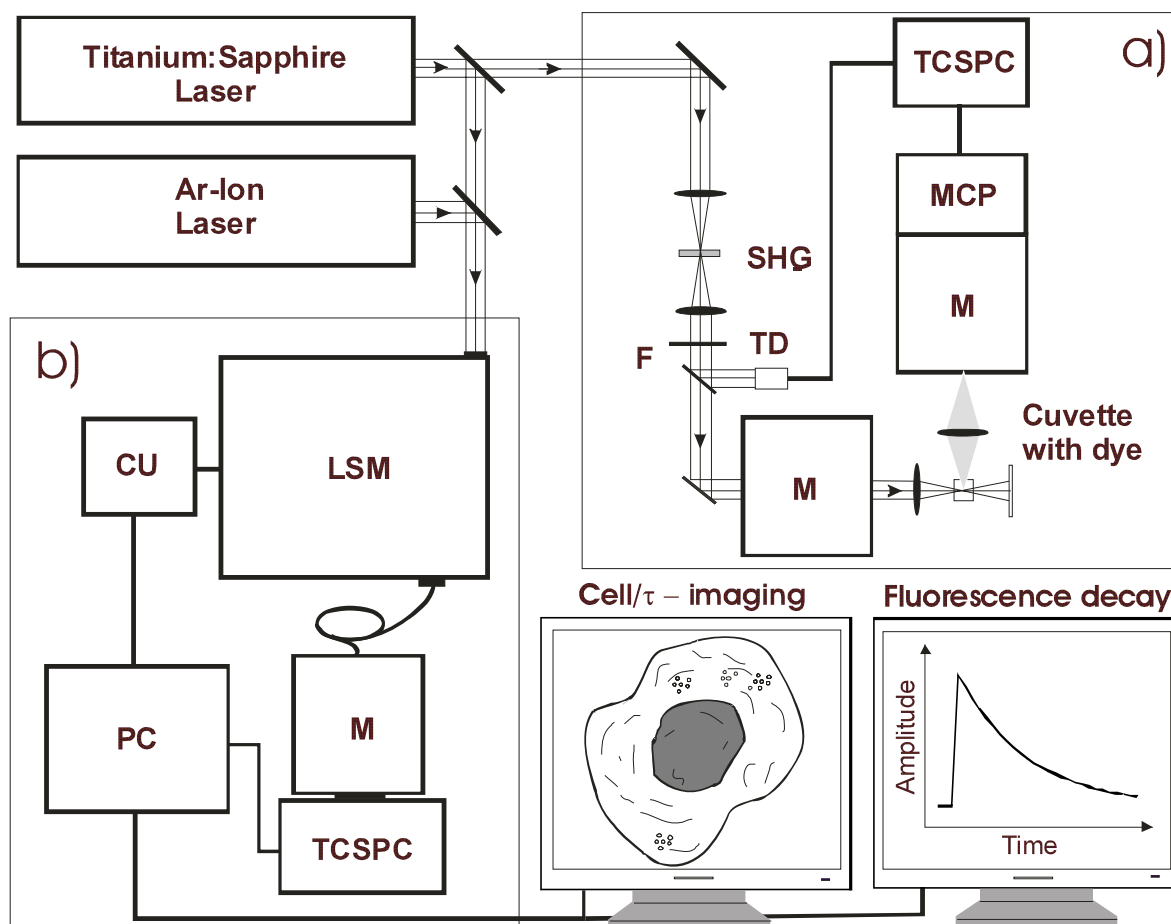


Fig. 2.10. Experimental arrangement for time-resolved spectroscopy in homogenous solutions (a) and cells (b). For cell imaging the Ar⁺ ion laser was used as the excitation source. The pulsed Ti:Sa laser was employed for both one- and two-photon excitation of fluorescence in the time-resolved measurements. AOM – acousto-optical modulator, TCSPC – time-correlated single photon counting unit, M – monochromators, CU – control unit, MCP – multi-channel plate photomultiplier, SHG – second harmonic generation, TD – trigger diode. The spatial resolution attained under two-photon excitation of the fluorescence was $<1\mu\text{m}^3$; the temporal resolution after deconvolution was ~ 20 ps

with a duration of 150 fs (FWHM) and an average power of 300 mW. The pulse repetition rate was 96 MHz. The excitation light was focused by a lens with a focal length of 5 cm on a glass cuvette containing the sensitizer. Fluorescence photons were collected under an angle of 90 degree to the excitation beam path by using another lens with the same focal length. The fluorescence light was focused onto the entrance slit of the monochromator. Additionally, an appropriate filter (BG39, Schott GmbH, Mainz, Germany) was used before the monochromator entrance in order to block scattered excitation photons.

d. Cell imaging

Microscopy experiments were conducted on the stage of a confocal laser-scanning microscope (LSM 510 Axiovert, Carl Zeiss, Jena, Germany) using a water immersion

objective (Achromplan 100x/1.0 W Ph3, Carl Zeiss Inc., Germany). Fluorescence was excited with an Ar⁺ ion laser or a titanium-sapphire laser. Cells were monitored using an appropriate filter combination for the wavelength regions of 505-550 nm, >560 nm and >650 nm, depending on the Ar⁺ ion laser line used for excitation. The autofluorescence of the cells was measured in the cell cultures prior to incubating with the sensitizers. Autofluorescence was excluded by adjusting the detection settings in the microscope (pinhole diameter and photomultiplier gain) so that no autofluorescence signal could be detected. These settings were used for the fluorescence measurements. When the Ti:Sa laser was used for two-photon excitation, an additional short-pass filter (<680 nm, BG39, Schott GmbH, Mainz, Germany) was used in the detection channel to block scattered excitation light.

e. Time-resolved fluorescence measurements in living cells

For *in vitro* measurements of fluorescence kinetics an Ar⁺ ion laser pumped, Kerr-lens mode-locked titanium:sapphire laser with a central wavelength of 800 nm, an average power of ~ 500 mW and a pulse duration of 140 fs (FWHM) was used as an excitation source (Fig. 2.10b). The excitation light was focused onto a Petri-perm dish containing the cell culture incubated with the sensitizer using one of three microscope objectives with different magnifications and numerical apertures (10x, 63x; and 100x; water immersion, with NA=0.45, 1.3, 1.4, respectively). Fluorescence light was collected by the same microscope objective and directed to the entrance slit of a monochromator via an optical fiber. Because of the weak fluorescence signals, the entrance and the output slits of the monochromator were set to 2 mm, resulting in a spectral width of 10 nm (FWHM). In order to correct for autofluorescence, control measurements were carried out prior to incubation with the sensitizers. In the wavelength region of 700-720 nm no autofluorescence signal could be detected. The fluorescence decay was recorded by the same TCSPC unit used for the measurements in homogenous solutions.

f. Time-resolved cell imaging (τ -imaging)

Imaging of cells based on both the fluorescence intensity and lifetime (τ -imaging) was performed using a modified TCSPC unit (SPC-730, Becker & Hickl) which allows for the measurement of the fluorescence kinetics of each pixel of a cell image. The data were analyzed using SPCImage software (Version 2.4.2, Becker & Hickl). The fit procedure was the same as described before.

Chapter 3

Results and discussion

3.1. Investigation of energy relaxation mechanisms and structure of the J-aggregates of TPPS₄

3.1.1. Steady-state measurements

To investigate characterize absorption and emission properties of different species of TPPS₄ steady state measurements were conducted with the experimental setup described in Section 2.2a (p. 38).

Fig. 3.1 shows the ground state absorption spectra of TPPS₄ in aqueous solution buffered at pH 7.5, 3.4 and 1.2. The absorption spectrum of H₂TPPS₄⁴⁻ at pH 7.5 is characteristic for the free-base porphyrins. It exhibits four Q bands located at 515, 553, 580 and 633 nm and an intense near-UV band (Soret band) with a maximum at around 414 nm. The absorption spectrum changes in acidic environment (pH 3.4) exhibiting a red-shifted and slightly broadened Soret band at 433 nm, a narrow intense band at 490 nm, and two broad weaker bands at 642 and 707 nm. The spectral bands at 433 and 642 nm can be attributed to the diprotonated ionic species H₄TPPS₄²⁻, whereas the band at 490 nm (B-band) and at 707 nm (Q-band) are characteristic for J-aggregates [17]. A further decrease of the solution pH to

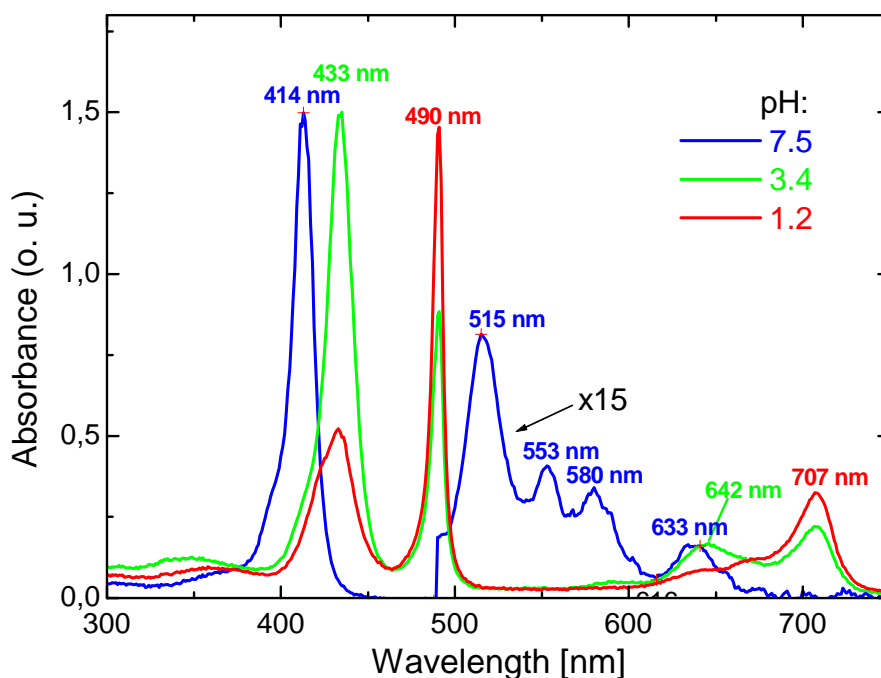


Fig. 3.1. UV-VIS absorption spectra of TPPS₄ in aqueous solution buffered at different pH values. Concentration of TPPS₄ in each case was 5×10^{-5} M. The blue curve (with a magnification factor of 15 for the region 500-750 nm) represents absorption of the free-base TPPS₄ with characteristic intense Soret band at 414 nm and four Q-bands in the region 500-700 nm. The lowering of pH results in the formation of the diprotonated form H₄TPPS₄²⁻ and increasing amount of J-aggregates (green and red curves), as indicated by the absorption bands at 490 nm and 707 nm.

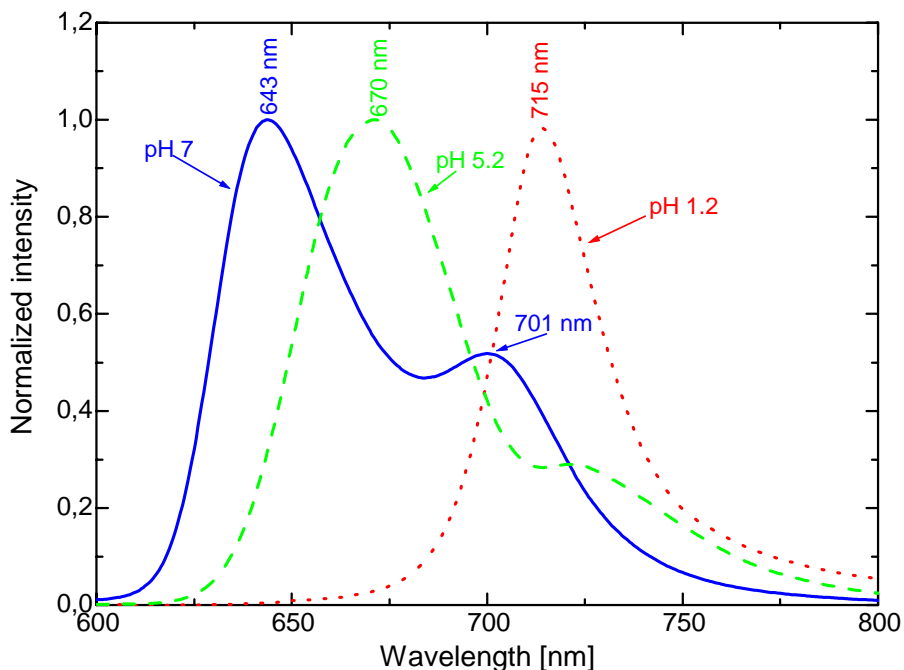


Fig. 3.2. Normalized fluorescence spectra of free-base (pH 7, blue solid curve), diprotonated ionic species (pH 5.2, green dashed curve) and J-aggregate (pH 1.2, red dotted curve) of TPPS₄. Concentration of TPPS₄ in all cases was 5×10^{-5} M. The spectra for the free-base and diprotonated forms were excited at 514 nm, the spectrum of J-aggregates was obtained by excitation at 488 nm.

1.2 results in an increase in the intensity of the absorption bands at 490 and 706 nm, and in the disappearance of the absorption bands related to the neutral and diprotonated species of TPPS₄. These changes in the absorption spectra have been assigned to the formation of the J-aggregates, derived from the dianionic H₄TPPS₄²⁻, as indicated by the diminution of the absorption at 433 nm [17]. A decrease in concentration of H₄TPPS₄²⁻ at low pH (~1-2) results in a decrease of the amount of J-aggregates.

The fluorescence spectra of the different species of TPPS₄ are shown in Fig. 3.2. The free-base H₂TPPS₄⁴⁻ species (pH 7) show emission with maxima at 643 nm and 701 nm, while the diprotonated H₄TPPS₄²⁻ (pH 5.2) exhibits a red shifted emission spectrum with a maximum at 670 nm and a shoulder at ~730 nm. The fluorescence spectrum of H₄TPPS₄²⁻ in aqueous solution (pH=1.2, excitation at 488 nm) exhibits a distinctive peak at around 715 nm, which is attributed to the fluorescence of J-aggregates [69].

In addition to the absorption and fluorescence measurements of TPPS₄ in aqueous solution at different pH, experiments on TPPS₄ were conducted in concentrated H₂SO₄. The absorption spectrum depicted in Fig. 3.3 shows no absorption bands which are characteristic to J-aggregates, but exhibits an intense band at 438 nm and a weaker one at 646 nm. The shape of the spectrum is similar to that measured for diprotonated species of TPPS₄ differing

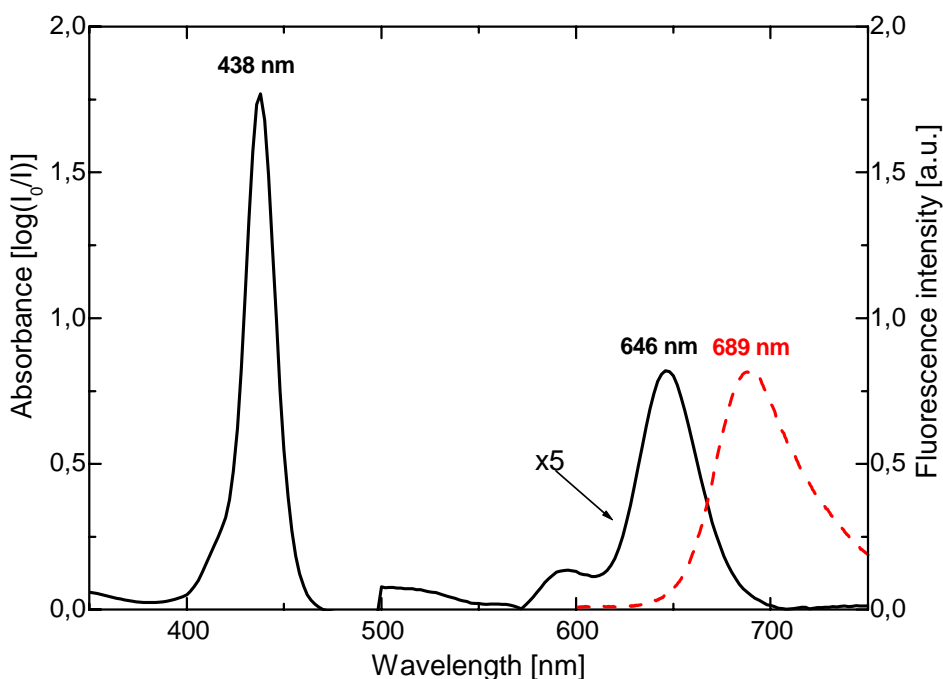


Fig. 3.3. Absorption (black solid curve) and fluorescence (red dashed curve) spectra of TPPS₄ in concentrated H₂SO₄. Concentration of TPPS₄ was 5x10⁻⁵ M. Excitation of the fluorescence was performed at 514 nm. The absorption spectrum corresponds to that of the diprotonated form. No formation of J-aggregates is observed. This fact can be explained by the protonation of the sulphonato groups in concentrated H₂SO₄, which precludes formation of J-aggregates

only by a slight shift in the red (~4-5 nm) of both absorption bands with respect to the diprotonated species.

The spectral changes, which occur when TPPS₄ is dissolved in concentrated H₂SO₄, imply that the J-aggregates break up. Since aggregation of TPPS₄ is thought to be mainly driven by the ion-pair formation of the diprotonated porphyrin ring and one of the anionic peripheral groups of neighboring porphyrins [123], the disintegration of the aggregates may be caused by the protonation of the peripheral sulphonato groups in the highly acidic medium. Because of the lack of the negative charges the sulphonato groups cannot interact with the cationic center on porphyrin moiety. The emission band (Fig. 3.3, red dashed line) is red-shifted to 689 nm. It is narrower than the emission band of the diprotonated species of TPPS₄ in aqueous solution and is red-shifted with respect to it. This differences may be due to the protonation of the sulfonato groups in the case of H₂SO₄, which may lead to a weaker interaction between porphyrin molecules and narrowing of the fluorescence band.

3.1.2. Fluorescence kinetics spectroscopy

The measurements of the fluorescence decay kinetics of TPPS₄ in aqueous solutions at different pH values and concentrations of the dye were performed with the time-correlated single photon counting (TCSPC) unit described in Section 2.2b (p. 39-40). The fluorescence kinetics of TPPS₄ in concentrated H₂SO₄ measured in a wavelength range of 630-740 nm was found to decay according to a mono-exponential law with a time constant of ~ 3.1 ns (Fig. 3.4a).

An increase of pH to 1.2 results in the formation of J-aggregates as evidenced by the

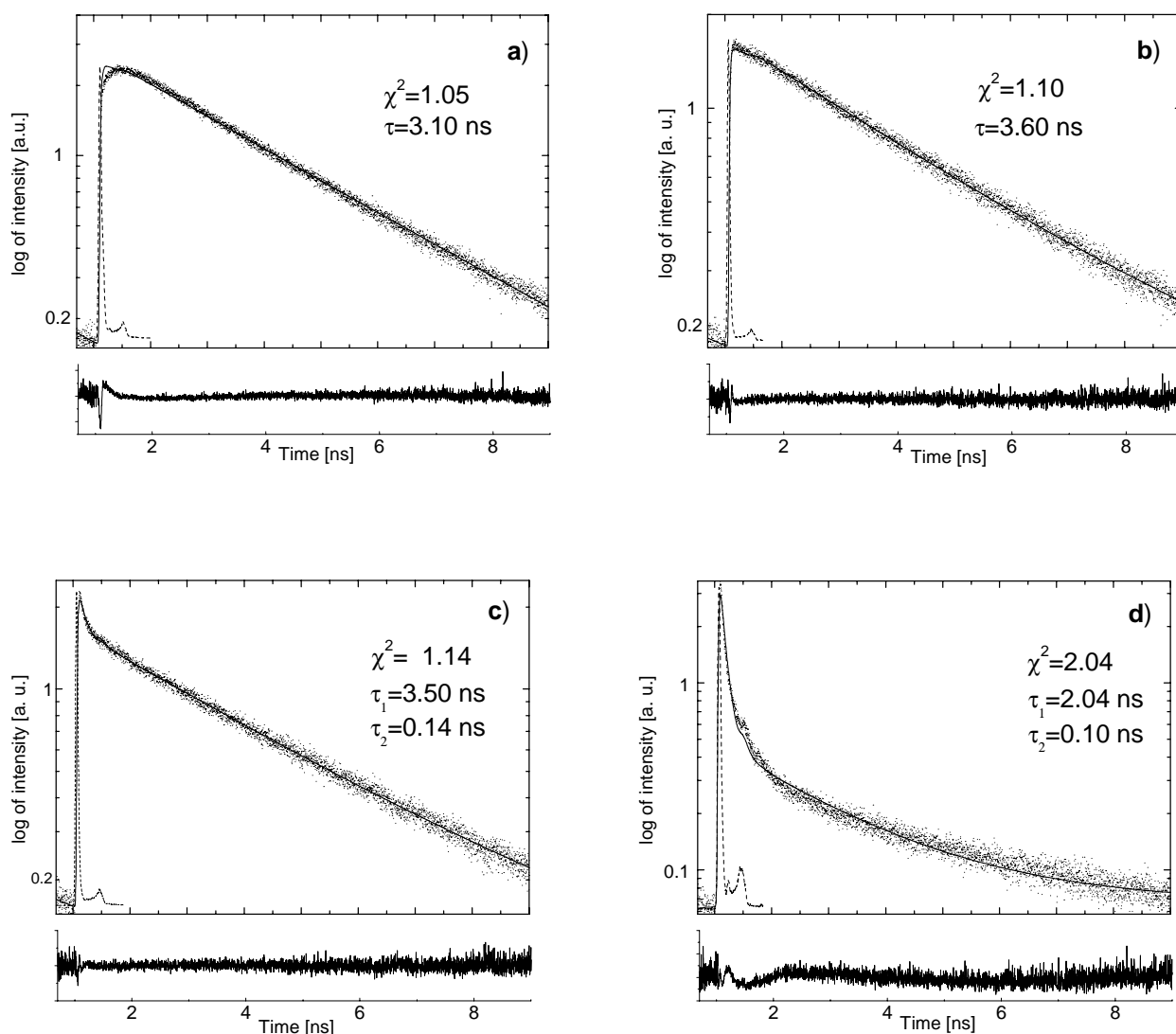


Fig. 3.4. Fluorescence decay of TPPS₄ in a) H₂SO₄, conc. 5×10^{-5} M $\tau=3.10$ ns, $\lambda_{em}=400$ nm, $\lambda_{em}=680$ nm and in aqueous solution at pH ~1 as a function of the concentration: b) 10^{-6} M, $\tau_1=3.6$ ns c) 10^{-5} M, $\tau_1=3.5$ ns, $\tau_2=0.14$ ns, d) 10^{-4} M, $\tau_1= 2.04$ ns, $\tau_2=0.1$ ns, in all three cases $\lambda_{ex}=400$ nm, $\lambda_{em}=720$ nm. The residuals are shown in the graphs below. The solid curves represent the theoretical fit, dashed line - instrument response function (IRF).

presence of the intense absorption band at 490 nm (see above). At low concentrations (10^{-6} M), the dominant species in such an acidic solution is the diprotonated form of TPPS₄ which exhibits a monoexponential fluorescence decay with a time constant value close to that obtained in concentrated H₂SO₄ (Fig. 3.4b). With concentrations above 10^{-5} M the amount of J-aggregates in solution increases. The aggregate formation is reflected in the fluorescence decay kinetics by the appearance of the short fluorescence decay component with a time constant of approx. 0.10 - 0.27 ns in the spectral region of 690-740 nm (Table III and Fig. 3.4

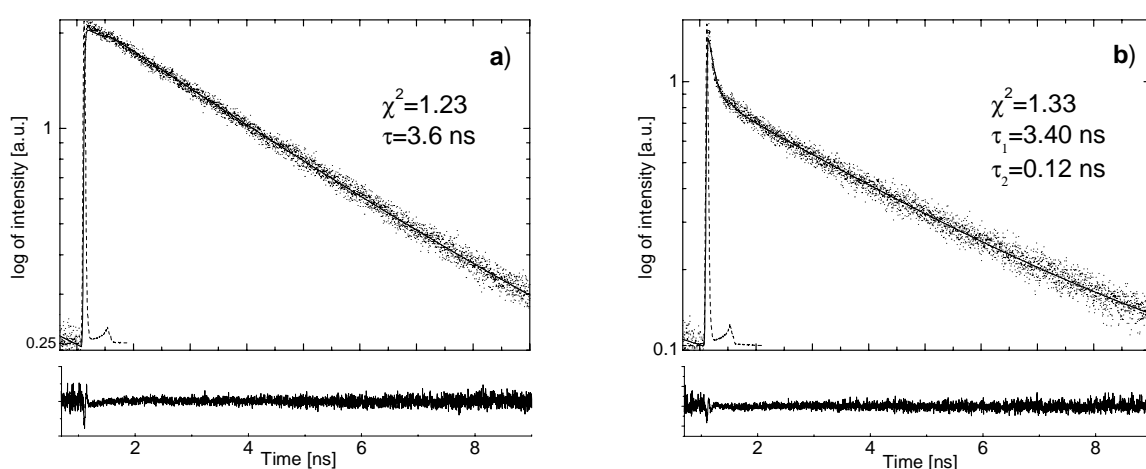


Fig. 3.5. Relaxation kinetics of TPPS₄ in aqueous solution at pH 3.2. $c = 5 \times 10^{-5}$ M: a) $\lambda_{em} = 670$ nm, $\tau = 3.6$ ns, b) $\lambda_{em} = 730$ nm, $\tau_1 = 0.14$ ns, $\tau_2 = 3.4$ ns. Solid line- theoretical fit, dashed line – instrument response function. Lower graphs represent residuals. The presence of the long-lived component at 660 nm and the short-lived component at 730 nm indicates that both the diprotonated form H₄TPPS₄²⁺ and J-aggregates are formed at pH 3.2.

c, d), where the fluorescence band attributed to J-aggregates was observed (Fig.3.2).

The increase of pH to 3 did not change the fluorescence relaxation kinetics significantly. Two decay constants were detected. In the spectral region where fluorescence of protonated species is dominant (630-680 nm, s. Fig. 3.2), the decay constant value is 3.6 ns, which is comparable to that obtained at the lower pH values (Fig. 3.4b-d). At the longer wavelengths (690-740 nm) an additional, short decay component of ca.140 ps was obtained.

A further increase of pH to 5 leads to the disappearance of J-aggregates and formation of free-base species of TPPS₄. This results in a monoexponential fluorescence decay process with a rate constant, that changes depending on the spectral region. At emission wavelengths between 630-650 nm and concentrations as low as $5 \cdot 10^{-6}$ M, the fluorescence decay time was determined to be about 6.9 ns. It becomes shorter with the increasing concentration (4.9 ns at 10^{-4} M) implying formation of higher aggregated species. Another decay component of ca.

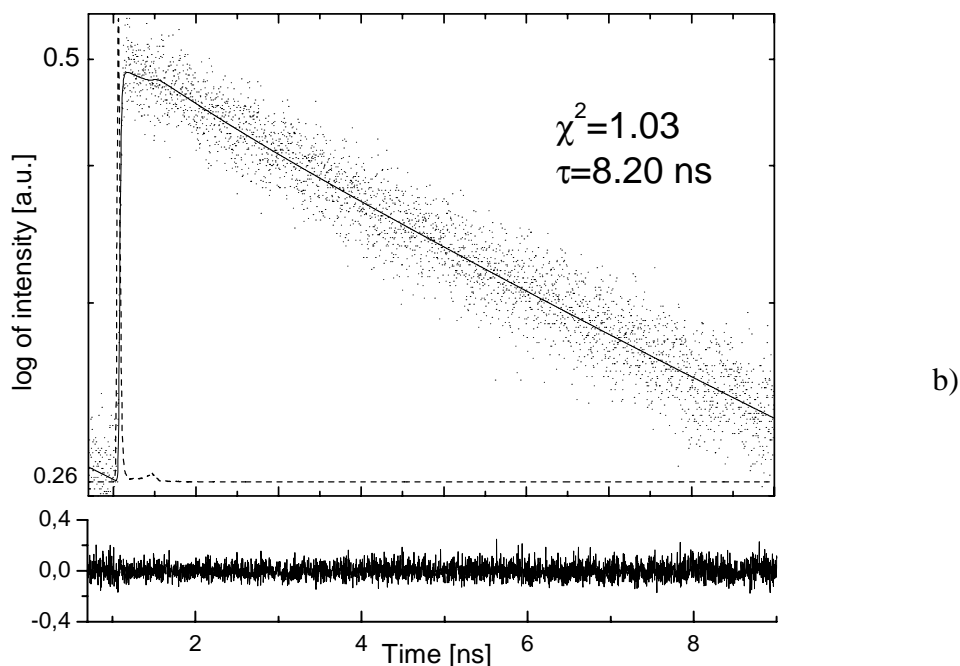


Fig. 3.6. Relaxation kinetics of TPPS₄ in aqueous solution at pH 7.2, $c=10^{-5}$ M, $\lambda_{\text{ex}}=400$ nm, $\lambda_{\text{em}}=720$ nm, $\tau_1=8.2$ ns. The solid line represents the theoretical fit to the experimental data, The IRF is represented by the dashed line. Residuals are presented in the graph below. The fluorescence decay constant of ~ 8 ns can be attributed to the non-protonated species H₂TPPS₄⁴⁻.

3.6 ns appears in the spectral region of 690-740 nm and is constant at various concentrations of TPPS₄.

In neutral solutions (pH 7.2) a monoexponential fluorescence decay with a time constant of ~ 8 ns was measured in neutral solutions (Fig. 3.6). The decay time was constant over the entire concentration range of TPPS₄.

The fluorescence decay values obtained in TPPS₄ solutions of different acidity are in good agreement with transient absorption relaxation lifetime reported by Frolov et al. [123]. The values of the fluorescence decay constants obtained for TPPS₄ in acidic aqueous solutions (Table III, Fig. 3.4a-c) are similar to the excited state lifetime (2-3 ns) measured by the pump-and-probe technique in aqueous solutions at pH = 3.5 and concentrations of TPPS₄ similar to those used in the fluorescence relaxation measurements. The fluorescence decay constant of approx. 3.5 ns obtained for TPPS₄ dissolved in concentrated H₂SO₄ can be attributed to the monomeric diprotonated species of TPPS₄ with characteristic absorption properties (Fig. 3.1). The relaxation constant differs only slightly from that measured by other authors when single-photon counting (3.87 ns) [83], phase modulation (3.9 ns) or streak camera (3.2 ns) [69] techniques have been used, independent of the excitation wavelength. Similarly, the short-lived fluorescence relaxation component (150-270 ps) measured in acidic solution in the region, where fluorescence of J-aggregates can be detected (690-740 nm) meets the

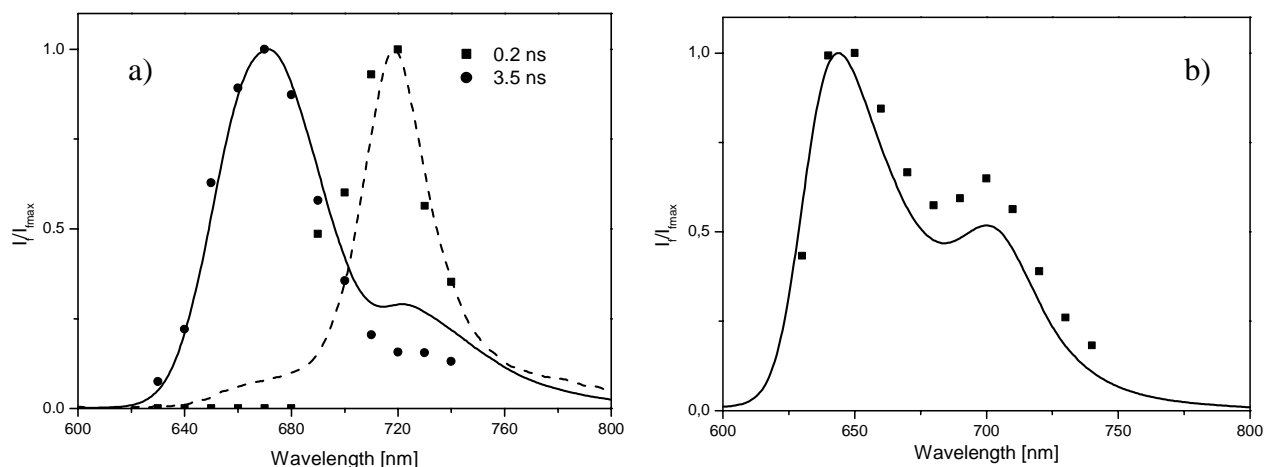


Fig. 3.7. a) Normalized emission spectra of the diprotonated form (solid line) and J-aggregates (dashed line) of TPPS₄ with the relative amplitudes of the long-lived (3.5 ns, circles) and short-lived (~200 ps, squares) fluorescence relaxation components measured by TCSPC. The amplitudes of the short and long component coincide with the emission spectra of the J-aggregates and diprotonated species, respectively. b) Normalized emission spectrum of the non-protonated TPPS₄ form in aqueous solution (solid line).

corresponding values of intermediate absorption decay constant of 290 ps obtained from the transient absorption measurements [123]. As it can be seen in Fig. 3.7a, where the relative amplitudes of the decay components and the fluorescence spectra of two different species are shown, there is a quite good correlation between the amplitudes and the fluorescence spectra of the corresponding species. Careful analysis of the relative amplitudes of the fluorescence decay components obtained in TPPS₄ solutions shows that the decay constant value of about 0.2 ns reflects the relaxation of excitation in J-aggregates. This is in good agreement with the values reported by others [64, 74], although the relative amplitudes of the decay components and, as in the case of single-photon counting, the number of decay components are different. This might be explained by different excitation wavelengths and different detection systems used. The fluorescence decay constants measured in neutral aqueous solutions of TPPS₄ (~8 ns, s. Fig. 3.6 and Table III) were found to be similar to the absorption relaxation lifetime obtained for TPPS₄ dissolved in ethanol [123]. The relative amplitude of the fluorescence decay measured at neutral pH correspond very well to the fluorescence spectrum of TPPS₄ measured in diluted aqueous solution at the same pH (Fig. 3.7b). Thus, the fluorescence decay time of ~8 ns can be attributed to the non-protonated monomeric species of TPPS₄. This lifetime is shorter as compared to that determined by others using the phase modulation and single-photon counting techniques (9.5 ns and 9.25 ns, respectively). However, it is in good agreement with the values obtained by streak camera system measurements [69].

Table III. Fluorescence decay constants of TPPS₄ in aqueous solutions at different pH. $\lambda_{exc}=400$ nm.

| pH | Concentration mol/L | Spectral region (nm) | τ_1 (ns) | τ_2 (ns) |
|------|------------------------|-------------------------|------------------|------------------|
| -1.1 | 5×10^{-5} | 630 – 740 | 3.1 ± 0.2 | |
| 1.19 | 10^{-6} | 640 – 740 | 3.7 ± 0.2 | |
| 1.22 | 10^{-5} | 640 – 680 | 3.6 ± 0.1 | |
| | | 690 – 740 | 3.6 ± 0.1 | 0.27 ± 0.13 |
| 1.2 | 5×10^{-5} | 640 – 670 | 3.5 ± 0.1 | |
| | | 690 – 740 | 2.8 ± 0.4 | 0.10 ± 0.05 |
| 1.28 | 10^{-4} | 630 – 680 | 3.3 ± 0.3 | |
| | | 690 – 740 | 3.6 ± 1 | 0.27 ± 0.13 |
| 3.22 | 5×10^{-5} | 640 – 680 | 3.5 ± 0.1 | |
| | | 690 – 740 | 3.6 ± 0.2 | 0.14 ± 0.37 |
| 4.85 | 5×10^{-6} | 640 – 650 | 6.9 ± 0.7 | |
| | | 660 – 740 | 3.6 ± 0.2 | |
| 5.15 | 10^{-4} | 630 – 650 | 4.9 ± 0.6 | |
| | | 660 – 740 | 3.7 ± 0.2 | |
| 7 | 10^{-6} | 630-740 | 7.9 ± 0.6 | |
| 7.15 | 10^{-5} | 630-740 | 7.7 ± 0.6 | |
| 7.15 | 10^{-4} | 630-740 | 7.9 ± 0.4 | |

The slightly faster decay constant value (6.9 ns) obtained for TPPS₄ in acidic medium (pH 4.85) at low concentrations (5×10^{-6} M) as compared to the decay in the neutral solution (~8 ns) might be caused by the fluorescence quenching effect induced by the diprotonated species present in the solution. However, the fluorescence decay time of 4.9 ns found at pH = 5.15 in solutions of higher TPPS₄ concentration needs further investigation. A similar fluorescence relaxation time has been measured in cells [31]. The corresponding fluorescence lifetimes of the non-protonated and diprotonated monomers of TPPS₄ presented in [17] are similar. However, for the J-aggregates there is a significant spread in fluorescence lifetimes obtained using different techniques, such as phase modulation, streak camera and single photon counting. The lifetimes of induced absorption in the J-aggregates obtained from experimental data are approximately in agreement with two of the three components, when three-exponential approximation was used ($\tau_1=50$ ps; $\tau_2=290$ ps; $\tau_3=2.08$ ns). The presence of the fast component of 50 ps may be caused by singlet-singlet annihilation within the J-

aggregates [83,123], since intensive pump pulses were used in the pump-and-probe experiments. An approximation of the fluorescence decay with exponential functions yields the values of process lifetimes that are usually applied to describe the systems consisting of monomers and small aggregates. However, in the case when molecules build large aggregates, singlet-singlet annihilation becomes possible. Therefore, due to a very large size of aggregates, pulses of very low energy should be used in all measurements in order to obtain annihilation-free conditions of the excitation relaxation. While another model bearing other specific parameters should be applied to describe relaxation processes in the presence of annihilation such systems more thoroughly, an exponential approximation giving excitation lifetimes is still commonly used for comparison purposes.

3.1.3. Investigation of nonlinear properties and structure of TPPS₄ J-aggregates

The fluorescence decay of TPPS₄ in acidic environment could not be approximated to an exponential law, when pulses of higher intensity were used for the excitation (Fig. 3.8a, b). Such a non-exponential fluorescence decay process persisted for excitation intensities down to $\sim 10^{14}$ photons/cm² per pulse, changing into a two-exponential process with time constants of ~ 150 ps and 3 ns at lower intensities. Moreover, measurements of the fluorescence quantum yield as a function of the excitation intensity revealed (Fig. 3.9) that the fluorescence quantum yield decreases remarkably at excitation intensities higher than 10^{15} photons/cm² per pulse. Such an intensity-dependent fluorescence behavior suggests that, in addition to the exponential energy relaxation in diprotonated species of TPPS₄ with a time-constant of 3 ns, other non-exponential decay mechanism of the excitation energy occur at high excitation intensities. A similar dependence of fluorescence relaxation characteristics on the excitation intensity has been reported for other organic molecules, such as 1,1'-diethyl-N,N'-quinocyanin (PIC) [19,124], thiocyanine [82], TTBC [80] and phthalocyanine films [87]. It has been explained by the exciton singlet-singlet annihilation within aggregated domains. Moreover, several recent studies carried out on porphyrin derivatives revealed the presence of exciton annihilation at sufficiently high excitation intensities [85,123]. Therefore, it is reasonable to expect that the intensity-dependent behaviour of the fluorescence relaxation of the J-aggregates at high excitation intensities might be caused by the exciton-exciton annihilation as well. At low excitation intensities, when only one exciton per domain is created and no annihilation takes place, the excitation energy decays through monomolecular relaxation processes, which reflect the natural excited state lifetime (150 ps) in J-aggregates.

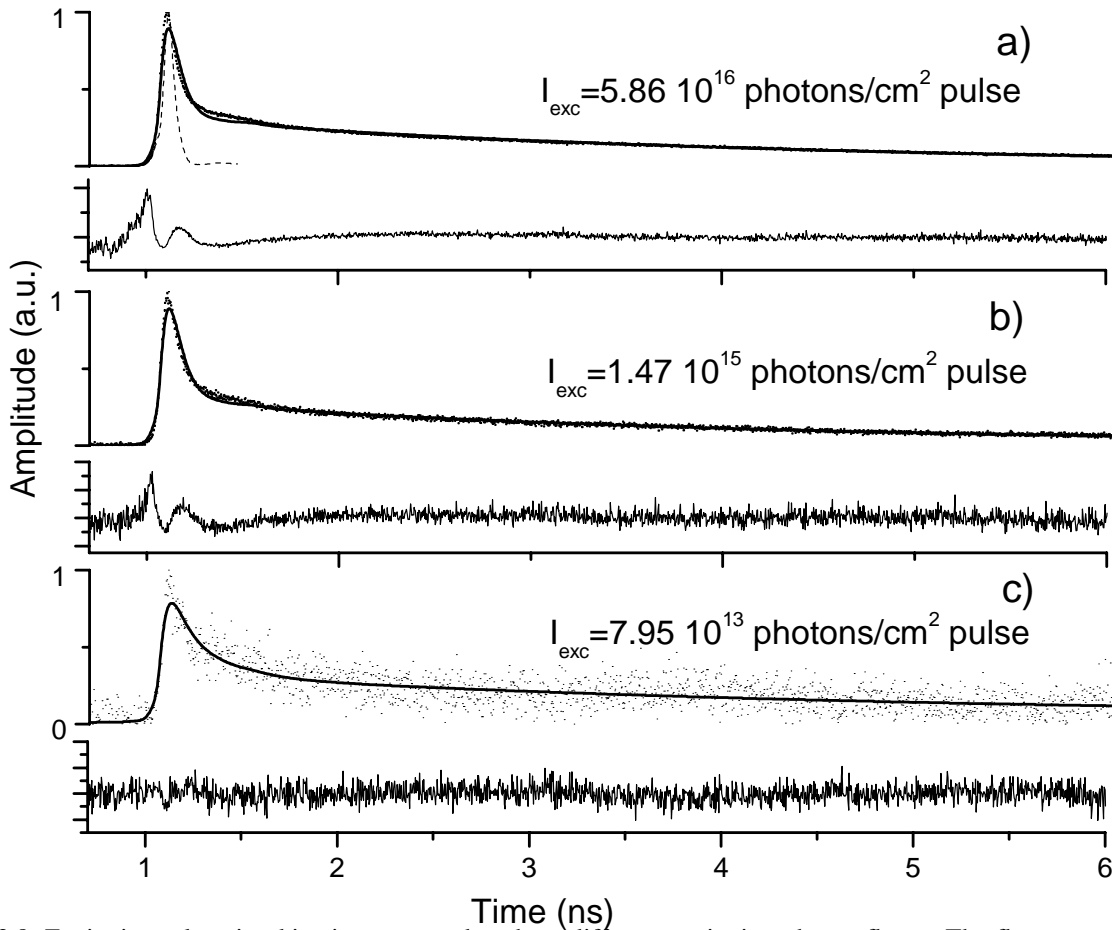


Fig. 3.8. Excitation relaxation kinetics measured at three different excitation photon fluxes. The fluorescence was excited at 430 nm and detected at 720 nm. a) Excitation intensity $5.86 \cdot 10^{16}$ photons/cm² s; the dashed line represents the instrument response function. b) excitation intensity – $1.47 \cdot 10^{15}$ photons/cm² s. c) Excitation intensity – $7.95 \cdot 10^{13}$ photons/cm² s. The solid line represents the theoretical fit of the fluorescence relaxation to a two-exponential law. The relaxation kinetics exhibit an additional, intensity-dependent and non-exponential relaxation channel as the excitation intensity increases. This implies, that the annihilation process between the excitons may be occurring.

When high excitation intensities are used, more than one exciton can be created simultaneously in a molecular aggregate (domain), and bimolecular exciton-exciton annihilation may occur resulting in a decrease of the detected excitation lifetime.

The fluorescence decay data were fitted using eq. (1.33). In order to obtain an absolute scale of fluorescence intensity, the number of measured fluorescence photons (counts) was divided by the excitation volume (in cm³) and multiplied with the geometrical factor G (see Techniques and methods). The iterative reconvolution method based on the non-linear Levenberg-Marguardt algorithm was employed for the fitting procedure. For excitation intensities from $5.86 \cdot 10^{16}$ down to $4.41 \cdot 10^{13}$ photons/cm²·pulse, the best-fit results were obtained with $h=0.5$. At lower excitations the experimental data deviated from the annihilation law. Using eq. (1.34) and (1.35) the exciton motion parameters- such as the diffusion coefficient D and the hopping time τ_h - were evaluated to be $(1.8 \pm 0.9) \cdot 10^{-3}$ cm²/s and

(1.2 ± 0.6) ps, respectively. Similar results were obtained for TPPS₄ when the transient absorption kinetics were measured by means of the pump-and-probe technique [123].

As shown by Fig.3.9, the fluorescence quantum yield starts to decrease when the excitation intensity reaches $\sim 1.5 \cdot 10^{15}$ photons/cm² pulse. This point marks the onset of the

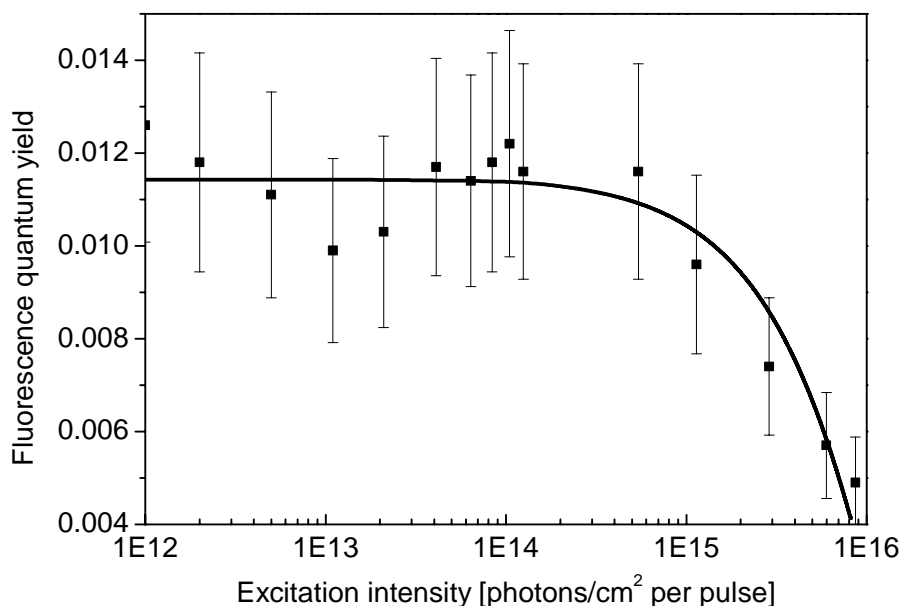


Fig. 3.9. Fluorescence quantum yield of TPPS₄ J-aggregates as a function of the excitation intensity. The solid

line – theoretical fit to $\phi(n(0)) = \phi_0 \sum_{j=0}^{\infty} \frac{(-n(0))^j \Gamma(r+1)}{(j+1)\Gamma(j+r+1)}$ [91], where $n(0)$ is the initial number of excitations, r is the ratio between the exciton lifetime in the presence of annihilation and the intrinsic exciton lifetime under annihilation-free conditions, ϕ_0 is the fluorescence quantum yield in the absence of annihilation. The fluorescence quantum yield decreases as a result of the annihilation which becomes stronger with the increasing excitation intensity.

annihilation process and corresponds to a threshold value of excitation intensity when only one exciton per domain exists. The mean number of molecules within one domain can then be calculated dividing the number of the molecules within the excitation volume by the number of absorbed photons at the threshold. Taking into account the concentration of the TPPS₄ molecules and the excitation volume in the sample, we found that the domain of the TPPS₄ J-aggregate consists of at least ~ 20 molecules.

It must be noted, however, that depending on the exciton motion characteristics and lifetime, this value may reflect either the physical size of the aggregate or the number of the molecules that an exciton visits within its lifetime in the absence of annihilation. Thus, if the migration

length of the exciton is shorter than the length of the aggregate, exciton collisions are confined to distances of $\sim 2d_{\text{migr}} = \sqrt{8\tau_{\text{exc}}D}$, with τ_{exc} being the exciton lifetime in the absence of the annihilation and D the diffusion coefficient. The annihilation process stops when the exciton density within the aggregate decreases to a value where the excitons do not collide as the distances between them are too large, even though more than one exciton does exist within the aggregate. Thus, it is obvious that only the exciton diffusion-limited size but not the actual physical size of the aggregate can be determined. With exciton motion parameters D , τ_{h} , and the exciton intrinsic lifetime all being known in the absence of annihilation, it is possible to determine which of the above mentioned cases occurs. The number of molecules visited by one exciton during its lifetime can be evaluated by calculating the distance that the exciton migrates during its lifetime in the absence of annihilation. This can be done using the equation for the exciton migration length d_{migr} (see above). The value of τ_{exc} was determined by fitting the fluorescence decay when low excitation intensities were used and no annihilation occurred. The short-lived component of ~ 150 ps can be attributed to the natural exciton lifetime within the aggregate in the absence of annihilation. Using this value and the diffusion coefficient determined previously, we found that the migration distance d_{migr} equals $\sim 7 \cdot 10^{-7}$ cm. Assuming that the distance between molecules is $\sim 5 \text{ \AA}$, the aggregate length can be calculated to be $\sim 10^{-6}$ cm, showing that the exciton diffusion length is shorter than the aggregate length. This result suggests that the number of molecules per aggregate determined represents the diffusion-limited size of the aggregate. The number of coherently conjugated molecules obtained in this work is in fairly good agreement with previous findings on the aggregation number of TPPS₄ obtained from UV/VIS absorption spectroscopy ($N=11$) [71], fluorescence anisotropy lifetime measurements ($N=22$) [84] and dynamic light scattering experiments ($N=6-32$) [77]. However, it has been proposed that J-aggregates of TPPS₄ tend to form large fractal-like structures or macroaggregates in organic solvents. Therefore, additional measurements of TPPS₄ embedded in polyvinyl alcohol (PVA) films were conducted by means of confocal laser-scanning microscopy. Fig. 3.10 shows a typical image of TPPS₄ fluorescence in a PVA film at acidic pH.

Fluorescence was excited at several wavelengths (488, 512, 633 nm) and detected using an appropriate filter set of wavelengths >650 nm. No differences were observed in the fluorescence pattern when different excitation wavelengths were used. As shown in Fig. 3.10, large structures on the scale of $\sim 1\mu\text{m}$ are formed in PVA films at acidic pH. The fluorescence kinetics of TPPS₄ in PVA matrix at acidic pH exhibit a two-exponential decay with decay

constants of 0.2 ns and 10.4 ns (Fig. 3.11). The short-lived relaxation component is similar to that of J-aggregates of TPPS₄ (~0.15 ns) measured at low excitations intensities. Therefore, the short decay time can be attributed to J-aggregates.

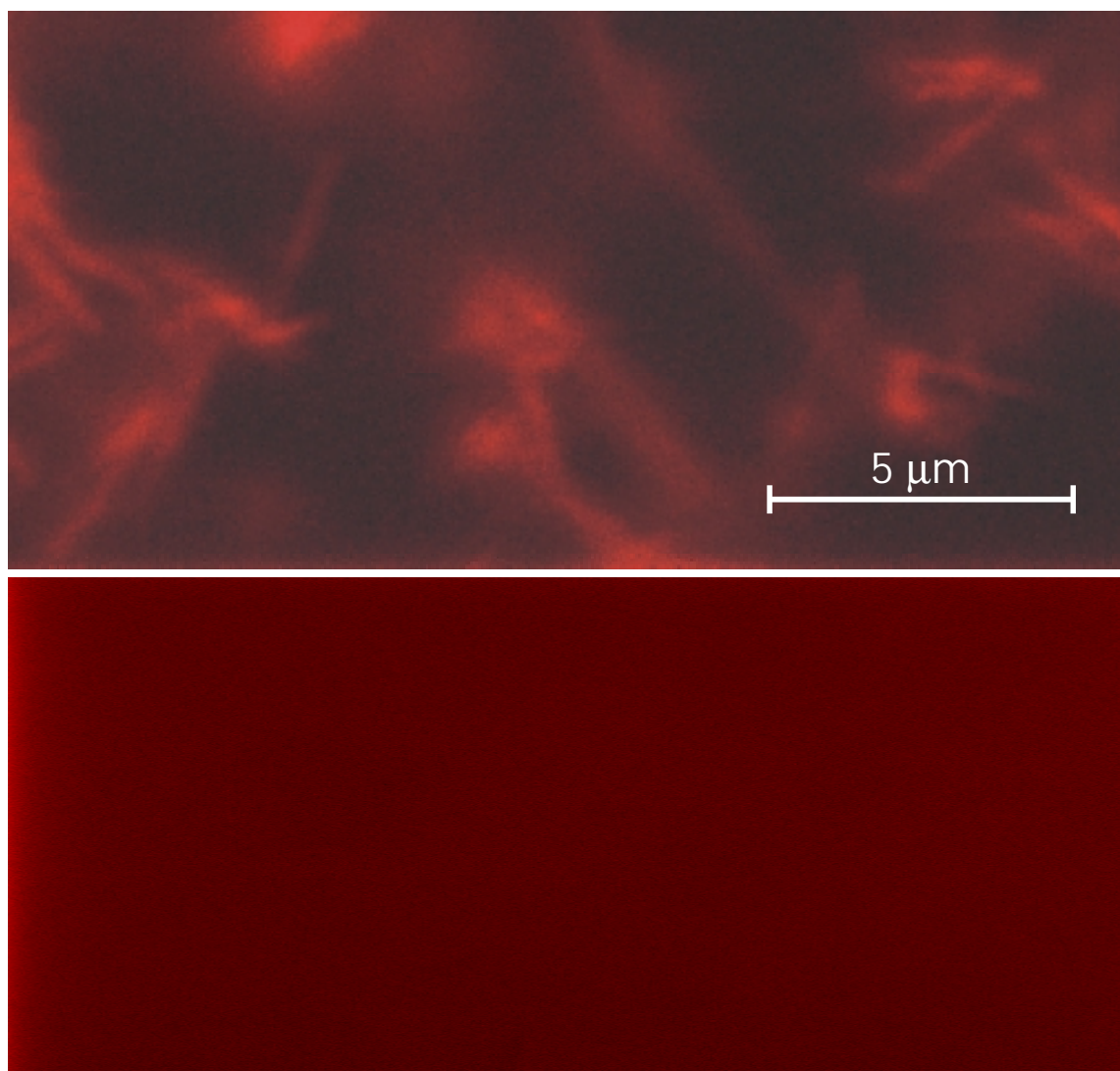


Fig. 3.10. TPPS₄ embedded in poliviny alcohol (PVA) matrices as measured by a laser-scanning microscope. a) at acidic pH (~2), b) at neutral pH. The fluorescence was excited at 633 nm, and detected between 650-750 nm. Macromoleular structures were observed at acidic pH, whereas at neutral pH no such structures are formed.

The fluorescence kinetics was also biexponential at neutral pH with decay constants of 2.3 ns and 10.6 ns. The faster component may arise from the interaction of the free-base species of TPPS₄ with PVA molecules. The long-living component is almost similar to the slow component measured in PVA at acidic pH. Due to the rather long decay constant, the slow component in both cases seems probably to arise from monomeric species of TPPS₄. However, further investigations are needed to clarify this more thoroughly.

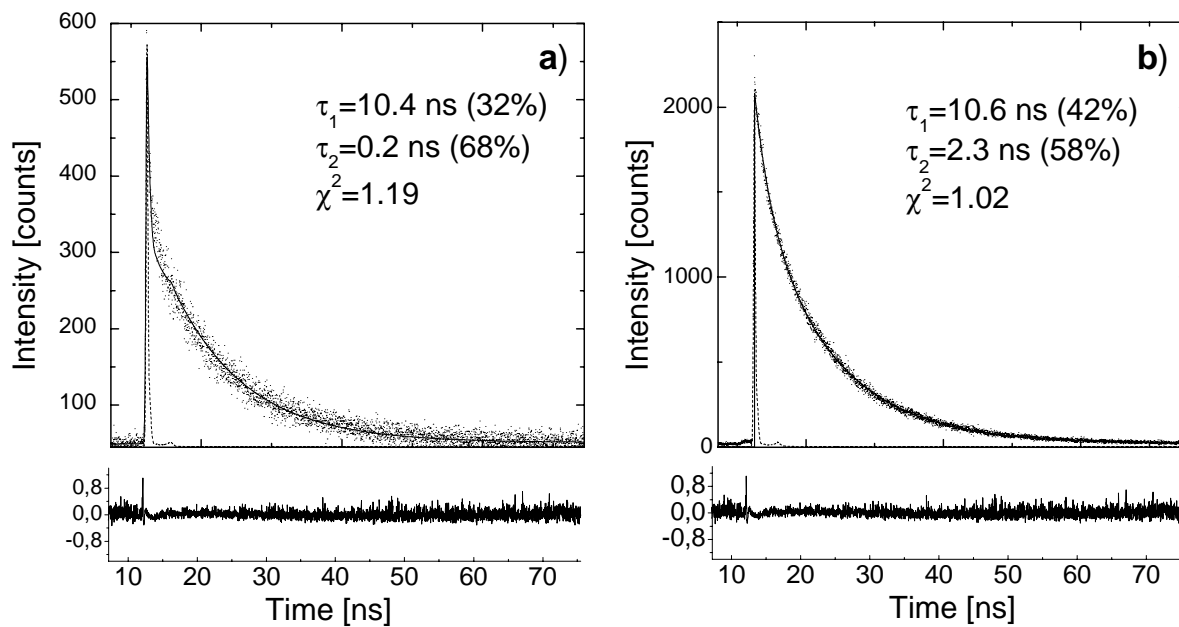


Fig. 3.11. Fluorescence relaxation kinetics of TPPS₄ in PVA films: a) at acidic pH, b) at neutral pH. The fluorescence was excited at 430 nm and detected at 720±10 nm. The dots are the experimental data. The solid curves represent the fitted data, the dashed curve – instrumental response function. The residuals are shown in the graph below.

3.2. Aggregation state and subcellular localization patterns of congeneric series of derivatives of pyropheophorbide a and chlorin e6

3.2.1. Steady-state absorption and fluorescence measurements

To characterize the aggregation conditions and important aggregation parameters of the sensitizers pyropheophorbide-a ethers, PpeC6 and PpeC9, and of the chlorin e6 derivative, ChlC9, steady-state absorption and fluorescence measurements were conducted

3.2.1.1. Photoproduct formation

Many sensitizers form photoproducts upon irradiation, and their fluorescence can interfere with that of the unmodified sensitizer. Therefore, the photochemical stability of the PS was investigated in order to determine whether fluorescent photoproducts are formed during irradiation. The irradiation dose, at which the fluorescence intensity decreased by 50%, was determined for a wavelength of 400 nm and yielded $D_{50} = 35 \text{ J/cm}^2$, $D_{50} = 25 \text{ J/cm}^2$ and $D_{50} = 770 \text{ J/cm}^2$ for PpeC6, PpeC9 and ChlC9, respectively. During the bleaching procedure, no formation of fluorescent photoproducts could be observed in either case (see Techniques and methods for details).

3.2.1.2. Absorption and emission properties

The absorption and emission properties were determined for three derivatives of Ppe, PpeC1, PpeC6 and PpeC9 in aqueous solutions and in MeOH and were similar for all three compounds. The absorption spectrum of PpeC9 (Fig. 3.12a) in MeOH consists of an intense Soret band peaking around 408 nm with two slight shoulders at higher energy due to B(0,0) and B(0,1) transitions and four weaker Q bands at 505 nm, 538 nm, 607 nm, and 662 nm. In contrast to the MeOH solutions, where the sensitizers are present in monomeric form [27], the absorption in PBS solution buffered at pH=7.3 exhibits a broadened Soret band and red-shifted ($\Delta\lambda \sim 7 \text{ nm}$) Q bands. The Q band with the longest wavelength peaks at 668 nm and shows a shoulder at 687 nm. The absorption spectrum changed towards the monomers when the fraction of MeOH was increased in aqueous solution. Similar changes have also been observed for the other compounds, PpeC1 and PpeC6 (data not shown).

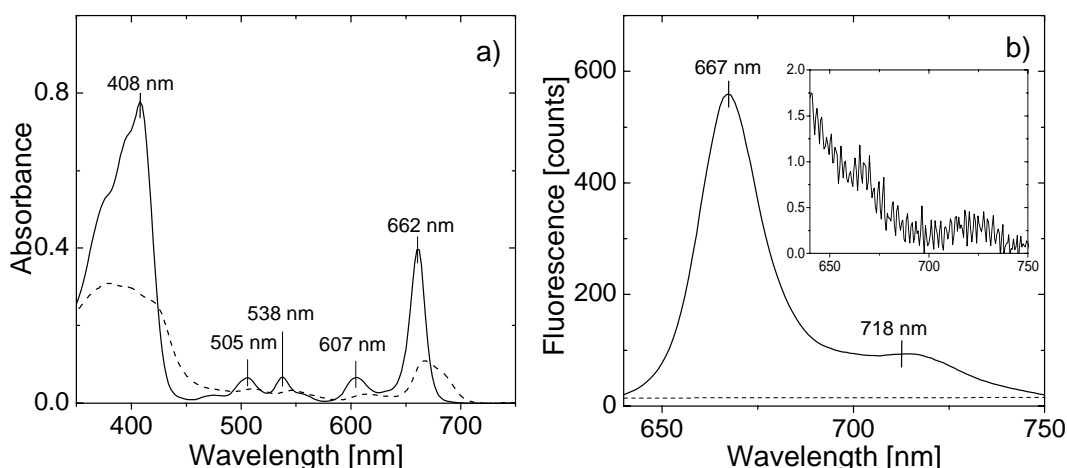


Fig. 3.12. a) - absorption spectra of PpeC9 in MeOH (—) and in aqueous solution (PBS, ---). In PBS, PpeC9 shows broadened and red-shifted absorption bands. b) – emission spectra of PpeC9 in PBS (---) and in PBS containing 1% vol./vol. of the detergent Triton X 100 (—). The inset in b) represents the emission spectrum in PBS on an enlarged intensity scale. Excitation was performed at 514 nm. The emission quantum yield is decreased in the solution without detergent by a factor of ~ 500 as compared to that containing detergent. The spectral changes in the absorption spectrum and the significant decrease of the emission quantum yield are indicative for strong aggregation of PpeC9 in aqueous solutions. The concentration of PpeC9 was in all cases $5 \mu\text{M}$.

The emission spectra of PpeC9 excited at 514 nm is shown in figure 3.12b. In PBS solution only a weak fluorescence signal was detected (Fig. 3.12b, dashed line and the inset). In PBS containing the detergent Triton X 100, the emission of PpeC9 (Fig. 3.12b, solid line) is characterized by two distinctive bands at 667 nm (transition $S_{10} \rightarrow S_{00}$) and 718 nm (transition $S_{10} \rightarrow S_{01}$). In this case, the fluorescence intensity increased by a factor of ~ 500 as compared to the detergent-free PBS solution. When aggregated, sensitizers exhibit only negligible fluorescence quantum yield [46,59,125,126] due to the fast radiation-less relaxation of the excitation energy within aggregates, which results from the strong interaction between aggregated molecules. Only when monomerization takes place, the fluorescence intensity increases dramatically with increasing monomerization degree. This is in accordance with the changes in the fluorescence before and after addition of the detergent to the PBS solution (Fig. 3.12b). A similar spectral behavior was also observed for other two derivatives (PpeC1 and PpeC6, data not shown).

The absorption spectrum of chlorin e6 nonyl ether, ChlC9, in MeOH (Fig. 3.13a, solid line) possesses a similar structure with the Soret band peaking at 394 nm and four Q bands at 495, 554, 599 and 654 nm. Similarly, the absorption spectrum of Chl e6 nonyl in aqueous solution (with 0.1 % MeOH) exhibits red-shifted and broadened absorption bands as compared with those measured in MeOH (Fig. 3.13a, dashed line). It shows a broadened Soret

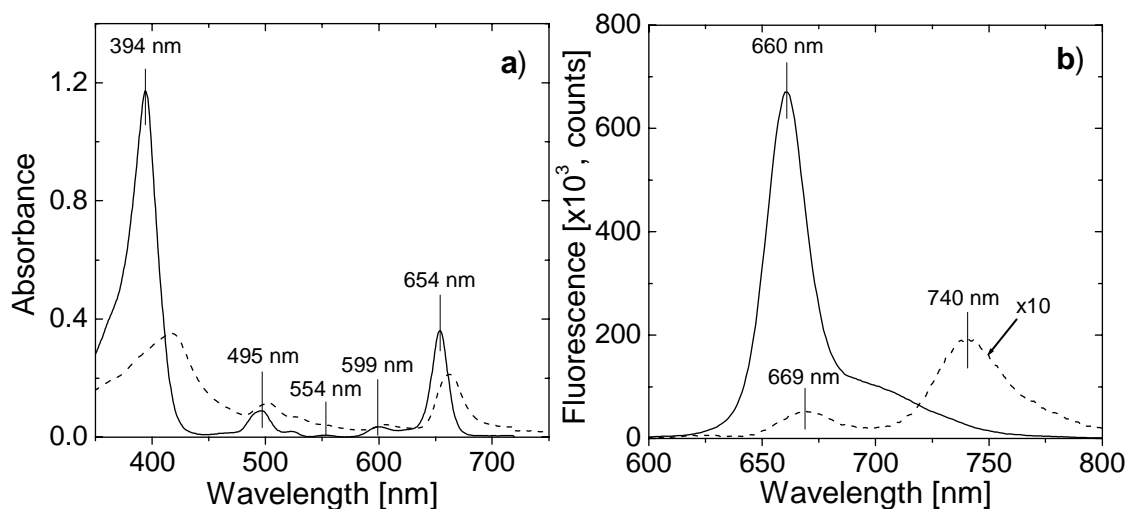


Fig. 3.13. a) - absorption spectra of ChlC9 in MeOH (—) and in aqueous solution (PBS, ---). In PBS, ChlC9 shows broadened and red-shifted absorption bands as compared in MeOH. b) – emission spectra of PpeC9 in MeOH (—) and in PBS (---). Excitation – 514 nm. The emission quantum yield is decreased in the solution without detergent by a factor of ~30 as compared to that in MeOH. The spectral changes in the absorption spectrum, the appearance of a new emission band at 740 nm and the significant decrease of the emission quantum yield are indicative for strong aggregation of ChlC9 in aqueous solutions. The concentration of ChlC9 was in all cases 5 μ M.

band with the maximum at 418 nm and broadened all four Q-bands being shifted by ~5-7 nm to the red with respect to the corresponding absorption bands of the monomers. Addition of MeOH to the solution resulted in a decreased red shift and narrowed absorption bands. At MeOH amounts of > 40 % vol./vol. the absorption spectrum changed toward the monomer spectrum and remained unchanged upon further increase of MeOH concentration.

The emission spectrum of the ChlC9 in MeOH consists of an emission band positioned at 660 nm and a shoulder at 706 nm (Fig. 3.13b, solid line). In aqueous solution, the fluorescence spectrum exhibits a weaker band peaking at 669 nm and a more intensive band with the maximum at 740 nm (Fig. 3.13b, dashed line). The fluorescence quantum yield in aqueous solution was decreased by a factor of 30 as compared to that in MeOH.

Such spectral changes, *i. e.* broadening and shifting of absorption bands as well as significant decrease of the fluorescence quantum yield, are characteristic for the self-association of the molecules. From the results presented above it can be supposed that all compounds investigated are self-associated in aqueous solutions.

It has been shown for other porphyrins that formation of ‘sandwich’-type or ‘face-to-face’ aggregates results in similar spectral changes as presented above [125,127,128]. The formation of aggregates of this kind may therefore also be supposed in the case of the pyropheophorbide molecules. Larger, micelle-like structures may also be formed as it has been suggested by other authors [42,129].

3.2.2. Time-resolved fluorescence measurements in homogenous solution

To better identify characteristic properties of aggregates, the energy relaxation kinetics of the sensitizers was studied by means of time-resolved fluorescence measurements.

Because the formation of fluorescent photoproducts upon irradiation could falsify the time-resolved fluorescence measurements, the photochemical stability of the pyropheophorbide-a derivatives used, PpeC6 and PpeC9, and of the chlorin e6 derivative, ChlC9, were tested. In homogenous solutions, no influence of the irradiation on the decay kinetics could be observed.

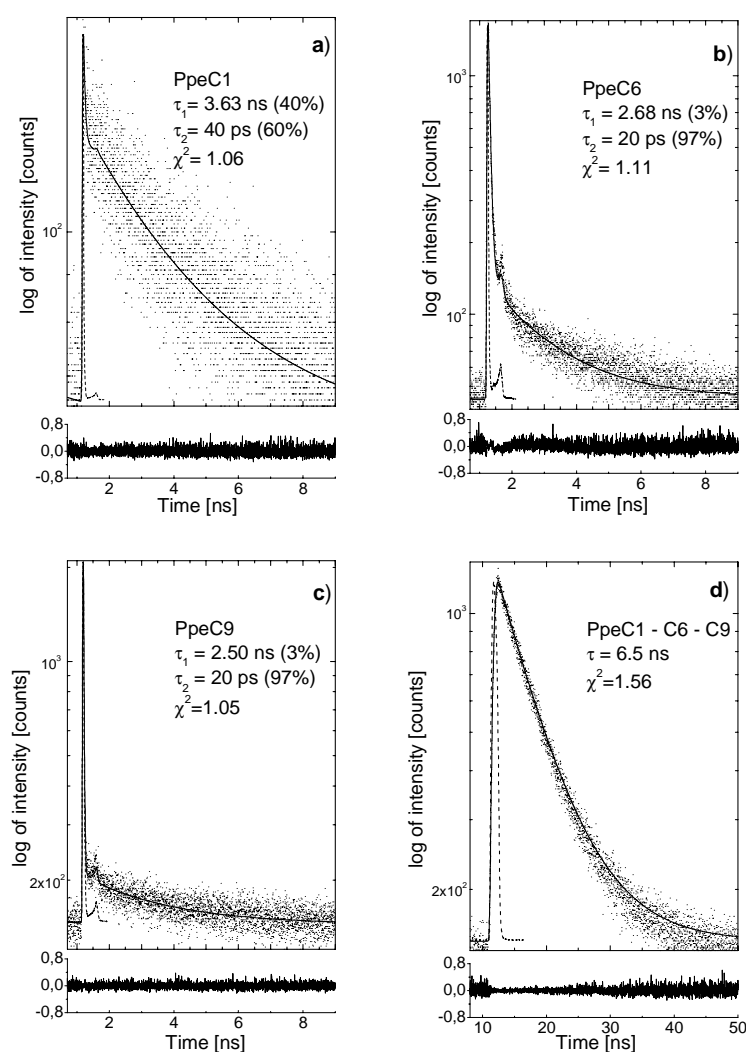


Fig. 3.14. Fluorescence relaxation kinetics of Ppe derivatives PpeC1, PpeC6, PpeC9. a) – PpeC1 in PBS; b) – PpeC6 in PBS; c) – PpeC9 in PBS. A biexponential decay law was fitted to the fluorescence decay to with the time constants and relative amplitudes given. d) - fluorescence relaxation kinetics of all three compounds in MeOH. A monoexponential decay law was fitted to the fluorescence kinetics. The solid lines represent the fitted function, the instrumental response function is shown by the dashed line, dots represent the experimental data. The fluorescence was excited in all cases at 400 – 405 nm, detection - >700 nm. Concentration was in all cases 5 μ M. The residuals are shown in the graphs below. The second weaker peak seen in the data and the fitted curve at ~1.5 ns is caused by the shape of the IRF, which is accounted for in the deconvolution procedure.

Ppe derivatives with alkyl side chains of different lengths were investigated. The fluorescence kinetics measured in PBS solution at 710 ± 10 nm for methyl and hexyl compounds are depicted in Fig. 3.14a,b. The relaxation kinetics of nonyl is presented in Fig. 3.14c. The results are summarized in Table IV.

The most lipophilic compounds investigated, PpeC6 and PpeC9, exhibit in PBS solution a two-exponential fluorescence decay with time constants of

Table IV. Excitation relaxation parameters of the investigated Ppe derivatives in PBS solution. $\lambda_{exc}=400$ nm

| Substance | λ_{em} , nm | τ_1 , ns | τ_2 , ps | A_1 | A_2 | Ampl. Ratio | χ^2 |
|-----------|---------------------|---------------|---------------|-------|-------|-------------|----------|
| C1 | 660 | 3,8 | - | 1,00 | - | - | 1,04 |
| C3 | | 3,15 | - | 1,00 | - | - | 1,45 |
| C5 | | 3,02 | - | 1,00 | - | - | 1,64 |
| C6 | | 3,78 | 130 | 0,66 | 0,34 | 0,02 | 1,44 |
| C9 | | 3,43 | 10 | 0,03 | 0,97 | 0,09 | 1,05 |
| C1 | 710 | 3,63 | 40 | 0,40 | 0,60 | 0,02 | 1,06 |
| C3 | | 2,77 | 60 | 0,16 | 0,84 | 0,12 | 1,23 |
| C5 | | 2,22 | 30 | 0,02 | 0,98 | 0,54 | 1,71 |
| C6 | | 2,68 | 20 | 0,03 | 0,97 | 0,23 | 1,23 |
| C9 | | 2,64 | 20 | 0,02 | 0,98 | 0,37 | 1,04 |

$\tau_1=2.5 - 2.7$ ns and $\tau_2= 20$ ps at 710 nm. The decay turns into a monoexponential process in methanol with a time constant of 6,5 ns (Fig. 3.14d), which is common for all three derivatives. In methanol only the monomeric form of the sensitizer exists. Thus, the decay time of 6.5 ns can be assigned to the fluorescence decay of the monomeric form.

The relaxation decay time obtained for Ppe in methanol agrees with the decay kinetics reported for the unmodified monomeric pyropheophorbide a (6.5 ns, [35]). The fluorescence decay times reported for monomeric mesoporphyrin, hematoporphyrin and protoporphyrin (~14 ns) [125,126] differ strongly from those obtained for the Ppe derivatives. This difference can be caused by the structure of the pyrrolic ring of the molecules, namely the number of the double bounds in the pyrrolic ring is reduced by 1 in the case of Ppe and Chl as compared with the porphyrin molecules.

The short-lived decay component of ~20 ps observed for PpeC6 and PpeC9 in aqueous solutions at 710 nm can be attributed to highly aggregated sensitizer species. The shortening

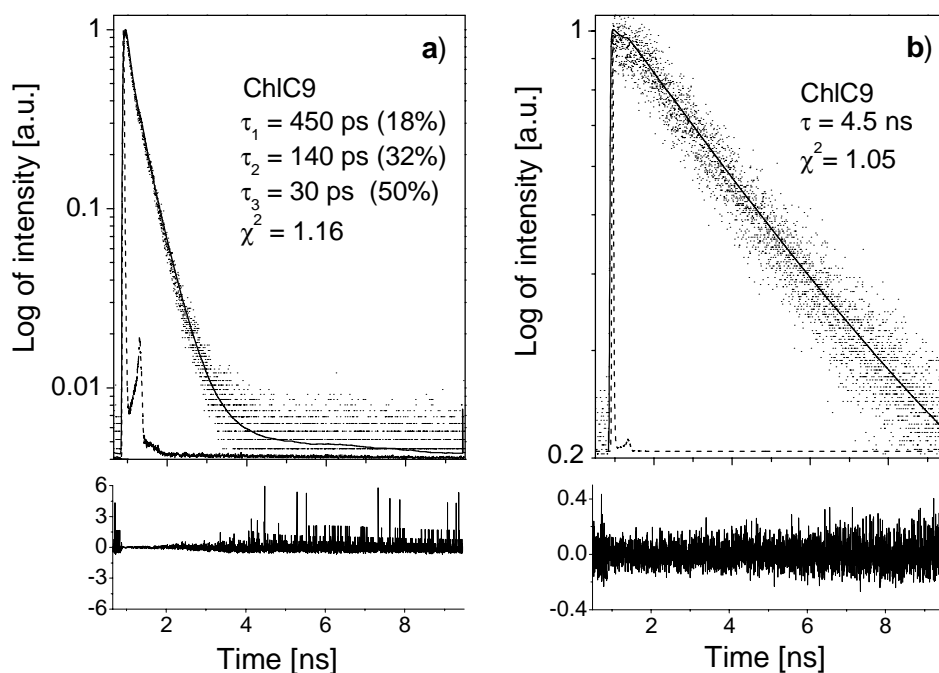


Fig. 3.15. Fluorescence relaxation kinetics of ChlC9 derivative in: a) PBS and b) MeOH. In PBS, a triexponential decay law was fitted to the fluorescence relaxation with time constants and relative amplitudes given. In MeOH ChlC9 exhibited a monoexponential decay character. The fluorescence was excited at 400 nm with 120 fs pulses. Detection > 700 nm. Concentration was in both cases 5 μ M.

of the lifetime of the excited energy level in aggregates arises from intermolecular interactions between individual molecules within aggregates, which causes a broadening of the energy levels and a shortening of their lifetimes. Previous studies on the energy relaxation kinetics of aggregated porphyrins revealed a fast component of ~100-300 ps, which has been assumed to originate from highly aggregated sensitizer species [28,37,51]. The difference in the decay rate reported earlier and those measured in this study can arise from different molecular structures of the compounds and the lower temporal resolutions of the former measurements.

The long-lived component of ~3 ns observed for PpeC1, PpeC6 and PpeC9 in aqueous solutions at 660 nm and 710 nm can be assigned to weaker aggregated species, such as dimers, trimers and oligomers. A similar fluorescence decay constant was obtained for other porphyrins and was ascribed to dimeric species [126]. However, in a later study a decay time of about 8 ns was reported and attributed to dimeric species of the porphyrins as well [130]. Therefore, the origin of the decay component with 3 ns lifetime measured for Ppe still remains unclear. On the other hand, a comparable fluorescence decay time of ~3.5 ns was obtained for the less lipophilic PpeC1 compound in aqueous solution. PpeC1 exhibits a monoexponential decay in both PBS solution and methanol, however, the decay time is by a

Table V. Fluorescence decay times of ChlC9 in aqueous solution as a function of MeOH amount. Excitation was performed at 400 nm, the emission was detected at 740 nm.

| Amount of MeOH (v./v. %) | Attributed species | τ_1 (A ₁) | τ_2 (A ₂) | τ_3 (A ₃) |
|--------------------------|---------------------------------|-------------------------------|-----------------------------|----------------------------|
| 0.1 | Aggregates | 0.3 - 0.5 ns (5%) - (20 %) | 80 - 220 ps (30 - 45 %) | 30 - 40 ps (50 %) |
| 20 - 50 | Partially disaggregated species | 0.5 - 3.4 ns (20%) (5 %) | 140 - 350 ps (30 - 45 %) | 30 - 40 ps (50 %) |
| 60 | | 4.2 - 4.5 ns (50 - 60)% | - | 40 - 50 ps (50%) (40%) |
| > 60 | Monomers | 4.5 ns (100 %) | - | - |

factor of ~ 2 shorter in PBS than in methanol (6.5 ns). This indicates, that PpeC1 self-associates in aqueous solution forming aggregates which are weaker associated than those of the more lipophilic PpeC6 and PpeC9. The monoexponential fluorescence decay with the shortened fluorescence lifetime measured for PpeC1 in PBS at 660 nm can be explained by a weaker aggregation degree as compared to the more lipophilic compounds PpeC6 and PpeC9, which exhibit a biexponential fluorescence decay with a short-lived component. The absence of short decay component indicates that highly associated species are not formed. This parallels the assumption made regarding the long-lived decay component of ~ 3 ns.

The fluorescence decay of ChlC9 measured at 740 nm in aqueous solution exhibited a tri-exponential character with time constants of $\tau_1=450$ ps, $\tau_2=140$ ps and $\tau_3=30$ ps (Fig. 3.15a). In a 100% MeOH solution the fluorescence decay was monoexponential with a time constant of 4.5 ns (Fig. 3.15b).

To examine the formation of self-associated sensitizer species, the fluorescence decay kinetics of ChlC9 were measured in aqueous solution containing different amounts of MeOH at an emission wavelength of 740 nm. The results are summarized in Table V. The fluorescence relaxation kinetics of ChlC9 exhibited a three exponential decay in aqueous solution. A single-exponential decay with a time constant of ≈ 4.5 ns was obtained for monomeric ChlC9 in pure MeOH. A partial disaggregation of the aggregates was observed

when the amount of MeOH in aqueous sensitizer solution was increased from 0.1 % vol./vol. to 60 % vol./vol. The slowest decay time τ_1 as well as its amplitude increased significantly upon the addition of MeOH. Complete monomerization was observed when the amount of MeOH in aqueous solution exceeded ~ 60%.

The short decay time $\tau_3 = 30 - 40$ ps is also present. Its amplitude $A_3 \sim 50\%$ is lower in comparison to ~ 80-95% measured at 660 nm wavelength (not shown), and the fractional contribution $f_i = \tau_i A_i$ of the slower decay times τ_1 and τ_2 at 740 nm are slightly increased in comparison to 660 nm. This implies the presence of the two different types of ChlC9 aggregates, type 660 and type 740, with different aggregation strength. All further fluorescence kinetics measurements were carried out at 740 nm wavelength in order to avoid reabsorption effects.

In summary, the results obtained from the fluorescence kinetics measurements point to the self-assembly of all derivatives investigated in aqueous solution. The degree of aggregation increases with the increasing lipophilicity of the molecules. The presence of aggregates demonstrated in the stationary studies parallels the identification of aggregates carried out by the measurements in the time domain. The results of the time-resolved fluorescence measurements correlate with those of the steady-state measurements, providing a basis for the identification of aggregated sensitizer species inside cells with high sensitivity.

3.2.3. Investigations on interaction of the sensitizers with biological membranes

The interaction of aggregated sensitizers with biological membranes is one of the essential factors influencing the uptake, intracellular distribution and photodynamic efficacy of sensitizers. The aim of the following experiment was to determine the degree of sensitizer aggregation, i. e. a quantification of the aggregation strength with regard to the ability of biological membranes to monomerize them.

The monomerization rates of the sensitizers were examined using isolated membranes of erythrocytes ('ghosts'). The sensitizers were incubated in a PBS solution containing ghosts and the fluorescence intensity was measured as a function of the incubation time. At 24 hours after incubation start the erythrocytes ghosts were extracted from the solution by centrifugation (15000 rpm, 25 min) and resuspended in PBS. The complete monomerization of the sensitizers was achieved by adding 1% vol./vol. Triton X-100 to the resuspended erythrocytes and to the supernatant. The monomerization degree was determined by calculating the ratio between the fluorescence intensities measured before and after addition of Triton X-100. The results obtained are summarized in Table VI. The monomerization

Table VI. Monomerization kinetics of the sensitizers incubated with biological membranes (erythrocyte ghosts). The lipophilicity is given as log of the octanol-water partition coefficient P. The relative amounts of the monomerized photosensitizers at 6 and 24 hours are given (see Fig. 1.6). a) ref. [64] b) ref. [137], c) theoretical calculations (see Appendix for details).

| Sensitizer | logP | Monomerized sensitizer fraction (%) | |
|------------|-------------------|-------------------------------------|----------|
| | | 6 hours | 24 hours |
| PpeC1 | 3.1 ^{a)} | 91 | 91 |
| PpeC6 | 5.5 ^{a)} | 54 | 83 |
| PpeC7 | 6.1 ^{a)} | 37 | 63 |
| PpeC9 | 7.1 ^{a)} | 11 | 22 |
| mTHPC | 9.4 ^{b)} | 35 | 62 |
| ChlC9 | 8.5 ^{c)} | 50 | 53 |

process was quantified by calculating the relative amount of the monomerized PS at 6 hours and at 24 hours after the incubation start (see also Fig. 1.6).

The monomerized fraction decreased within the Ppe series with increasing lipophilicity (logP) (Table VI). However, the amount of monomeric species in erythrocyte membranes was found to be significantly higher for the more lipophilic tetra(m-hydroxyphenyl)chlorin (mTHPC, logP 9.4) as compared to that of the less lipophilic PpeC9 (logP 7.1). The monomerization amount observed for mTHPC is comparable to that of the much less lipophilic PpeC7 (logP 6.1). A similar relation was observed for ChlC9 (logP 8.5), which at 6 hours after incubation exhibited a higher amount of monomeric species than the less lipophilic PpeC9 and PpeC7. At 24 hours after incubation, however, it was monomerized to a lesser extent than PpeC7. This implies that the degree of aggregation of PS which belong to different classes (such as e.g. chlorins and porphyrins), is determined in a biological sense not only by the lipophilicity but also by structural properties of PS molecules.

The PpeC6 and PpeC7, which have been found to exhibit the highest photodynamic efficacy *in vivo*, show a relatively fast monomerization at 6 hours after incubation with a much slower increase of the amount of monomers up to 24 hours. A ‘steady-state’ was not observed. In contrast, mTHPC, which possess only a low tumor selectivity [138], exhibit similar kinetics up to 6 hours, but reaches a ‘steady-state’ at ~ 10 hours of incubation (not shown). PpeC9 exhibit a significantly lower monomerization (no ‘steady-state’ during the entire incubation), whereas the less lipophilic PpeC1 is monomerized much faster. It is

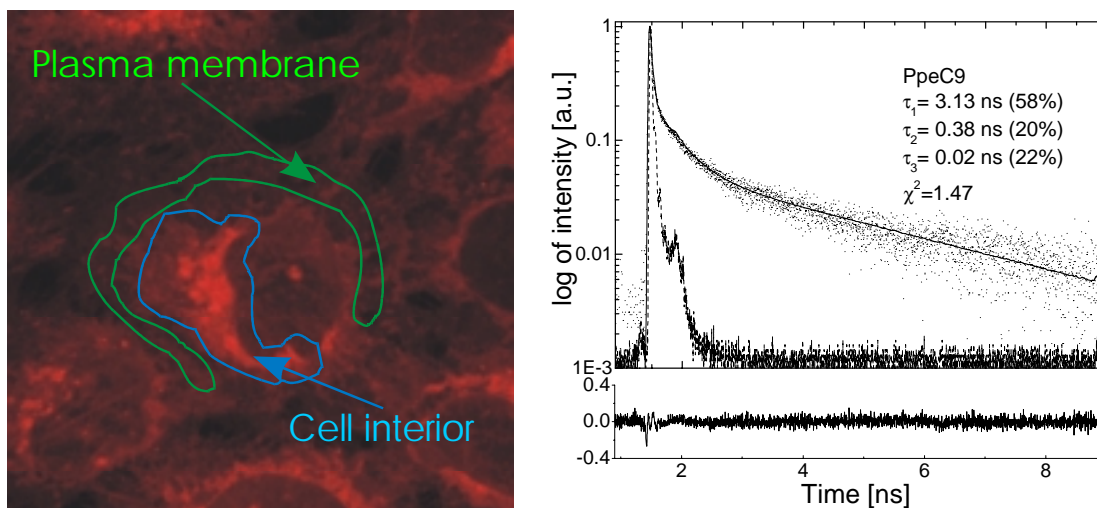


Fig. 3.16. a) - intracellular regions where the fluorescence kinetics were measured. b) - fluorescence relaxation kinetics of PpeC9 in A431 cells measured at 9 h after incubation in the cell interior with the plasma membrane region being excluded from detection. The kinetics were best fitted to a tri-exponential decay law with time constants and relative amplitudes given. Excitation was performed at 800 nm with 120 fs pulses. Emission was detected at 650 – 720 nm.

obvious that the monomerization kinetics of the PS investigated exhibiting significantly different photodynamic efficacy *in vivo* differ also significantly. Thus, the suppose, that the monomerization kinetics of PS in biological membranes can be used as a biological measure for the photodynamic efficacy of PS.

3.2.4. Time-resolved fluorescence measurements in tumor cells

3.2.4.1. Derivatives of pyropheophorbide a ether

In order to investigate the uptake and the aggregation/disaggregation in living cells, time-resolved fluorescence measurements were conducted *in vitro* in different regions of interest in cells (Fig. 3.16a). After the incubation cells were rinsed twice with PBS, and the fluorescence decay was measured for PpeC9 in the cell interior (Fig. 3.16b). The fluorescence relaxation in the region of the plasma membrane (Fig. 3.17a) at 2 h 30 min after incubation could be best fitted to a two-exponential decay law with time constants of 1.1 ns and 30 ps. The kinetics changed to a three-exponential time course (time constants: 5 ns, 400 ps, and 20 ps) after prolonged incubation at 9 h (Fig. 3.17b). The short-lived decay component corresponds to that found in PBS solution (~20 ps, s. Fig. 3.14c).

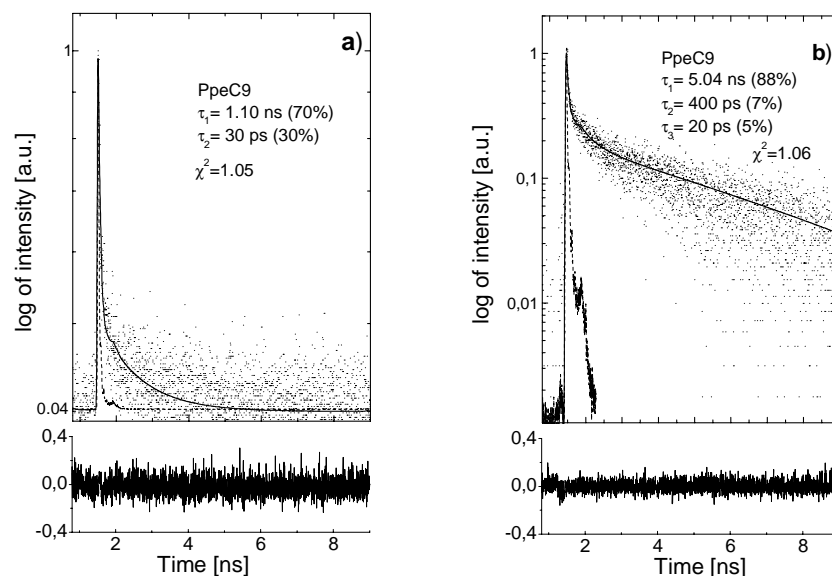


Fig. 3.17. Excitation relaxation kinetics of PpeC9 in the plasma membrane of A431 cells. a) at 2 h 30 min after incubation; b) at 9 h after incubation. The concentration of sensitizer was $5\mu\text{M}$. The fluorescence was excited by two-photon absorption at 800 nm. $\lambda_{\text{em}}=650 - 720$ nm. The solid line represents the theoretical fit, dashed line – instrumental response function

No fast (< 50 ps) fluorescence decay component was observed for the less lipophilic PpeC6 compound, when fluorescence kinetics were measured at distinct cellular regions at different incubation times (3.18a). Since it is known, that the porphyrin molecules may bind covalently and non-covalently to certain kinds of biomolecules (proteins and lipids) [30,131,132], changes of the fluorescence kinetics due to the interaction with intracellular components have to be considered. In other words, if the shortest decay measured for C9 within cells ($\sim 20\text{-}30$ ps) results from the interaction with cellular components, a comparable (< 100 ps) fluorescence decay time should occur for PpeC6 compound as well. As this is not the case, the shortest fluorescence relaxation component seems not to be caused by covalent bond of sensitizer molecules to intracellular biomolecules. In addition, the fluorescence kinetics obtained for TPPS₄ in cells exhibits no such a short component (Fig. 3.18b), but shows two decay constants similar to those measured for PpeC9 in the cell interior after longer incubation. On the other hand, in case of non-covalent interaction of PpeC9 molecules with cellular components, the interacting PpeC9 and the lipid or protein molecules should be situated at least as near to each other as the PpeC9 molecules in the aggregates in order to interact strong enough and open an additional fast energy decay channel with a time constant of ~ 30 ps. Since it is difficult to expect that such a strong non-covalent interaction between the sensitizer molecules and cellular components can contribute to a great extent to the overall interaction process, the shortest decay component measured for PpeC9 can only be attributed

Table VII. Fluorescence decay times (τ_i) and their relative amplitudes (A_i , given in parenthesis in per cent) of Ppe derivatives in A431 cells. Excitation was performed at 800 nm with 120 fs pulses. Emission was detected at > 700 - 750 nm.

| Incubation time (hours) | τ_1 (A_1) | τ_2 (A_2) | τ_3 (A_3) |
|-------------------------|------------------------------|---------------------------|-----------------------------|
| PpeC6 | | | |
| 2 | 2 - 5 ns (25 - 40 %) | - | 70 - 180 ps (75 %) (60%) |
| 6 | 5.7-6.5 ns (100 %) (98 %) | 260 ps (2 %) | - |
| PpeC9 | | | |
| 2 | 2 ns (2 %) | 180 ps (8 %) | 20 - 25 ps (90 %) |
| 5 - 6 | 3.6 - 5.5 ns (4 - 25 %) | 210- 600 ps (6 - 25 %) | 20 - 50 ps (90%) (50 %) |

to the aggregated species of the sensitizer. From the above it is obvious, that aggregates of PpeC9, the most lipophilic compound investigated, are present in the cell interior.

The longer decay times in the order of some 100 ps obtained for PpeC9 at 2 h 30 min after incubation can be ascribed to weaker associated aggregates or to weak association of sensitizer molecules to intracellular components, as shown for hematoporphyrin derivative [30,132]. While the shortest component remains nearly constant over the entire incubation time, the slower part of the fluorescence decay changes with the increasing incubation time, resulting in two decay constants of ~ 5 ns and 0.4 ns at 9 h after incubation. These decay times are similar to those measured for PpeC6 derivative after 6 h 30 min incubation (6.7 ns and ~ 0.3 ns, Fig. 3.18a), and can be ascribed to both monomerized and bound fractions of the sensitizer. The increasing fractional contribution and the decay times of the long-living compounds of PpeC9 with the incubation time point to a monomerization of the aggregated sensitizer in cells.

The fractional contribution of the short decay component of PpeC9 to the fluorescence signal in the plasma membrane decreases from 30% at 2 h 30 min after incubation to about 5% at 9 h (Fig. 3.17). The amount of the aggregated species decreases more slowly inside the cell as compared to the plasma membrane. Here, the short component contributes to 22% to the entire fluorescence at 9 h after administration with the sensitizer (Fig. 3.16b). This points to a higher concentration of aggregated species inside the cell for the PpeC9 compound. The difference in the amounts of the aggregated species in the plasma membrane and in the cell

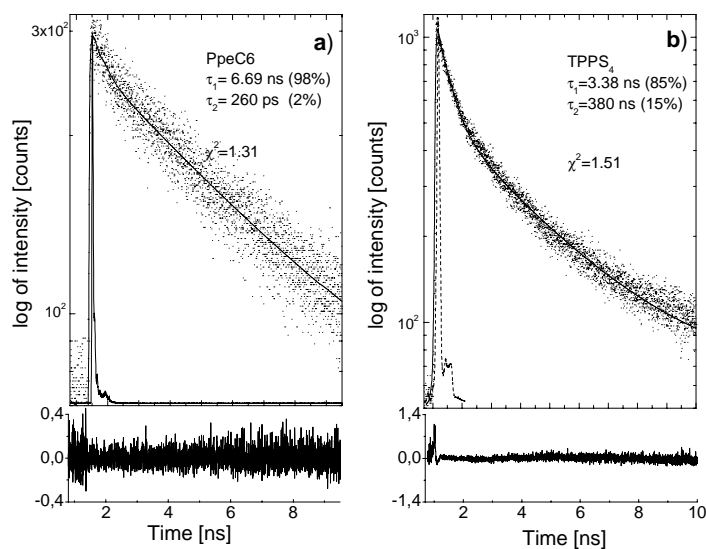


Fig. 3.18. Fluorescence decay kinetics of a) PpeC6 in A431 cells (whole-cell detection), incubation – 6 h 30 min and b) TPPS₄ in A431 cells (whole-cell detection), incubation – 4 h 15 min. A two-exponential decay was fitted to the decay kinetics. The time constants and the relative amplitudes are given in graphs. The residuals are shown in the graphs below. Excitation was at 430 nm, emission was detected between 650-720 nm.

interior (perinuclear region) may result from the endocytotic uptake of the PpeC9 compound. The results of PpeC6 and PpeC9 measurements are summarized in Table VII.

3.2.4.2. Chlorin e6 derivatives

Fluorescence kinetics observed in cells incubated with ChlC9, are shown in Fig. 3.19. The fluorescence decay measured in the cytosol was best fitted to a triexponential decay law (see Table VIII).

Interestingly, the shortest fluorescence decay time τ_3 , ($40 \text{ ps} \leq \tau_3 \leq 75 \text{ ps}$), was present over the entire period of incubation. The presence of the short-lived decay component indicates the internalization of ChlC9 aggregates by the A431 cells.

Furthermore, it can be shown that the aggregates could not be sufficiently monomerized by the cells. The slowest fluorescence decay constant τ_1 remained below that of the monomers (s. Table VIII) during the incubation period and its amplitude did not exceed 40% - 50%. Washing the cells and replacing the aqueous medium with MeOH resulted in the disappearance of the triexponential decay and occurrence of a monoexponential relaxation with a decay time comparable to that of the monomeric form, $\tau = 4.6 \text{ ns}$ (Fig. 3.19b). The slow increase in the decay times τ_1 , τ_2 , τ_3 during the incubation period indicated only a restricted, partial disaggregation of the internalized aggregates of the lipophilic ChlC9. This is

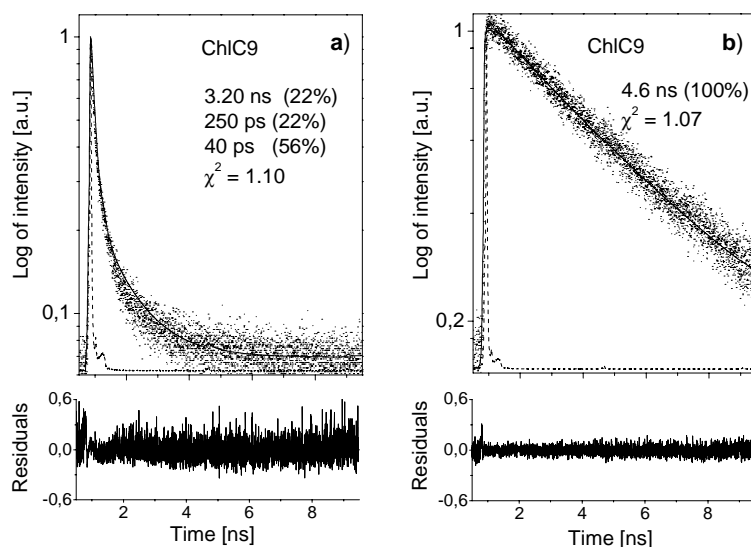


Fig. 3.19. a) Fluorescence relaxation kinetics of ChlC9 in A431 cells measured at 3 h after incubation start. The decay could be best fitted to a triexponential decay law with time constants $\tau_1=3.2$ ns (22%), $\tau_2=250$ ps (22%), and $\tau_3=40$ ps (56%).

b) fluorescence relaxation kinetics of ChlC9 in A431 cells with MeOH added. The decay could be best fitted to a monoexponential law with a time constant of $\tau_1 = 4.6$ ns. The concentration of the sensitizer was $5\mu\text{M}$, excitation was performed with 120 fs pulses at 430 nm, detection was at >710 nm.

in contrast to the complete monomerization observed for the amphiphilic PpeC6. It has been shown that amphiphilic PpeC6 is a very effective sensitizer, whereas PpeC9 exhibits a considerably reduced tumor response [20]. This can be explained nicely on the basis of the results presented here. The aggregates of PpeC9 and ChlC9 can be taken up by the tumor cells, but they can not be sufficiently monomerized to become photodynamically active.

Table VIII. . Fluorescence decay times τ_i and the corresponding relative amplitudes A_i (given in % in parenthesis) of ChlC9, measured in A431 cells in the wavelength interval of 700 – 760 nm. The cells were incubated for the indicated incubation times with a sensitizer concentration of $5\mu\text{M}$ at 37°C and washed with PBS prior to measurements. Fluorescence was excited by TPE (PpeC6 and PpeC9) at 800 nm or by OPE (ChlC9) at 430 nm using ~ 120 fs laser pulses.

| Incubation time (hours) | τ_1 (A_1) | τ_2 (A_2) | τ_3 (A_3) |
|--|-----------------------------|-----------------------------|----------------------------|
| 1 - 2 | 2.8 - 3.3 ns (15 - 50 %) | 250 - 330 ps (25 %) | 40 - 75 ps (60%) (25%) |
| 2 - 3 | 3.2 - 3.3 ns (20 - 40 %) | 240 - 280 ps (20 - 30 %) | 40 - 45 ps (30 - 60 %) |
| 3 - 6 | 3.1 - 4.3 ns (15 - 40 %) | 270 - 450 ps (20 %) | 70 - 75 ps (70%) (40 %) |
| 10 min after addition of MeOH to the washed cells (6 h inc.) | 4.6 ns (100 %) | - | - |

3.2.5. Investigation on the uptake kinetics and subcellular localization patterns of PS in tumor cells

To investigate the structure-property relationship of the pyropheophorbide a and chlorin e6 derivatives in tumor cells, measurements on the uptake kinetics and subcellular localization were conducted.

3.2.5.1. Derivatives of pyropheophorbide a ether

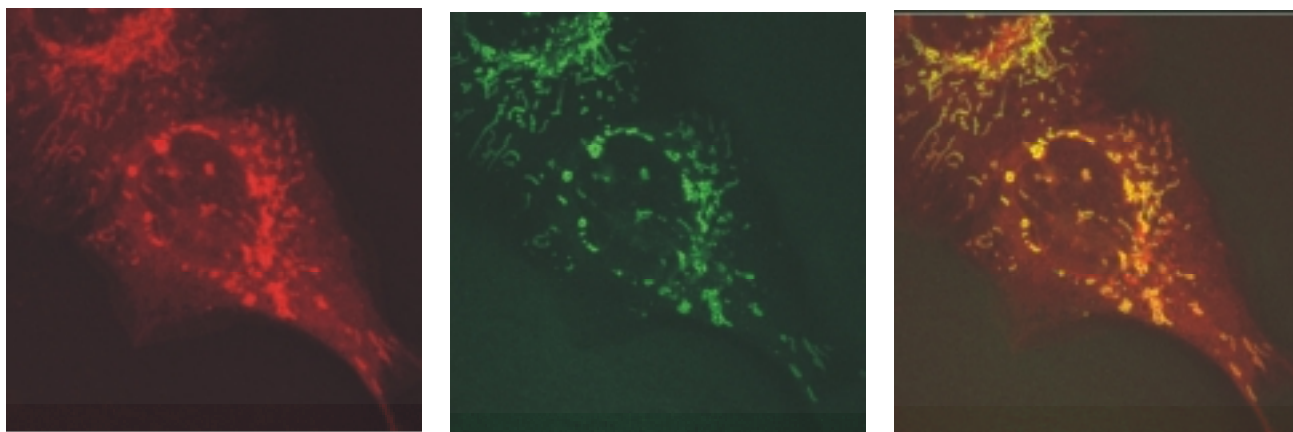
The cells of the human epidermoid carcinoma cell line (A431) were used for the experiments. Cells were administered with 5 μ M PpeC1, PpeC6 and PpeC9 derivatives for different times. Fluorescence was excited with 488 nm Ar⁺ laser line. The fluorescence was detected with a set of fluorescence filters, which transmitted light at wavelengths longer than 650 nm. As can be seen in the case of the most hydrophilic compound PpeC1 a strong fluorescence signal was detected at 10 min after incubation (Fig. 3.20). The cells administered with PpeC6 and PpeC9 compounds showed a weaker fluorescence signal at 3 and 5.5 h after incubation, respectively. This correlates with the disaggregation kinetics observed in erythrocyte ghosts, where the most hydrophilic compounds PpeC1..C3 were monomerized much faster than the more lipophilic ones (PpeC6...C12).

The cells were additionally co-incubated with 50 nM of the mitochondria marker MitoFluor Green (Molecular Probes Inc., Eugene, Oregon, USA). This allowed for a better visualization of the mitochondria and co-localization with the sensitizer.

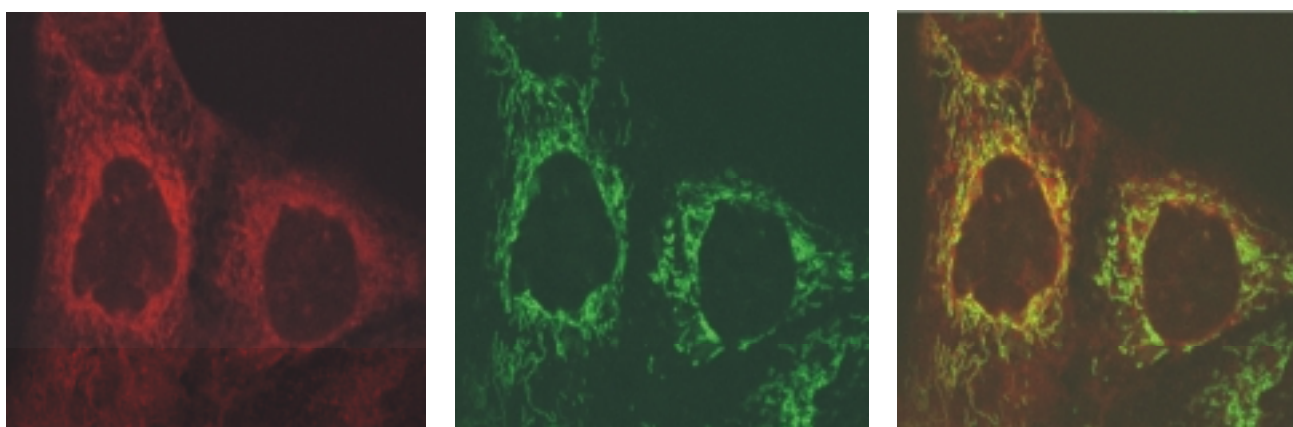
As can be seen (Fig. 3.20), the cellular localization patterns also differ for all compounds used. Besides the strong fluorescing areas the PpeC1 distributes diffuse in the cell. Unlike PpeC1, the most lipophilic PpeC9 exhibits exceptionally a point-like, endosomic/lysosomal localization pattern (see the weakly fluorescent red points in Fig. 3.20), while the C6 represents an intermediate case, being localized both in the cytoplasm as well as at the mitochondria and lysosomes.

The diffuse distribution of the fluorescence for the PpeC1 compound in A431 cells can be explained in two ways: i) internalization of PpeC1 can be mediated via passive diffusion through the plasma membrane, resulting in the diffuse distribution of the monomerized sensitizer over the entire cell. As the Ppe molecule possesses affinity for both the lipid media and aqueous solution (due to the non-symmetrically distributed charge and the lipophilic alkyl side chain on the opposite sides of the molecule), it may be incorporated in the

C1 , $t_{inc.} = 10 \text{ min}$



C6 , $t_{inc.} = 3 \text{ h}$



C9 , $t_{inc.} = 5,5 \text{ h}$

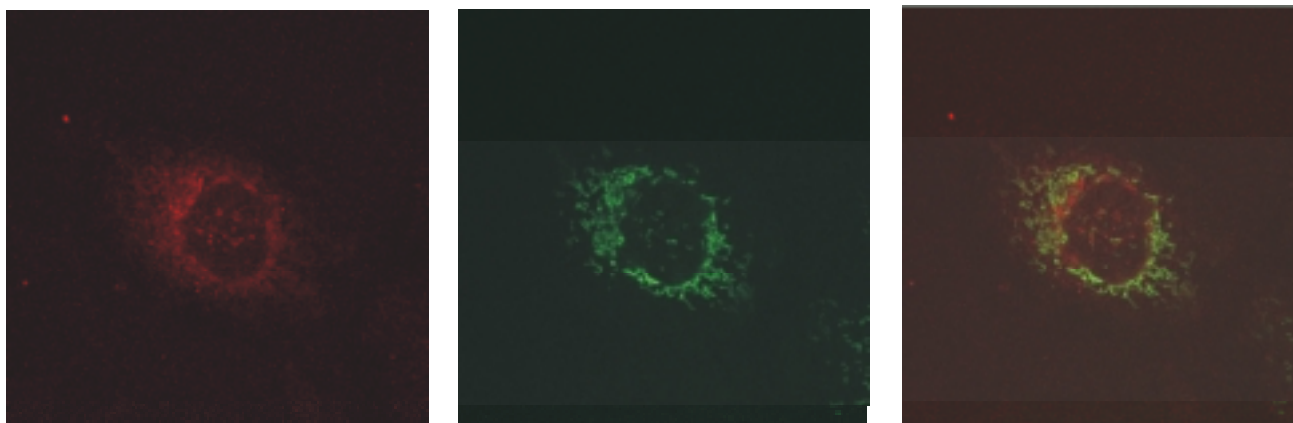


Fig. 3.20. Uptake kinetics and subcellular localization patterns of Ppe methyl (C1; first line), hexyl (C6; middle line) and nonyl (C9; lower line) in A431 cells. Left column – fluorescence of the compounds detected between 650 – 750 nm, middle column – fluorescence (detected at 505-550 nm) of the mitochondrial marker MitoFluor Green, incubated for 20 min, right column – overlay of both channels. The concentration of the sensitizers was 5 μM in all three cases. The uptake kinetics and localization patterns shows clear differences depending on the lipophilicity of the compound.

aqueous-lipid barrier. Owing to the fast monomerization in the plasma membrane, the sensitizer molecules may penetrate the plasma membrane and further distribute diffusely in the cytoplasm. ii) the diffuse fluorescence distribution of PpeC1 accumulation may also be mediated by the endocytotic uptake and the subsequent release of the internalized monomers from the endocytic vesicles into the cytoplasm. The weak endo-/lysosomal localization of PpeC1 in cells indicates, that this pathway plays only a minor role in the internalization process. In contrast to PpeC1, the endocytosis seems to be more pronounced in the uptake of the most lipophilic compound PpeC9. This can be concluded from the exceptional endosomic/lysosomal intracellular localization pattern and the absence of a diffuse distribution in the cytoplasm of this compound. From the above it may be concluded, that the internalization pathway strongly depends on the lipophilicity of the sensitizer.

3.2.5.2. Chlorin e6 derivatives. Fluorescence lifetime imaging (FLIM, τ - imaging)

To obtain information on how the aggregates of the sensitizers are internalized by tumor cells, the uptake of ChlC9 was observed using LSM and FLIM. The high resolution lifetime imaging allows for the measurement of the fluorescence kinetics in each pixel of the fluorescence image. The τ -images of the cells incubated with ChlC9 for 2h are presented in Fig. 3.21a-c. Three different time windows ((a)10 - 100 ps, (b)100 ps - 1 ns, and (c) 1 ns - 10 ns are shown. The bright point-like structures seen in Fig. 3.21a represent the localization of the sensitizer fraction exhibiting the short-lived fluorescence decay component (10 – 100 ps) and are attributable to aggregated species. This was shown by the fitting procedure of the fluorescence kinetics, which revealed a short-lived decay component with a time constant of ~50 - 80 ps and a relative amplitude of 70 - 80 % in the bright points in Fig. 3.21a.

. In the later time intervals (Fig. 3.21b, c) the point-like structures disappear. The fluorescence distribution is more homogenous with some higher intensity in the perinuclear area. The fluorescence kinetics exhibited a mostly bi- or monoexponential character with time constants varying between ~0.5 - 3 ns. These longer decay times measured in the perinuclear area and the cytoplasm provide evidence for the presence of partial disaggregated species of ChlC9.

Comparing cell images obtained using specific lysosomal markers, such as LysoTracker Blue and Acridine Orange (not shown), the point-like structures seen in the time window 10 - 100 ps (Fig. 3.21a) can be attributed to endosomes/endo-lysosomes. This led us

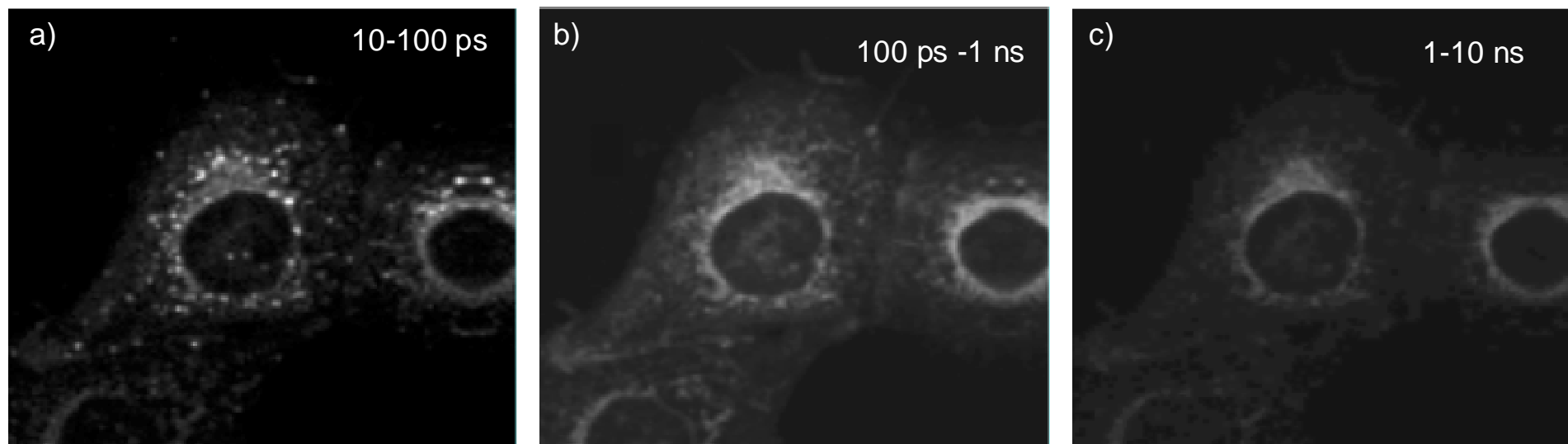


Fig. 3.21. FLIM of A431 cells incubated with ChlC9. The images represent three time windows: 10 - 100 ps (a), 100ps - 1 ns (b), 1ns - 10 ns (c). The bright point-like structures seen in a) represent the localization of the sensitizer fraction exhibiting the short-lived fluorescence decay component (10 - 100 ps) and are attributable to aggregated species. They disappear in the next time windows b) and c). The weaker fluorescent perinuclear area in b) and c) exhibited mostly biexponential decay character with decay constants of $\sim 0.5 - 3$ ns. These longer decay times measured in the perinuclear area and the cytoplasm show the presence of partial disaggregated species of ChlC9. Concentration of the sensitizer was $5\mu\text{M}$, incubation was at 37°C for 2 hours, excitation was performed with 120 fs pulses at 430 nm, detection at > 710 nm.

to suppose that the aggregated species of ChlC9 are most probably internalized via the endocytotic pathway. This suggestion is supported by studies on the endocytotic uptake pathway of tumor cells performed by other authors. It has been found that tumor cells can preferentially internalize nanoparticles and microspheres, e.g. nanoparticles of coated iron oxide [133] and chlorin e6-conjugated microspheres [134]. Furthermore, so-called photochemical internalization [135] is based on the endocytotic internalization of membrane-impermeable macromolecules into the endosomes/lysosomes of cancer cells. In addition, it has been suggested in former studies that phagocytosis is the uptake mechanism of aggregates of the tumor localizing fraction of haematoporphyrin derivative (HpD) [30].

The fluorescence of the partially disaggregated species, Figs. 3.21b and 3.21c, appearing in the vicinity of the point-like structures seen in Fig. 3.21a., indicates that the lysosomes are most probably involved in the disaggregation of the sensitizers, may be due to their “additional” ability to enzymatically degrade a series of macromolecules. Other cellular areas, especially the plasma membrane, exhibit no or only a relatively weak fluorescence at the time of observation. This suggests that disaggregation at the cell membrane and diffusion of monomerized sensitizer species into the cells are less probable. However, this can not be completely excluded for the less lipophilic compounds such as PpeC1...C6, because of their relatively fast monomerization at the plasma membrane (see investigations with erythrocytes Sec. 3.2.3 on p. 64).

The short-lived fluorescence decay component observed for the lipophilic ChlC9 indicates that the highly aggregated portion of the PS is present in the cell throughout the entire incubation time. The relative constant decay time of the short-lived component imply a rigid structure of aggregated ChlC9 species, which cannot sufficiently be disaggregated/monomerized by the interaction with cell compartments/biomolecules or by enzyme actions.

3.5.2.3. Endocytotic uptake in tumor cells

The ability of the neoplastic cells to internalize molecules via endocytosis was examined using latex particles of 100 nm size conjugated with FITC fluorescence marker. A incubation of the tumor cells revealed the presence of latex particles inside cells (see Fig. 3.22a). It shows that particles of up to 100 nm size can be internalized. Because particles of this size cannot cross the outer membrane of cells, endocytosis is the only possible way of

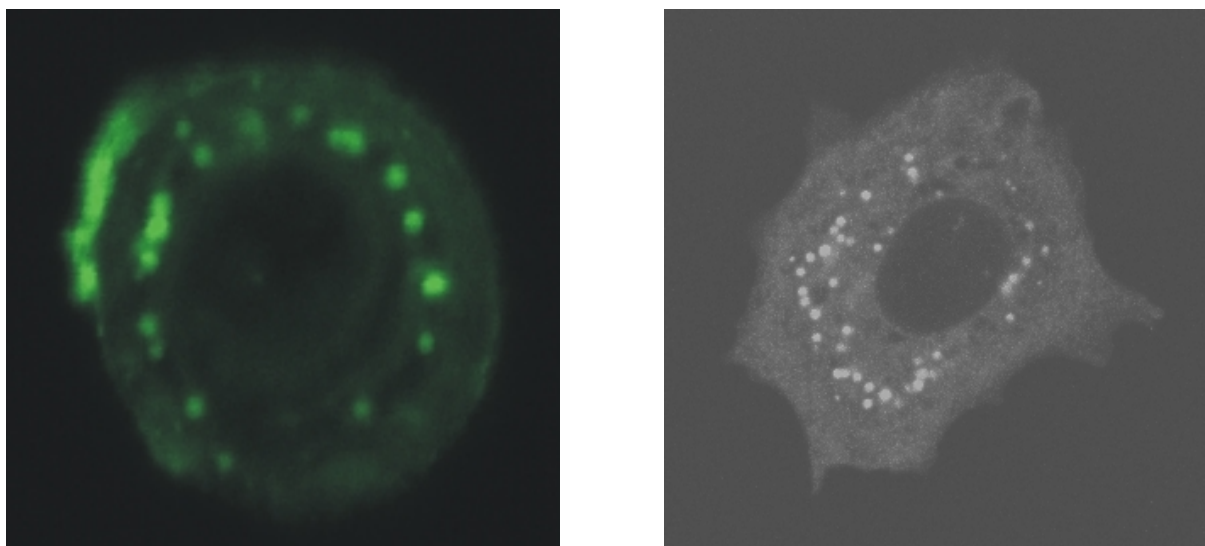


Fig. 3.22. a) - fluorescence image of a cell of HTB-22 line incubated with latex particles of 100 nm size conjugated with the green fluorescing tag FITC. The image represents a z- slice in equatorial plane of the cell. Contributions from the outer cell membrane lying above and below the scan plane are excluded from the image (confocal LSM). Incubation - 1 h, excitation - 514 nm, emission 505 – 550 nm.
 b) – fluorescence image of a HTB-22 cell incubated with PpeC6 for 3 h 20 min. The bright spots imply an endocytotic uptake of the sensitizer. The diffuse fluorescence which is seen in the cytoplasm shows that the sensitizer can also be internalized by passive diffusion through the plasma membrane. Excitation was performed at 800 nm, fluorescence was detected in a wavelength region of 550 – 685 nm.

uptake. The size of aggregates of PpeC9 has been evaluated by means of dynamic light scattering and yielded ~80 – 140 nm.

Fig. 3.22b shows the intracellular fluorescence distribution pattern of PpeC6 in a cell of HTB-22 tumor cell line. The bright spots seen in the figure can be attributed to endosomes. This distribution pattern points to endocytotic internalization of the sensitizer.

3.2.6. Summary and discussion of the results obtained

- The fluorescence relaxation time constants of the monomers, aggregates and weaker associated species of a series of pyropheophorbide a ether and chlorin e6 derivatives were determined.
- The measurements of the fluorescence kinetics indicate, that all derivatives investigated aggregate in aqueous solutions. The degree of aggregation depends strongly on the lipophilicity of the sensitizer, i.e. on the length of the alkyl chain attached to the tetrapyrrolic ring.
- Phospholipid bilayers of the plasma membrane are able to monomerize aggregates of sensitizers.
- Within a congeneric series of the sensitizer, the monomerization is determined by the length of the alkyl side chains and the resulting lipophilicity. In general, the

monomerization is determined by the degree of aggregation, which has to be defined in a biological sense. It is proposed to quantify the degree of aggregation on the basis of monomerization kinetics of a sensitizer at appropriate biological membranes (e. g. erythrocyte ‘ghosts’).

- Two-photon time-resolved fluorescence microscopy proved to be a powerful tool for following the aggregation/disaggregation kinetics of the sensitizer inside living cells with high spatial and temporal resolutions. The measured fluorescence relaxation kinetics *in vitro* enabled the differentiation of aggregates from sensitizer molecules bound to the cellular proteins and lipids, and monomers.
- By means of intracellular time-resolved fluorescence measurements with a temporal resolution of 10 – 20 ps, it was demonstrated that aggregates of the sensitizers can be internalized by tumor cells. The fluorescence decay constants (< 50 ps) of aggregated sensitizers, which were measured in aqueous solutions, were also observed in intracellular regions.
- By means of fluorescence τ - imaging (FLIM) it was directly demonstrated that aggregates of the investigated sensitizers exhibit a point-like distribution pattern in the cell interior. This implies an endocytotic uptake of the aggregated sensitizer.
- Uptake of 100 nm latex beads via endocytosis was observed. In general, it can be supposed that the tumor cells exhibit a more intensive endocytosis, which is caused by their higher metabolism as compared to that of the non-malignant cells.
- It was demonstrated that the degree of aggregation within a congeneric series (Ppe) increases with increasing number of carbon atoms in the alkyl chain. The short-chained (less lipophilic) compounds (PpeC1...C3) show a fast monomerization at the phospholipid bilayer as demonstrated by experiments in erythrocyte ghosts and a fast internalization in tumor cells. In contrast to the short-chained compounds, the long-chained sensitizers (PpeC9...C12) are monomerized only partially, even after longer incubation times. Furthermore, the long-chained compound PpeC9 exhibit only negligible fluorescence in the cytoplasm of tumor cells. It shows a weak point-like fluorescence pattern in the perinuclear area.
- These measurements demonstrate that the endocytosis-mediated internalization increases with increasing length of the alkyl chain. However, the ability of tumor cells to monomerize aggregated sensitizers decreases with increasing chain length. The short-chained sensitizers undergo rapid monomerization and internalization. However, they are

also rapidly cleared from cells [20]. This can explain why the photodynamic efficacy is highest for PpeC6 and PpeC7 at 24 hours after *in vivo* administration.

- In general, it can be concluded that ‘too hydrophilic’ and ‘too lipophilic’ sensitizers have only a limited range of application in PDT. In fact, a maximum of photodynamic efficacy *in vivo* was found for the amphiphilic sensitizers.
- The rapid monomerization of the more hydrophilic short-chained sensitizers (PpeC1-C3) at the plasma membrane is a process which can take place at plasma membranes of both, malignant and non-malignant cells. Therefore, it is expected not to be selective for tumor cells. On the other hand, it may be supposed that selectivity for tumor cells can be achieved by choosing substances which rely on the endocytotic uptake mechanism, such as the more lipophilic sensitizers PpeC6...C9.

Summary

Molecular self-assemblies have been found to play a decisive role in many processes of the living and non-living nature as well as in many technological fields. Despite numerous studies on the structure and properties of such molecular formations, their structure-property relationship remains unclear.

The **first aim** of this work was *to investigate the structure and energy relaxation processes of J-aggregates*. The investigations were carried out on the water-soluble tetrapyrrolic sensitizer 5,10,15,20-tetrasulphonatophenyl porphine (TPPS₄).

J-aggregates are a particular case of molecular self-assemblies. Due to the strong molecular interaction and alignment of individual molecules within aggregates, they exhibit collective properties arising from the delocalised eigenstates of the molecular wave function. Because of their large application potential, elucidation of the structure-property relationship of J-aggregates is of particular interest.

The experiments were carried out by using steady-state and time-resolved spectroscopy methods. Structure and energy relaxation properties of J-aggregates were investigated by means of time-correlated single photon counting (TCSPC) technique. A part of these measurements was conducted at the stage of a confocal laser-scanning microscope (LSM). The realized experimental set-up enabled space- and time-resolved measurements with resolutions of $\sim 1 \mu\text{m}^3$ and $\sim 15 - 25 \text{ ps}$, respectively.

It was found that TPPS₄ dissolved in aqueous solutions at neutral pH shows a single exponential fluorescence decay with a time constant of $7.9 \pm 0.6 \text{ ns}$ at concentrations of $10^{-6} - 10^{-4} \text{ M}$. This decay constant was attributed to the *neutral monomeric* form of TPPS₄. By using concentrated H₂SO₄ as a solvent, it was possible to shift the equilibrium completely from the aggregated form of TPPS₄ to the diprotonated form and to determine for the first time the characteristic fluorescence decay constant of the *diprotonated form* ($3.1 \pm 0.2 \text{ ns}$) [139].

Because non-linear intermolecular effects, such as exciton-exciton interaction occurring within an aggregate can influence fluorescence decay characteristics, the fluorescence kinetics of the TPPS₄ J-aggregates were investigated as a function of the excitation intensity. Structural properties of J-aggregates and exciton migration characteristics were determined. It was observed that in solutions containing high amounts of J-aggregates, the increase of the excitation intensity resulted in an additional, intensity-dependent non-exponential decay component in the fluorescence decay kinetics. Theoretical investigations

showed that the measurement data can be best described by the model of exciton singlet-singlet annihilation in restricted domains.

The exciton migration parameters, diffusion length D , and the hopping time τ_h of TPPS₄ J-aggregates were determined. The intrinsic exciton lifetime, i.e. the exciton lifetime in the absence of annihilation, was measured to be ~150 ps and the mean physical size of the J-aggregate was determined to be ~20 molecules per aggregate. This value is similar to those determined by other groups using different experimental techniques. It was observed that the J-aggregates of TPPS₄ do not decompose in polyvinyl alcohol matrices, but form large assemblies (macroaggregates) on a scale of ~1 μm . This fact implies that formation of molecular nanostructures on TPPS₄ basis is possible due to the rigid structure of the macroaggregates [140].

The **second aim** of the work presented *was to investigate the structure-property relationship of selected sensitizers using appropriate physical methods and to gain additional knowledge on how the structure of a sensitizer molecule can modulate its photodynamic efficacy.*

Molecular self-assembly also plays an important role for PDT and is still a matter of discussions. It has been demonstrated before that within a congeneric series of sensitizer derivatives, the photodynamic efficacy *in vivo* increases with increasing lipophilicity of the derivatives up to a certain point, whereas a further increase causes a decrease in photodynamic cytotoxicity. This important finding could not be explained so far and was a matter of discussions. Furthermore, factors determining the efficacy and the tumor selectivity could not be clearly defined so far. Gaining information on the structure-property relationship of sensitizers could elucidate this essential finding, which can significantly assist the further development of the sensitizers for photodynamic therapy of tumors.

The aggregation/disaggregation behavior of selected sensitizers (modified pyropheophorbide a and chlorin e6 series) was examined in homogenous solutions and in tumor cells by means of time-resolved fluorescence spectroscopy using one- and two-photon excitation.

It was found that all sensitizers under study aggregate in aqueous solutions. The lipophilicity was varied by attaching alkyl side chains of different lengths to the host molecule. It was found that highly aggregated species of pyropheophorbide a ethers and chlorin e6 derivatives exhibit relative short fluorescence decay times of ~20 – 40 ps and 30-40 ps, respectively. Fluorescence decay times of 6.5 ns and 4.5 ns were obtained for monomeric pyropheophorbide a (Ppe) and chlorin e6 (Chl) derivatives, respectively. The difference in the

decay times of aggregated and monomeric forms of the sensitizers made it possible to distinguish them clearly on the subcellular level in time-resolved fluorescence lifetime measurements in cells.

Measurements of the time course of the intensity in erythrocyte membranes ('ghosts') during incubation with the sensitizers enabled us to quantify the monomerization process and the aggregation degree in a biological sense. The results obtained indicate that the monomerization degree in the plasma membrane correlates with the results of the time-resolved fluorescence measurements (decay times and amplitudes of the fluorescence kinetics) of the sensitizer in homogenous solutions. The compounds bearing short alkyl side chains are monomerized much faster than those with longer chains.

By using the TCSPC imaging technique with a high temporal resolution (20 – 30 ps), aggregates of sensitizers can be detected directly in tumor cells. For the most lipophilic compounds studied, PpeC9 and ChlC9, aggregates were found inside A431 cells [141]. The presence of aggregated sensitizer species in the cell, the endosomic/lysosomal intracellular distribution pattern, and the fact that such large molecular formations can hardly cross the outer cell membrane by passive diffusion imply an uptake of the sensitizers via the endocytotic uptake pathway.

It was found that the degree of aggregation of the sensitizers increases with increasing lipophilicity within a congeneric series. The degree of aggregation of sensitizers belonging to different classes seems to be related not only to the lipophilicity but seems also to be influenced by the structure and the charge distribution of the molecule.

A certain degree of aggregation of the sensitizer can cause an efficient loading of cells, since highly packed portions of sensitizer can be internalized. Too strongly aggregated sensitizers, however, cannot be sufficiently monomerized to become photodynamically active. On the other hand, too weakly aggregated sensitizers can be easily monomerized by the cell membrane and cross it via passive diffusion. Thus, such sensitizers can be washed out easily and their retention time in cells is relatively short. As such, no high selectivity between healthy and neoplastic cells can be expected, because the monomerization process occurs at all cell membranes to the same extent. It can be concluded that there has to be a maximum of photodynamic efficacy within a congeneric series (C5, C6, C7) in the case of Ppe.

These findings can be used as a basis for a better understanding of the structure-activity relationship of sensitizers for photodynamic therapy of tumors and hopefully help to design more efficient drugs for PDT.

Zusammenfassung

Molekulare Aggregate spielen in vielen Prozessen sowohl in der belebten und unbelebten Natur als auch auf vielfältigen technologischen Gebieten eine Schlüsselrolle. Trotz zahlreicher bisher durchgeführter Studien zur Korrelation von Struktur und Eigenschaften solcher molekularen Assoziante, sind noch viele Fragen auf diesem Gebiet ungeklärt.

Der erste Teil der Arbeit beschäftigt sich mit der *Aufklärung der Struktur und der Prozesse der Energierelaxation von J-Aggregaten*. Als Modellsubstanz diente ein wasserlösliches tetrapyrrolisches Photosensibilisator 5, 10, 15, 20- Tetrasulphonatophenylporphin (TPPS₄).

J-Aggregate sind ein besonderer Fall von molekularen Selbst-Assoziaten. Aufgrund der starken molekularen Wechselwirkung und Ausrichtung von individuellen Molekülen innerhalb der Aggregate zeigen sie kollektive Eigenschaften, die auf den delokalisierten Eigenzuständen der molekularen Wellenfunktion beruhen. Wegen ihres großen Anwendungspotentiales, ist die Aufklärung der Struktur-Eigenschafts-Beziehung von J-Aggregaten von besonderem Interesse.

Die Struktur und die nichtlinearen Eigenschaften von J-Aggregaten wurden mit dem Verfahren der zeitkorrelierten Einzelphotonenzählung (TCSPC) untersucht. Ein Teil der Messungen wurde unter Verwendung eines konfokalen Laser-Scan-Mikroskops (LSM) in Kombination mit einem TCSPC Modul durchgeführt. Die realisierte Versuchsanordnung ermöglichte raum- und zeitaufgelöste Messungen mit Auflösungen von jeweils $\sim 1 \mu\text{m}^3$ bzw. $\sim 15 - 25 \text{ ps}$.

Die Fluoreszenzlebensdauermessungen zeigten, dass TPPS₄ in wässrigen Lösungen bei neutralem pH-Wert und Konzentrationen von 10^{-6} bis 10^{-4} M einen monoexponentiellen Fluoreszenzabfall mit einer Zeitkonstante von $7.9 \pm 0.6 \text{ ns}$ aufweist, die der nicht protonierten monomeren Form von TPPS₄ zugerechnet werden kann. Durch Lösen in konzentrierter H₂SO₄ konnte das chemische Gleichgewicht von der aggregierten Form von TPPS₄ zur diprotonierten Form verschoben werden und erstmals die charakteristische Fluoreszenzabklingzeit der diprotonierten Form mit $3.1 \pm 0.2 \text{ ns}$ bestimmt werden [139].

Da nichtlineare zwischenmolekulare Wechselwirkungen, wie z. B. die innerhalb eines Aggregates auftretende Exciton-Exciton-Wechselwirkung, die Fluoreszenzabklingzeit beeinflussen können, wurde die Fluoreszenzkinetik der J-Aggregate von TPPS₄ als Funktion der Anregungsintensität untersucht. Damit bot sich auch die Möglichkeit, die strukturellen

Eigenschaften und die Migrationscharakteristiken von Excitonen in J-Aggregaten zu bestimmen.

Es wurde beobachtet, dass in Lösungen, die J-Aggregate enthielten, mit einer Zunahme der Anregungsintensität eine zusätzliche, intensitätsabhängige und nicht-exponentielle Relaxationskomponente im Fluoreszenzabfall von TPPS₄ auftritt. Die Messdaten lassen sich mit einem Modell der Exciton-Singulett-Singulett-Annihilation in beschränkten Domänen gut beschreiben.

Die Migrationssparameter - die Diffusionslänge D und die Sprung-Zeit („hopping time“) τ_h von TPPS₄ J-Aggregaten - wurden bestimmt. Die eigentliche Lebensdauer des Excitons, d. h. die Lebensdauer in Abwesenheit von Annihilation, wurde gemessen (~150 ps) und die mittlere physische Größe der J-Aggregate bestimmt (~20-Moleküle pro Aggregat). Dieser Wert ist vergleichbar mit Resultaten, die andere Gruppen mit unterschiedlichen experimentellen Verfahren erzielten.

TPPS₄ J-Aggregate können auch stabil in Polivinyl-Alkoholmatrizen eingebettet werden. Sie bilden dann große Strukturen (Makroaggregate) auf einer Skala von ~1- μm aus. Dies zeigt, dass wegen der starren Struktur der Makroaggregate die Bildung von molekularen Nanostrukturen auf TPPS₄ Grundlage möglich ist [140].

Im zweiten Teil der Arbeit wird die *Struktur-Eigenschafts-Beziehung von ausgewählten Photosensibilisatoren (PS) unter Benutzung geeigneter physikalischer Messmethoden untersucht sowie der Einfluss der Struktur eines Photosensibilisator-Moleküls auf seine photodynamische Wirksamkeit betrachtet*. Die Untersuchungen wurden mittels Methoden stationärer und zeitaufgelösten Spektroskopie durchgeführt.

Molekulare Selbst-Assoziation von Photosensibilisatoren (PS) spielt auch bei der photodynamischen Therapie eine grosse Rolle und wird jetzt noch kontrovers diskutiert. So ist bekannt, dass die photodynamische Wirksamkeit *in vivo* sich innerhalb einer konjugierten Reihe eines PS mit Zunahme der Lipophilität bis zu einem gewissen Grad vergrössert, während jedoch ein weiterer Anstieg eine Verminderung der photodynamischen Zytotoxizität verursacht. Die Faktoren, die die Effizienz und die Tumorselektivität bestimmen, konnten bisher nicht eindeutig definiert werden. Weiterführende Erkenntnisse über die Struktur-Eigenschafts-Beziehung von PS könnten wesentlich zu der Weiterentwicklung der Photosensibilisatoren für die photodynamische Tumorthherapie beitragen.

Das Aggregations/Deaggregations-Verhalten von ausgewählten PS (konjugierte Reihen von Pyropheophorbid a (Ppe) und Chlorin-e6 (Chl) Derivaten) wurde in homogenen

Lösungen und in Tumorzellen mit Verwendung zeitaufgelöster Fluoreszenzspektroskopie unter Ein- und Zweiphotonenanregung untersucht.

Es wurde gefunden, dass alle untersuchten PS in wässrigen Lösungen aggregieren. Durch Variation der Länge der an das Molekül-Grundgerüst angehängten Alkyl-Seitenketten wurde die Lipophilität der PS sukzessiv verändert. Es wurde festgestellt, dass hochaggregierte Spezies von Pyropheophorbid a und Chlorin-e6 Derivaten einen multiexponentiellen Fluoreszenzabfall zeigen, wobei Komponenten mit ~20 - 40 ps bzw. 30 - 40 ps auftreten. Für die Monomere von Pyropheophorbid a und Chlorin-e6 Derivaten wurden Fluoreszenzabklingzeiten von 6.5 ns bzw. 4.5 ns gemessen. Der Unterschied der Abklingzeiten von aggregierten und monomeren Formen der Photosensibilisatoren ermöglicht es, sie durch zeitaufgelöste Fluoreszenzmessungen auf subzellulärer Ebene deutlich zu unterscheiden.

Durch eine Messung der Fluoreszenzintensität in Erythrocyten-Membranen ('Ghosts') während der Inkubation mit dem PS, war es möglich, den Monomerisierungsprozess und die Aggregationsstärke in einem biologischen Kontext zu quantifizieren. Die gewonnenen Ergebnisse zeigen, dass der Monomerisierungsgrad der Photosensibilisatoren in der Plasmamembran mit den Ergebnissen der zeitaufgelösten Fluoreszenzmessungen (Abklingzeiten und relative Amplituden der Fluoreszenzkinetik) korrespondiert. Die Komponenten mit kürzeren Alkyl-Seitenketten werden viel schneller monomerisiert als die mit den längeren Ketten.

Durch Kombination eines Laser-Scanning-Mikroskops mit einem zeitlich hoch auflösenden TCSPC-Modul (Auflösung 20 – 30 ps) konnten Aggregate von PS in Tumorzellen direkt nachgewiesen werden. Auf diese Weise konnte gezeigt werden, dass die am meisten lipophilen Komponenten, PpeC9 und ChlC9, in Zellen der Tumor-Zelllinie A431 in aggregierter Form vorliegen [141].

Die Anwesenheit von Aggregaten in der Zelle der PS, ihre endosomal/lysosomale intrazelluläre Verteilung und die Tatsache, dass solch große molekulare Strukturen kaum durch passive Diffusion die Plasmamembran durchqueren können, legt nahe, dass diese Aggregate durch Endozytose aufgenommen werden.

Der Grad der Aggregation eines PS wird innerhalb einer konjugierten Reihe mit zunehmender Lipophilität größer. Der Grad der Aggregation der PS, die zu den verschiedenen Klassen gehören, scheint aber nicht nur von der Lipophilität sondern auch von anderen Parametern wie der Struktur und Ladungsverteilung des Moleküles abzuhängen.

Ein geeigneter Aggregationsgrad des PS kann eine effektive Beladung von Zellen ermöglichen, da besonders kompakte Strukturen gut aufgenommen werden können. Allerdings können stark aggregierte PS durch die Zellmembran nicht hinreichend monomerisiert werden, um photodynamisch aktiv zu sein. Andererseits werden zu schwach aggregierte PS an der Zellmembran zwar schnell monomerisiert und durch passive Diffusion aufgenommen, haben jedoch nur eine relativ kurze Verweilzeit in den Zellen, da sie leicht ausgewaschen werden können. Da die Monomerisierung an allen äusseren Zellmembranen auftritt und eine vergleichbare Kinetik aufweist, kann keine hohe Selektivität zwischen den gesunden und neoplastischen Zellen erwartet werden. Es liegt nahe, dass es ein Maximum der photodynamischen Wirksamkeit in Tumorzellen innerhalb einer konjugierten Reihe geben muss. Beispielsweise liegt das Maximum der photodynamischen Wirksamkeit der untersuchten PS bei C5 und C6 Komponenten.

Die Ergebnisse können als Grundlage für ein besseres Verständnis der Struktur-Wirkungs-Beziehung von Photosensibilisatoren bei der photodynamischen Therapie dienen und möglicherweise zur Entwicklung besserer Pharmaka beitragen.

References

1. S. Creighton, J.-K. Hwang, A. Warshel, W. W. Parson and J. Norris. *Biochemistry*, 27, (1988).
2. W. Kühlbrandt. *Nature*, 374, (1995) 497.
3. K. E. Michel-Beyerle, M. Plato, J. Deisenhofer, H. Michel, M. Bixon and L. Jorter. *Biochem. Biophys. Acta*, 632, (1988) 52.
4. P. M. Borsenberger, A. Chowdry, D. C. Hoesterey and W. Mey. *J. Appl. Phys.*, 44, (1978) 5555.
5. E. Hanamura. *Phys. Rev. B*, 37, (1988) 1273.
6. F. Sasaki, S. Kobayashi. *Appl. Phys. Lett.*, 63, (1993) 2887.
7. S. Kobayashi. *Mol. Cryst. Liq. Cryst.*, 217, (1992) 77.
8. Y. Wang. *Chem. Phys. Lett.*, 126, (1986) 209.
9. Y. Wang. *J. Opt. Soc. Am. B*, 8, (1991) 981.
10. P. G. Schouten, J. M. Warman, M. P. de Haas, M. A. Fox and H. L. Pan. *Nature*, 353, (1991) 736.
11. A. H. Herz. *Adv. Colloid Interface Sci.*, 8, (1977) 237.
12. T. H. James *The Theory of the Photographic Process*. Macmillan (1977).
13. G. Scheibe. *Angew. Chemie*, 49, (1936) 563.
14. G. Scheibe. *Angew. Chemie*, 50, (1937) 212.
15. E. E. Jelley. *Nature*, 138, (1936) 1009.
16. E. E. Jelley. *Nature*, 139, (1937) 631.
17. D. L. Akins (1996) in *J-aggregates* (T. Kobayashi, ed.), Structure and exciton emission dynamics of molecular aggregates: cyanines and porphyrins. pp. 67-94, World Scientific.
18. T. Kobayashi. *J-aggregates*. World Scientific (2001).
19. V. Sundström, T. Gillbro, R. A. Gadonas and A. Piskarskas. *J. Chem. Phys.*, 89, (1988) 2754.
20. B. W. Henderson, D. A. Bellnier, W. R. Greco, A. Sharma, R. K. Pandey, L. A. Vaughan, K. R. Weishaupt and Thomas J. Dougherty. *Cancer Research*, 57, (1997) 4000.

21. I. J. MacDonald, J. Morgan, D. A. Bellnier, G. M. Paszkiewicz, J. E. Whitaker, D. J. Litchfield and Th. J. Dougherty. *Photochem. Photobiol.*, 70, (1999) 789.
22. P. Vehlenger, M. Zellweger, G. Wagnieres, L. Inillerat-Jeanneret and H.van den Berg. *J. Photochem. Photobiol.*, 54, (2000) 36.
23. P. Margaron, G. Marie-Josee, V. Scasnar, H. Ali and J. E. Van Lier. *Photochem. Photobiol.*, 63, (1996) 217.
24. R. Pandey, W. R. Potter and T. J. Dougherty. US Patent No. 5,952,366: Jun 15, 1999.
25. R.Cubeddu, G. Canti, A. Pifferi, P. Taroni and G. Valentini. *Photochem. Photobiol.*, 66, (1997) 229.
26. H. Schneckenburger, M. H. Gschwend, R. Sailer, A. Rück and W. S. L. Strauss. *J. Photochem. Photobiol.*, 27, (1995) 251.
27. M. Ambroz, A. J. MacRobert J. Morgan G. Runbles M. S. C. Foley D. Phillips. *J. Photochem. Photobiol. B: Biol.*, 22, (1994) 105.
28. M.Yamashita, M. Nomura, S. Kobayashi, T. Sato and K. Aizawa. *IEEE Journal of quantum electronics*, 20, (1984) 1363.
29. M. Yamashita, T. Tomono, S. Kobayashi, K. Torizuka, K. Aizawa and T. Sato. *Photochem. Photobiol.*, 47, (1988) 189.
30. R. Cubeddu, R. Ramponi, W. Q. Liu ND F. Docchio. *Photochem. Photobiol.*, 50, (1989) 157.
31. J. M. Wessels; W. Strauss; H. K. Seidlitz; A. Rück and H. Schneckenburger. *J. Photochem. Photobiol. B: Biol.*, 12, (1992) 275.
32. R.Cubeddu, R. Ramponi and P. Taroni. *J. Photochem. Photobiol. B: Biol.*, 11, (1991) 319.
33. A. Andreoni, R. Cubeddu, S. de Silvestri, G. Jori, P. Laporta and E. Reddi. *Z. Naturforsch*, 38 c, (1982) 83.
34. F. Docchio, R. Ramponi, C. A. Sacchi, G. Bottiroli and I. Freitas. *Chem. -Biol. Interactions*, 50, (1984) 135.
35. B. Roeder, H. Wabnitz. *J. Photochem. Photobiol.*, 1, (1987) 103.
36. H. K. Seidlitz, H. Schneckenburger and K. Stettmaier. *J. Photochem. Photobiol. B: Biol.*, 5, (1990) 391.
37. H. K. Seidlitz, K. Stettmaier, J. M. Wessels and H. Schneckenburger. *Opt. Eng.*, 31, (1992) 1482.
38. C.S.Foote. *Proc. SPIE Institute*, 115 (1990).
39. H.von Tappeiner. *Münch. Med. Wochenschr.*, 1, (1900) 5.
40. A. Andreoni and R. Cubeddu. *Chem. Phys. Lett.*, 108, (1984) 141.

41. G. Bottiroli, F. Docchio, I. Freitas, R. Ramponi and C. A. Sacchi. *Chem. -Biol. Interactions*, 50, (1984) 153.
42. S. B. Brown, M. Shillock and P. Jones. *Biochemical journal*, 153, (1976) 279.
43. D. Dolphin. *The Porphyrins*. Academic Press (1978).
44. D. Kessel and E. Rossi. *Photochem. Photobiol.*, 35, (1982) 37.
45. C. R. Lambert, E. Reddi, J. D. Spikes, M. A. Rodgers and G. Jori. *Photochem. Photobiol.*, 44, (1986) 595.
46. R. Margalit and M. Rotenberg. *Biochem. J.*, 219, (1984) 445.
47. G. J. Smith, K. P. Ghiggino, L. E. Bennett and T. L. Nero. *Photochem. Photobiol.*, 49, (1989) 49.
48. J. K. Atkins. *Physical Chemistry*. Academic Press (1996).
49. B. S. Suhindra and J. H. Fuhrkop. *Int. J. Quantum Chem.*, 20, (1981) 747.
50. B. Roeder. *Einführung in die molekulare Photobiophysik*. Teubner (1999).
51. H. Schneckenburger, H. K. Seidlitz and J. Eberz. *J. Photochem. Photobiol. B: Biol.*, 2, (1988) 1.
52. G. Valduga, E. Reddi, G. Jori, R. Cubeddu, P. Taroni and G. Valentini. *J. Photochem. Photobiol. B: Biol.*, 16, (1992) 331.
53. E. Zenkevich, E. Sagun, V. Knyukshto, A. Shulga, A. Mironov, O. Efremova, R. Bonnett, S. Phinda Songca and M. Kassem. *J. Photochem. Photobiol.*, 33, (1996) 171.
54. J. Moan. *Photochem. Photobiol.*, 39, 445 (1984).
55. C. Emiliani and M. Delmelle. *Photochem. Photobiol.*, 37, (1983) 487.
56. R. W. Boyle and D. Dolphin. *Photochem. Photobiol.*, 64, (1996) 469.
57. I. Eichwurz, H. Stiel and B. Röder. *J. Photochem. Photobiol.*, 54, (2000) 194.
58. B. M. Aveline, T. Hasan and R. W. Redmond. *J. Photochem. Photobiol.*, 30, (1995) 161.
59. G. J. Smith. *Photochem. Photobiol.*, 41, (1985) 123.
60. T. J. Dougherty. *Photochem. Photobiol.*, 38, (1983) 377.
61. W. Dietel and R. Wendenburg. *SPIE*, 2370, (1994) 63.
62. F. Ricchelli, D. Stevanin and G. Jori. *Photochem. Photobiol.*, 48, (1988) 13.
63. F. Ricchelli, P. Nikolov, S. Gobbo, G. Jori, G. Moreno and Ch. Salet. *Biochim. Biophys. Acta*, 1196, (2001) 165.

64. W. R. Potter, B. W. Henderson, D. A. Bellnier, R. K. Pandey, L. A. Vaughan, K. R. Weishaupt and Th. J. Dougherty. *Photochem. Photobiol.*, 70, (1999) 781.
65. K. W. Woodburn, N. J. Vardaxis, J. S. Hill, A. H. Kaye and D. R. Phillips. *Photochem. Photobiol.*, 54, (1991) 725.
66. D. Kessel, P. Thompson, K. Saatio and K. D. Nantwi. *Photochem. Photobiol.*, 45, (1987) 787.
67. K. S. Mellish. 13th International Congress of Photobiology. (2000).
68. R. K. Pandey and T. J. Dougherty. *Photochem. Photobiol.*, 1, (1996) 194.
69. D. L. Akins, S. Özcelik, Han-Ru Zhu and C. Guo. *J. Phys. Chem.*, 100, (1996) 14390.
70. E. B. Fleischer, J. M. Palmer, T. S. Strivastava and A. Chatterjee. *J. Am. Chem. Soc.*, 93, (1970) 3162.
71. O. Ohno, Y. Kaizu and H. Kobayashi. *J. Chem. Phys.*, 99, (1993) 4128.
72. R. F. Pasternack, C. Fleming, S. Herring, P. J. Collings, J. dePaula, G. DeCastro Esther and J. Gibbs. *Biophys. J.*, 79, (2000) 550.
73. J. M. Ribo, R. Rubires, Z. El-Hachemi, J. A. Farrera, L. Campos, G. L. Pakhomov and M. Vendrell. *Mater. Sc. Eng. C*, 11, (2000) 107.
74. R. Lauceri, S. Gurrieri, E. Bellacchio, A. Contino, L. Monsu'Scolaro, A. Romeo, A. Toscano and R. Purrello. *Supramol. Chem.*, 12, (2000) 193.
75. T. Kobayashi. *Supramol. Sci.*, 5, (1998) 343.
76. K. Misawa and T. Kobayashi. *J. Chem. Phys.*, 110, (1999) 5844.
77. N. Micali, F. Mallamace, A. Romeo, R. Purrello and L. Monsu Scolaro. *J. Phys. Chem.*, 104, (2000) 5897.
78. R. Rubires, J.-A. Farrera and J. M. Ribo. *Chem. Eur. J.*, 7, (2001) 436.
79. N.L.Vekshin. *Energy Transfer in Macromolecules*. SPIE (1997).
80. S. Özcelik and D. L. Akins. *J. Phys. Chem.*, 101, (1997) 3021.
81. V. Gulbinas, M. Chachisvilis, A. Persson, S. Svanberg and V. Sundström. *J. Phys. Chem.*, 98, (1994) 8118.
82. J. Moll, W. J. Harrison, D. V. Brumbaugh and A. A. Muentzer. *J. Phys. Chem.*, 104, (2000) 8847.
83. N. C. Maiti, M. Ravikanth, Sh. Mazumdar and N. Periasamy. *J. Phys. Chem.*, 99, (1995) 17192.
84. N. C. Maiti, Sh. Mazumdar and N. Periasamy. *J. Phys. Chem.*, 102, (1998) 1528.
85. R. F. Khairutdinov and N. Serpone. *J. Phys. Chem.*, 103, (1999) 761.

86. I. Renge and U. P. Wild. *J. Phys. Chem.*, 101, (1997) 7977.
87. V. Gulbinas, M. Chachisvilis, L. Valkunas and V. Sundström. *J. Phys. Chem.*, 100, (1996) 2213.
88. Th. Förster. *Ann. Phys.*, 2, (1948) 55.
89. Th. Förster. *Z. Naturforsch.*, 4a, (1949) 321.
90. M.D. Galanin. *JETP*, 28, (1955) 485.
91. G. Paillotin, C. E. Swengerg, G. Breton and N. E. Gencintov. *Biophys. J.*, 25, (1979) 513.
92. A. J. Campillo, V. H. Kollman and S. L. Shapiro. *Science (Wash. D. C.)*, 193, (1976) 227.
93. N. E. Geacintov and J. Breton. *Biophys. J.*, 17, (1977) 1.
94. A. Suna. *Phys. Rev. B*, 1, (1970) 1716.
95. L. Valkunas, G. Trinkunas, V. Liuolia and R. van Grondelle. *Biophys. J.*, 69, (1995) 1117.
96. L. Valkunas, G. Trinkunas and V. Liuolia. *Biophys. J.* 76, (1999) 244.
97. A. Bunde and S. Havlin. *Fractals in Disordered Systems*. Springer (1991).
98. C. J. R. Sheppard T. Wilson. *Theory and Practice of Scanning Optical Microscopy*. Academic Press (1984).
99. T. Wilson. *Confocal Microscopy*. Academic Press (1990).
100. D. A. Agard. *Annu. Rev. Biophys.*, 13, (1984) 191.
101. W. Denk, J. H. Strickler and W. W. Webb. *Science*, 248, (1990) 73.
102. C. L. Caylor, I. Dobrianov, C. Kimmer, R. E. Thorne, W. Zipfel and W. W. Webb. *Phys. Rev. E*, 59, (1999) 3831.
103. I. Choupa, M. Pereira, J. M. Millot, H. Morjani and M. Manfait. *SPIE*, 3604, (1999) 51.
104. M. L. Coleno, V. P. Wallace, C. H. Sun, A. K. Dunn, M. W. Berns and B. J. Tromberg. *SPIE*, 3604, (1999) 67.
105. A. Diaspro and M. Robello. *Microsc. Anal.*, 58, (1999) 5.
106. I. Gryczynski, H. Malak and J. R. Lakovicz. *Bioimaging*, 4, (1996) 138.
107. M. Gu. *Opt. Lett.*, 21, (1996) 988.
108. X. S. Gan and M. Gu. *Bioimaging*, 4, (1996) 129.

109. G. S. He, J. B. Bhawalkar, P. N. Prasad and B. A. Reinhardt. *Opt. Lett.*, 20, (1995) 1524.
110. S. W. Hell. *Bioimaging*, 4, (1996) 121.
111. S. W. Hell, K. Bahlmann, M. Schrader, A. Soini, H. Malak, I. Gryczynski, J. R. Lakowicz. *J. Biomed. Opt.*, 1, (1996) 71.
112. K. Hean Kim, Ch. Buehler, C. Y. Dong, and B. R. Masters. *SPIE*, 3604, (1999) 60.
113. H. J. Koester, D. Baur, R. Uhl and S. W. Hell. *Biophys. J.*, 77, (1999) 2226.
114. O. Nakamura. *Microsc. Res. Tech.*, 47, (1999) 165.
115. A. Periasamy. *SPIE*, 3604, (1999) 74.
116. J. M. Song, T. Inoue, H. Kawazumi and T. Ogawa. *Anal. Sci.*, 14, (1998) 913.
117. H. Schneckenburger and Th. P. Wustrow. *Photochem. Photobiol.*, 47, (1987) 471.
118. I. Choupa, M. Pereira, J. M. Millot, H. Morjani and M. Manfait. *SPIE*, 3604, (1999) 51.
119. E. H. K. Stelzer, S. Hell, S. Lindek, R. Stricker, R. Pick, C. Storz, G. Ritter and N. Salmon. *Opt. Communications*, 104, (1994) 223.
120. J. P. Hermann and J. Ducuing. *Phys. Rev. A*, 5, (1972) 2557.
121. J. N. Demas and G. A. Crosby. *J. Phys. Chem.*, 75, (1971) 991.
122. Ch. Xu, J. Guild, W. Webb and W. Denk. *Opt. Lett.*, 20, (1995) 2372.
123. D. Frolov, S. Bagdonas and R. Rotomskis. *Lithuanian journal of physics*, 40, (2000) 228.
124. Ph. J. Reid, D. A. Higgins and P. F. Barbara. *J. Phys. Chem.*, 100, (1996) 3892.
125. D. Kessel, C. J. Byrne and A. D. Ward. *Photochem. Photobiol.*, 53, (1991) 469.
126. D. Kessel, C. J. Byrne and A. D. Ward. *J. Photochem. Photobiol.*, 13, (1992) 153.
127. G. A. Karns, W. A. Gallagher and W. B. Elliott. *Bioorg. Chem.*, 8, (1979) 69.
128. M. Gouterman, D. Holten and E. Lieberman. *Chem. Phys.*, 25, (1977) 139.
129. T. B. Melo and G. Reiseater. *Biophysical chemistry*, 25, (1986) 99.
130. F. Ricchelli. *J. Photochem. Photobiol.*, 29, (1995) 109.
131. J. D. Spikes. In *Porphyrins in Tumor Therapy* (A. Andreoni, R. Cubeddu, ed.) Photosensitizing properties of porphyrins in model cell systems. pp. 51-60 (1984).
132. R. Cubeddu, R. Ramponi and G. Bottioli. 701, (1987) 316.
133. A. Moore, E. Marecos, A. Bogdanov and R. Weissleder. *Radiology*, 214, (2002) 574.

134. R. Bachor, Cr. Shea, R. Gillies and T. Hasan. *Proc. Natl. Acad. Sci. USA*, 88, (1991) 1580.
135. P. K. Sebo, G. Sivam, O. Fodstad, K. Sandvig and K. Berg. *Int. J. Cancer*, 92, (2001) 761.
136. Klopman G, Li JY, S. Wang and M. Dimayuga. *J. Chem. Inform. Comput. Sci.* 34, (1994) 752.
137. SciFinder Scholar, Reg. No.: 122341-38-2, Database: REGISTRY (COPYRIGHT 2002 ACS), 2002.
138. S. Andrejevic Blant, P. Grosjean, J.-P. Ballini, G. Wagnieres, H. van den Bergh, Ch. Fontolliet, Ph. Monnier. *J. Photochem. Photobiol.* 61, (2001) 274.
139. D. Frolov, S. Bagdonas, L. Kelbauskas, W. Dietel, G. Streckyte and R. Rotomskis. *Lithuanian journal of physics.* 41, (2001) 484.
140. L. Kelbauskas, S. Bagdonas, W. Dietel and R. Rotomskis. *J. Luminescence*, 101, (2003) 253.
141. L. Kelbauskas and W. Dietel, *Photochem. Photobiol.*, 76, (2002) 686.

Appendix

i. TPPS₄ spectroscopy

Chemicals

The TPPS₄ was purchased from Porphyrin Products Inc. of Logan, Utah, and used without further purification. The stock solution of TPPS₄ was prepared in 0.02 M phosphate buffered saline (PBS) at pH 7, at a concentration of 9×10^{-3} M. The TPPS₄ solutions used in the experiments were prepared by diluting the stock solution to a concentration of 5×10^{-5} M. Only freshly prepared TPPS₄ solutions were used. The J-aggregates were obtained through the lowering of pH upon addition of HCl to the solution.

The polyvinyl alcohol (PVA) solution was prepared by dissolving 100 mg of crystalline PVA in 1 mL 0.1 M HCl solution at pH 1. The stock solution of TPPS₄ in polyvinyl alcohol (PVA) was prepared by dissolving TPPS₄ in PVA solution until saturation. The films at five different TPPS₄ concentrations (100%, 50%, 33%, 20% and 10%) were obtained by diluting the stock solution with PVA solution and further applying 1 drop (appr. 1 mL) of the PVA solution onto the 2 cm² area of the microscope cover glasses. The samples were dried on a flat surface at room temperature for 24 h.

ii. Steady-state and time-resolved spectroscopic studies on pyropheophorbide a ether derivatives in homogenous media and in tumor cells

Chemicals

The pyropheophorbide ethers were prepared according to the procedure described in [68]. The PS were dissolved in 0.1 N sodium hydroxide and stirred over 12 hours at 40-50° C. After cooling, the pH was carefully adjusted to 7.4 and the non-dissolved material was removed by centrifugation (30 minutes, 15000 g). The concentration of the monomeric PS was determined from the extinction at 660 nm in a 1 cm cuvette, measured for the stock solution diluted to 1:40 with methanol.

Lipophilicity.

The lipophilicity of the compounds was determined as the logarithm of the octanol-water partition coefficient (log P, base 10) .

The lipophilicity of Chl derivatives was calculated at the UFZ Center for Environmental Research, Leipzig, using the method described in [136]. The calculated log P values were found to vary linearly with the length of the alkyl chain yielding 7.5 and 8.5 for ChlC6 and ChlC9, respectively. Preliminary experimental log P values were obtained using reversed-phase HPLC analysis and were found to be approximately 15% higher than the calculated values (A. Paschke, private communication).

Cells

The human endothelial carcinoma cell line (A431) was used for the experiments. The cells were seeded on 50x50 mm Petriperm dishes (Helmut Saur Laborbedarf, Reutlingen, Germany) and grown for 116 h in nutrient solution in the presence of 10% fetal calf serum (FCS) and 1% penicillin-streptomycin at 37°C and 5% CO₂ in a humid environment before measurements. Prior to microscopy, the cell cultures were rinsed with PBS and re-incubated in nutrient solution without FCS. Further, the cells were administered with the PS for distinct times.

iii. Two-photon absorption spectra of fluorescent probes and photosensitizers

Sample preparation

The fluorescent probes were purchased from Molecular Probes, Eugene, OR, USA. The pyropheophorbides were sensitized in the group of T. Dougherty [12]. Rhodamine 6G was purchased from Lambda Physics GmbH, Darmstadt, Germany. Hematoporphyrine IX, Protoporphyrin IX, Chlorin e6, meso-tetra-porphyrin were purchased from Porphyrin Products Inc., Logan, Utah, USA. The stock solutions of the fluorescent probes were prepared at 2 mM and then diluted by a factor of 100 to 100 μM concentration. The preparation of the solutions is summarized in Table A1.

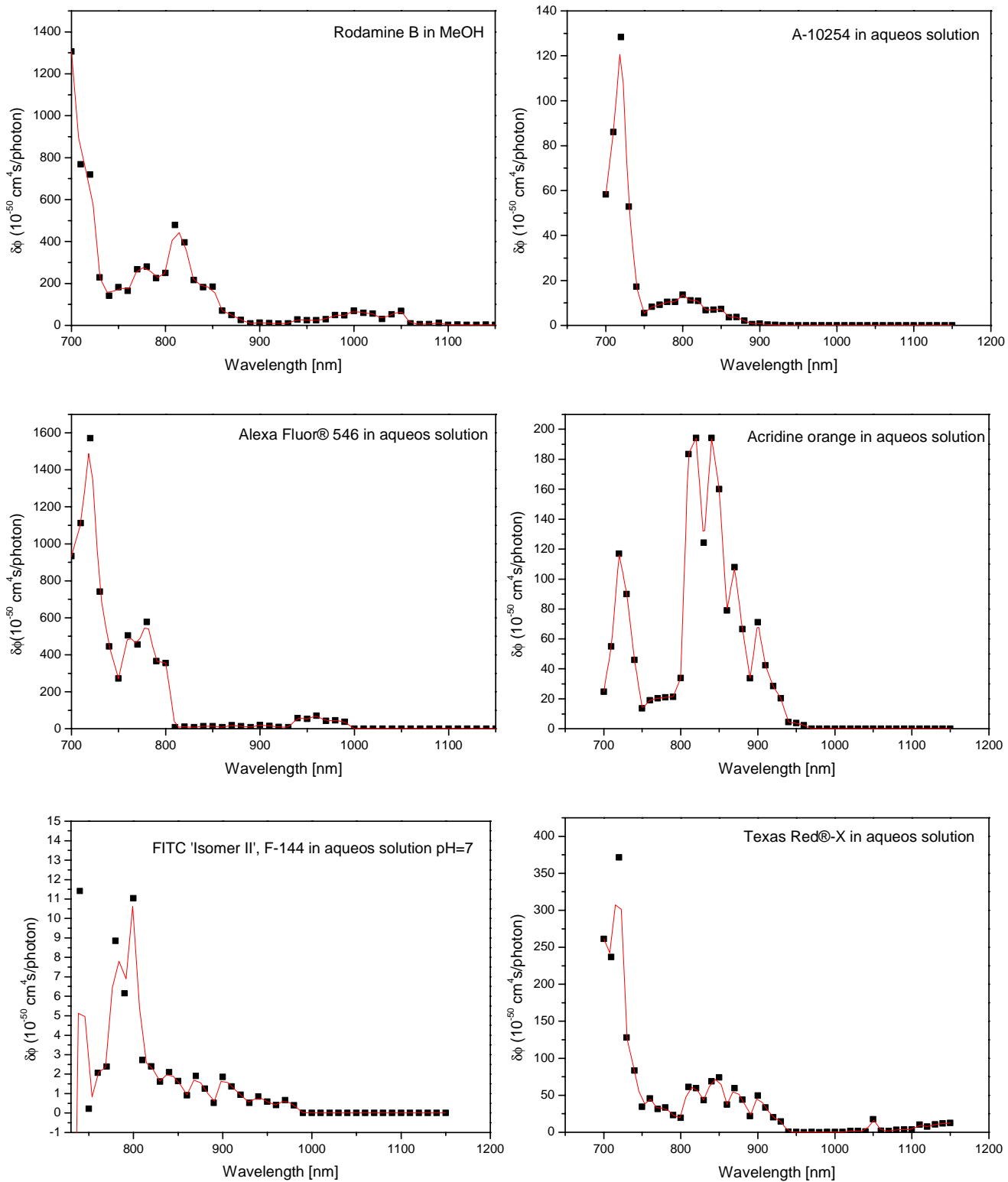


Fig. A1. Two-photon absorption cross-section of the investigated fluorescent probes in the wavelength region 700-1150 nm.

Table A1. Preparation of solutions (Catalog numbers of fluorescent cellular markers obtained from Molecular Probes Europe BV are given in the brackets)

| Substance ('MP' Cat. No.) | Solvent | Concentration (μM) |
|--|-------------------------------|---------------------------------|
| Rhodamine B | MeOH | 500 |
| Alexa Fluor TM 546 (A- 10258) | H ₂ O | 100 |
| Alexa Fluor TM 350 (A- 10439) | H ₂ O | 100 |
| Acridine orange (A- 1301) | H ₂ O | 100 |
| Dextran, rhodamine B (D- 1824) | H ₂ O | 100 |
| CellTracker TM (C- 7001) | DMSO | 100 |
| Texas Red ^{R-X} (T- 10125) | H ₂ O | 100 |
| Indo-1 (I- 1202) | Aqueous buffer, pH=7 (PBS) | 100 |
| DAPI (D- 1306) | H ₂ O | 100 |
| Hoechst 33342 (H- 1399) | H ₂ O | 100 |
| Propidium iodide (P- 1304) | H ₂ O | 100 |
| AMCA-X (A- 6118) | DMSO | 100 |
| Lucifer yellow (A- 629) | H ₂ O | 100 |
| FITC 'Isomer I' (F- 143) | aqueous buffer pH=7 | 100 |
| FITC 'Isomer II' (F- 144) | aqueous buffer pH=7 | 100 |
| Alexa Fluor TM 488 (A- 10254) | H ₂ O | 100 |
| Nile red (N- 1142) | DMSO | 100 |
| Chlorin e6 | DMSO | 100 |
| Deuteroporphyrin IX | DMSO | 100 |
| Pyropheophorbide a-nonyl | PBS+Triton 100 | 34,5 |

Ehrenwörtliche Erklärung

Ich erkläre hiermit ehrenwörtlich, dass ich die vorliegende Arbeit selbständig, ohne unzulässige Hilfe Dritter und ohne Benutzung anderer als der angegebenen Hilfsmittel und Literatur angefertigt habe. Die aus anderen Quellen direkt oder indirekt übernommenen Daten und Konzepte sind unter Angabe der Quelle gekennzeichnet.

Weitere Personen waren an der inhaltlich-materiellen Erstellung der vorliegenden Arbeit nicht beteiligt. Insbesondere habe ich hierfür nicht die entgeltliche Hilfe von Vermittlungs- bzw. Beratungsdiensten (Promotionsberater oder andere Personen) in Anspruch genommen. Niemand hat von mir unmittelbar oder mittelbar geldwerte Leistungen für Arbeiten erhalten, die im Zusammenhang mit dem Inhalt der vorgelegten Dissertation stehen.

Die Arbeit wurde bisher weder im In- noch im Ausland in gleicher oder ähnlicher Form einer anderen Prüfungsbehörde vorgelegt.

Die geltende Promotionsordnung der Physikalisch-Astronomischen Fakultät ist mir bekannt.

Ich versichere ehrenwörtlich, dass ich nach bestem Wissen die reine Wahrheit gesagt und nichts verschwiegen habe.

Jena, den 09. April 2003

(Laimonas Kelbauskas)

Liste der wissenschaftlichen Veröffentlichungen und wissenschaftlichen Vorträge

Artikel

D. Frolov, S. Bagdonas, L. Kelbauskas, W. Dietel, G. Strečkyte, R. Rotomskis TPPS₄ spectroscopy: investigation of aggregation and protonation properties, Lithuanian journal of physics, 41 (2001) 484.

L. Kelbauskas, S. Bagdonas, W. Dietel, R. Rotomskis. Excitation relaxation and structure of TPPS₄ J-aggregates Journal of Luminescence, 101, (2003) 253.

L. Kelbauskas, W. Dietel. Internalization of aggregated photosensitizers by tumor cells: subcellular time-resolved fluorescence spectroscopy on derivatives of pyropheophorbide-a ethers and chlorin e6 under femtosecond one- and two-photon-excitation, Photochemistry and Photobiology, 76 (6) (2002) 686.

Vorträge

L. Kelbauskas, R. Wolleschensky F. Ewald, Th. Feurer and W. Dietel
Temporal and spectral resolved laser scanning microscopy studies on the internalization and localization of an amphiphilic photosensitizer of second generation in tumor cells
World Congress on Cellular and Molecular Biology, 8-13 Oct 2000, Jena

L. Kelbauskas, W. Dietel, Structure-activity relationship of sensitizers: lipophilicity, aggregation state and subcellular localization patterns of a series of pyropheophorbide a derivatives
9th ESP Congress of European Society for Photobiology, 3-8. Sept. 2001, Lillehammer, Norwegen

Poster

L. Kelbauskas, W. Dietel, T. Feurer, J. Kobelke
Femtosecond spectroscopy of materials with high n_2 values for an all-optical Kerr shutter
XIV Lithuanian-Bellorussian Workshop „Lasers and optical nonlinearity“
poster, August 1-10 1999, Preila, Lithuania

F.Ewald, L. Kelbauskas, W. Dietel

Structure-activity relationship: Aggregation/deaggregation behavior and loading of tumor cells
13th International Congress on Photobiology, 1-6. Juli 2000, San Francisco, USA

L. Kelbauskas, W. Dietel, Th. Feurer, E. Ewald and R. Wolleschensky

Two-photon excitation of photosensitizers and molecular fluorophores: excitation spectra and subcellular localization patterns

3rd European Biophysics Congress, 9-13. Sept. 2000, München

L. Kelbauskas, Th. Feurer, F. Ewald and W. Dietel

Two-photon fluorescence excitation spectra of biologically relevant sensitizers and fluorescent markers

World Congress on Cellular and Molecular Biology, 8-13 Oct 2000, Jena

L. Kelbauskas, W. Dietel

Internalization of aggregated photosensitizers by tumor cells probed by subcellular time-resolved spectroscopy under femtosecond one- and two-photon excitation

IX International Conference on Laser Applications in Life Sciences, 7-11. Juli 2002, Vilnius, Litauen

Lebenslauf

- 07.12.73 geboren in Jonava, Litauen
- 1979 – 1991 Allgemeinbildende Schule Jonava
- 1991 – 1995 Physik Studium an der Universität Vilnius
Abschluss mit dem Bakalaureat-Diplom (Bachelor of science)
Thema der Diplomarbeit:
„Untersuchung der Struktur des Bewegungsanalysators des Sehsystems“
- 1995 – 1997 Studium Angewandte Physik an der Universität Vilnius
Abschluss mit dem Magister-Diplom (Master of science).
Thema der Diplomarbeit:
„Elektrophysiologische Charakterisierung von 14-3-3-Protein
überexprimierten Tabakpflanzen“
- 1996-1997 Teilstudium an der Friedrich-Schiller-Universität Jena im Rahmen des EU-
Programms „Tempus“. Mitarbeit in der Arbeitsgruppe von Prof. Dr. R.
Sauerbrey.
- 1997-2001 Wissenschaftlicher Mitarbeiter in der Arbeitsgruppe von Prof. Dr. R.
Sauerbrey
Institut für Optik und Quantenelektronik
der Friedrich-Schiller-Universität Jena
- seit 01.01.2002 Wissenschaftlicher Mitarbeiter in der Arbeitsgruppe von Prof. Dr. K.
Benndorf
Institut für Physiologie II
der Friedrich-Schiller-Universität Jena

Jena, den 09. April 2003

(Laimonas Kelbauskas)

Danksagung

Vor allem möchte ich mich bei Herrn Dr. Wieland Dietel für die wertvollen Diskussionen, sein intensives Engagement und ständige Hilfsbereitschaft bedanken.

Mein besonderer Dank geht auch an Herrn Prof. Dr. Thomas Feurer, der mich mit anregenden Diskussionen und neuen Ideen bei der Arbeit jederzeit unterstützt hat.

Ich danke Herrn Prof. Dr. Roland Sauerbrey für die Möglichkeit, die Arbeit im Institut für Optik und Quantelektronik durchzuführen und für die Unterstützung mit hochentwickelter Messtechnik.

Für die interessante Fragestellung und Anregungen zum Thema „J-Aggregate“ habe ich mich bei Herrn Prof. Ricardas Rotomskis zu bedanken.

Ich bedanke mich bei Herrn Prof. Dr. Klaus Benndorf und Dr. Cristoph Biskup für die wertvollen Diskussionen und die Unterstützung bei Bereitstellen von Zellkulturen und Messtechnik.

Ausserdem möchte ich mich hiermit bei allen jenen bedanken, die mit ihren Leistungen mir zur Seite standen:

- Herrn Dipl.-Phys. Marko Hellwing für die Unterstützung bei technischen Fragen und Problemen.
- Herrn Dr. Leo Wollweber und seinen Mitarbeiterinnen für die zur Verfügung gestellten Zellkulturen und Hilfe bei den biologischen Fragestellungen.
- Herrn Dipl.-Phys. Ralf Wolleschensky für seine Hilfe bei dem Laser-Scan-Mikroskop.
- Herrn Prof. Edward Zenkevich und Dr. Aleksander Shulga für die nutzvollen Diskussionen und die Synthese von Sensitizern.
- Frau Petra Mämpel für ihre Unterstützung als technische Assistentin bei den Messungen und insbesondere der Bereitstellung von Zellkulturen.
- Frau Dipl.-Phys. Friederike Ewald für die hervorragende Zusammenarbeit und die Diskussionen.
- Vielen anderen Mitarbeitern des Instituts für Optik und Quantenelektronik für die grosse Freundlichkeit und Hilfsbereitschaft bei technischen und administrativen Problemen aller Art.
- Meiner Familie und allen meinen Freunden die mich unterstützt haben.

Diese Arbeit wurde zum Teil über das Projekt Nr. Di 481/2-1 der DFG gefördert.